The heart of oxygenic photosynthesis illuminated

Janssen, G.J.

THE HEART
OF
OXYGENIC PHOTOSYNTHESIS
illuminated

Geertje Jacoba Janssen

Geertje Jacoba Janssen
The Heart of Oxygenic Photosynthesis illuminated
Ph.D. Thesis, Leiden University, 4th December 2013

ISBN: 978909028000

Cover design painting “Klaprozen” by Herman van der Wal
Thesis Printed by Smart Printing Solutions, www.sps-print.eu

THE HEART OF OXYGENIC PHOTOSYNTHESIS illuminated

PROEFSCHRIFT

ter verkrijging van
de graad van Doctor aan de Universiteit Leiden,
op gezag van de Rector Magnificus Prof. Mr. C.J.J.M. Stolker,
volgens besluit van het College voor Promoties
te verdedigen op Woensdag 4 December 2013
klokke 08:45

door

Geertje Jacoba Janssen

geboren te Londen, Verenigd Koninkrijk in 1984

Promotiecommissie:

Promotor:
Prof. dr. H. J. M. de Groot

Copromotor:
Dr. A. Alia

Overige leden:
Prof. dr. J. Matysik
Prof. dr. M. Ubbink
Prof. dr. J. Golbeck
Prof. dr. J. Brouwer

In liefdevolle herinnering aan Siska Pothof

TABLE OF CONTENTS

LIST OF ABBREVIATIONS

A	Electron acceptor
A_0	Chl *a* primary electron acceptor in PSI
A_1	Quinone secundairy electron acceptor in PSI
ALA	δ-aminolevulinic acid
BBY	PSII enriched membrane
BChl	Bacteriochlorophyll
Chl *a*	Chlorophyll a
Car	Carotenoid
CS	Chemical shift
D	Electron donor
DD	Differential decay
DFT	Density functional theory
DNP	Dynamic nuclear polarization
DR	Differential relaxation
ENDOR	Electron nuclear double resonance
EPR	Electron paramagnetic resonance
ET	Electron transfer
Hb.	Heliobacter
ISC	Intersystem crossing
LCMS	Liquid Chromatography Mass Spectroscopy
MAS	Magic-angle spinning
n.a.	Natural abundance
ns	Nanosecond
NMR	Nuclear magnetic resonance

NPQ	non-photochemical quenching
OEC	Oxygen evolving complex
P_{D1}	Donor Chl *a* of PSII attached to the D1 branch of the RC
P_M	BChl *a* of P attached to the M branch of the RC
P_L	BChl *a* of P attached to the L branch of the RC
Phe *a*	Pheophytin *a*
Photo-CIDNP	Photochemically induced nuclear polarization
PSI	Photosystem I
PSII	Photosystem II
QM/MM	Quantum mechanics/molecular mechanics
Rb.	*Rhodobacter*
RC	Reaction center
rf	Radio-frequency
RPM	Radical pair mechanism
RT	Room temperature (293K)
TNP	Transient nuclear polarization
TOP	Transiently obscured polarization
TSM	Three-spin mixing
WT	Wild type
Φ	Bacteriopheophytin

LIST OF SYMBOLS

A_{zz}	(3,3) element of the hyperfine tensor
A_{zx}, A_{zy}	Pseudosecular elements of the hyperfine interaction
B	Absolute pseudosecular hf interaction

D	Magnitude of the electron-electron dipolar coupling
d	Electron-electron coupling
d_{vdW}	van der Waals distance
I	measured LCMS peak intensity
$I_{\%}$	relative LCMS peak intensity
I_t	calculated true LCMS peak intensity
J	Electron-electron exchange coupling
ρ_i	Electron spin density
S	Singlet radical state
T_0	Triplet state with magnetic quantum number 0
T_{ev}	Evolution time
T_S	Lifetime of the singlet radical state
T_T	Lifetime of the triplet radical state
τ_p	Laser pulse duration
ΔA	Hyperfine anisotropy
Δt	delay time between laser pulse and NMR detection
$\Delta \Omega$	Difference of the electron Zeeman interaction between the two radicals
ω_I	Nuclear Zeeman interaction

Chapter 1

INTRODUCTION

1.1 OXYGENIC PHOTOSYNTHESIS

1.1.1 Solar energy

Over the past 3.5 billion years, nature has developed a highly efficient mechanism to harvest solar energy resulting in the process we now know as photosynthesis (Blankenship 2002). Today photosynthesis is crucial for life on earth just as energy is crucial to maintain our current state of human civilization. Besides the production of oxygen, photosynthetic processes lead to the formation of fossil fuels. In addition, photosynthetic organisms are the start of the food chain and as such sustain living beings on the planet.

The capability to harvest energy from sunlight by 'soft' biological proteins has triggered an extensive amount of research. By increasing our understanding about photosynthesis, we ultimately aim to find sustainable solutions for man's increasing demand for energy while avoiding both the excessive use of fossil fuels that cause environmental problems and the danger involved with nuclear power plants. The accident at the nuclear power plant of Fukushima in Japan 2011 underlined once again the necessity to find a safe and green alternative source of energy (Knip 2011).

1.1.2 Photosynthetic proteins

The primary photosynthetic processes of energy conversion occur inside the reaction center (RC), a pigment-protein complex located at the heart of the photosynthetic complexes. Upon the absorption of a photon in the visible region, a cascade of electron transfer reactions occurs along a series of protein-bound cofactors, leading to the formation of a trans-membrane potential. There are two types of RCs distinguished based upon their final electron acceptor: Type I RCs have iron-sulfur clusters as electron acceptors while Type II RCs contain pheophytin and quinone as acceptors. Photosynthetic purple bacteria and green non-sulphur bacteria have Type II RCs while Type I RCs are found in heliobacteria and green sulphur bacteria.

Photosynthesis in cyanobacteria, algae and higher plants involves the participation of both types of RCs, photosystem I (PSI, Type I) and photosystem II (PSII,

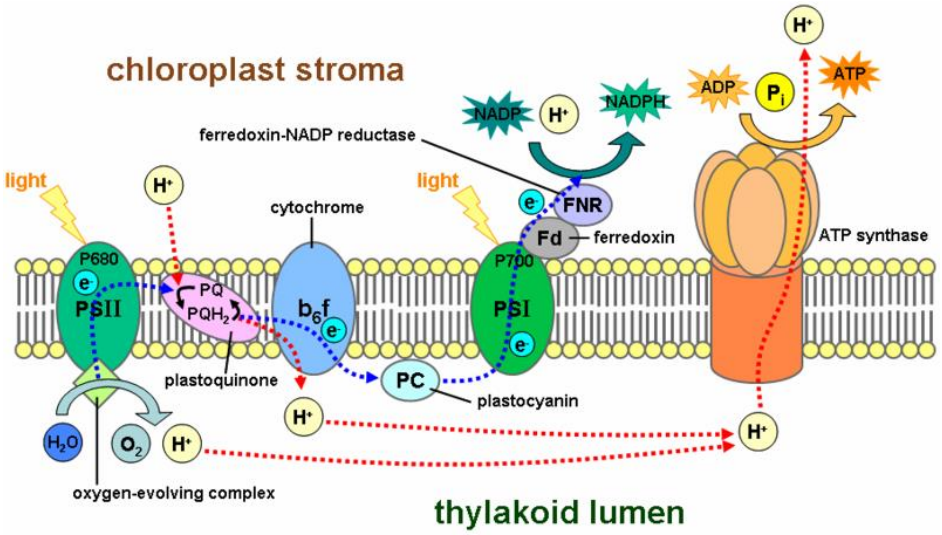

Figure 1.1: Schematic model of the photosynthetic machinery of oxygenic photosynthesis as found in plants, green algae and cyanobacteria located in the thylakoid membrane. Electron transfer starts at photosystem II (PSII) and proceeds via the plastoquinone pool to cytochrome b_6f and via plastocyanin to photosystem I (PSI). The proton gradient that is generated drives the synthesis of ATP by the ATP synthase complex. The electron transport chain is depicted in blue dotted arrows; the proton transport chain is depicted in red dotted arrows.

Type II). The coupling of these two photosystems allows for the pumping of electrons across the photosynthetic membrane, transforming the energy from the sun into a stable trans-membrane potential that is strong enough to split water and reduce $NADP^+$. During this process, which is known as oxygenic photosynthesis, free oxygen is produced as a side product while carbon dioxide is fixed from the air into organic material. Figure 1.1 shows a schematic representation of the complexes involved in oxygenic photosynthesis and the proton and electron flows. The photosynthetic complexes are embedded inside the thylakoid membrane and while electrons are transferred from PSII to PSI, protons are pumped from the stroma (outer) to the lumen (inner) site of the thylakoid membrane. The potential difference generated by this movement is used to generate ATP. The active site of PSII, where water splitting occurs, protrudes into the acidic (pH 6.5) lumen space of the membrane while PSI functions at the stroma side where the pH is normally around 8 (Magnitskii and Tikhonov 1998; Kramer *et al.* 1999; Trubitsin and Tikhonov 2003). In plants and algae the thylakoid is located in specialized organelles called chloroplasts, with each cell containing 10 to 100 chloroplasts (Allen *et al.* 2011). Cyanobacteria are single cell organisms without separate chloroplasts, instead they contain a network of circular thylakoid membranes (Nowaczyk *et al.* 2010).

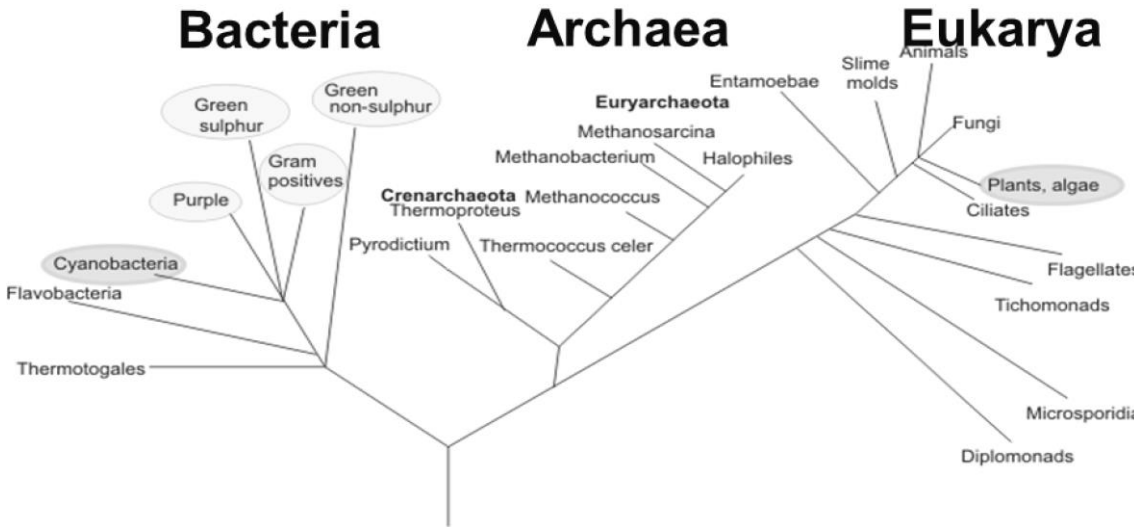

Figure 1.2: Phylogenetic tree based on the small subunit RNA method with the groups containing photosynthetic organisms marked by the grey circles (Blankenship 2002). Groups containing the full oxygenic photosynthesis machinery (PSI and PSII) are dark grey encircled. In bright grey are the groups that contain non-oxygenic photosynthetic organisms with either Type I or Type II photosystems.

1.1.3 Bacterial Reaction Centers

Figure 1.2 shows a phylogenetic tree indicating the groups that contain photosynthetic organisms (Blankenship 2002; Jankowiak *et al.* 2003). Although the occurrence of photosynthesis is widespread among distinct groups and different species, the overall three-dimensional structure of the photochemically active RC is highly conserved. In 1988 Deisenhofer, Michel and Huber shared the Nobel Prize in chemistry. They received the award for the determination of the first crystal structure of the RC of the purple bacteria *Rb. sphaeroides* (Deisenhofer *et al.* 1984; 1985), which was also the first resolved membrane protein complex. Because until the mid 80's this remained the only RC from which a high resolution X-ray structure was available, the Type II bacterial reaction center of purple bacteria is the most extensively studied photosynthetic RC (Hunter *et al.* 2008). The understanding of its function and structure has been used as a guideline for further research on other photosynthetic RCs.

Figure 1.3 shows the photosynthetic RC complex and the cofactor arrangement of the Type II bacterial reaction center of *Rb. sphaeroides* based on the 2.55 Å resolution X-ray structure solved by Camara-Artigas *et. al.* (Camara-Artigas *et al.* 2002). The RC consists of three membrane spanning polypeptides, L, M and H, referring to their relative (light, medium and heavy) weight (Yeates *et al.* 1987; Ermler *et al.* 1994; Camara-Artigas *et al.* 2002). The L and M proteins bind the cofactors. Two bacteriochlorophyll *a* (BChl *a*)

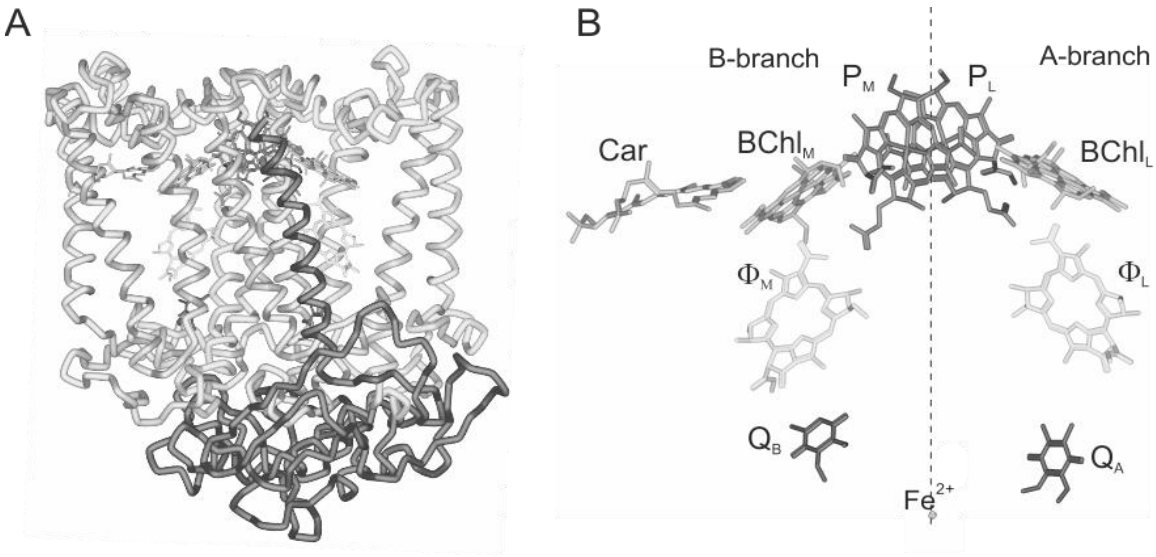

Figure 1.3: (A) The complex arrangement of 3 polypeptide subunits, L, M and H, that surround the bacterial RC are represented with a ribbon representation. (B) The cofactors in the bacterial reaction center (RC) of *Rb. sphaeroides* wild type (WT). The primary electron donor, the special pair, is formed by the two BChl *a* molecules P_L and P_M. $BChl_L$ and $BChl_M$ are accessory BChl cofactors. Φ_A and Φ_B are bacteriopheophytin (BPhe) *a* cofactors. On the acceptor side, two ubiquinone-10 cofactors Q_A and Q_B with a non-heme iron in between are localized. Side chains are omitted for clarity of representation. The near symmetric cofactor arrangement is broken by a carotenoid (Car). The light-induced electron transfer occurs selectively via branch A. [PDB entry 1M3X (Camara-Artigas *et al.* 2002), the figure has been made with Accelrys Discovery Studio adapted with permission from (Gupta 2011), page 17]

P_L and P_M form together the 'special pair' (P) or P840 donor. Although they are strongly coupled, P_L and P_M are not a perfect symmetric dimer (Hoff and Amesz 1991) and are therefore referred to as the 'special pair' rather than a BChl dimer. In addition two accessory BChl's ($BChl_{L,M}$), and two bacterial pheophytins ($\Phi_{L,M}$) are bound, with the subscripts representing the respective polypeptide chain to which the cofactor is bound (Deisenhofer *et al.* 1984). The Type II bacterial RC contains two ubiquinone-10 cofactors; Q_A and Q_B, with Q_B being more loosely bound and functioning as a two electron shuttle by dissociating from the RC after take up of two electrons and two protons. In addition the bacterial RC contains one spheroidene carotenoid (Car) and a non-heme iron (Fe^{2+}). The cofactors are arranged in two branches, A and B, around a pseudo-C_2 symmetry axis perpendicular to the membrane plane. The electron flow is asymmetric, occurring almost exclusively along the active A branch.

The carotenoid that is bound to the M subunit and located on the inactive branch near the $BChl_M$, breaks the apparent symmetry of the cofactor arrangement. Carotenoids are known to play an important role as light-harvesting pigments and in the prevention of the photochemical formation of highly reactive singlet oxygen species (Cogdell *et al.* 2000). Singlet oxygen is an extremely damaging species produced for example via the

triplet state of a Chl. The triplet Chl can be quenched by carotenes according to the Dexter triplet quenching mechanism (Dexter 1953; Cogdell *et al.* 2000), producing triplet Car (^{3}Car) that decays to the ground state by dissipating heat through molecular vibrations (Telfer 2005). The Dexter mechanism requires an electronic exchange coupling of the (BChl) donor and acceptor (Car) through an overlap of the respective wave functions. This mechanism is only efficient when donor and acceptor are in van der Waals contact. In the bacterial RC this condition is met with a distance between the $BChl_M$ and the Car of ~3.3 Å (Camara-Artigas *et al.* 2002). The *Rb. sphaeroides* R26 strain (R26) is a widely studied mutant that lacks the carotenoid. It has been found that after Car reconstitution into the R26 RC, two stereoisomers (13,14 -cis and 15,15'-cis) of the Car occur (Wirtz *et al.* 2007; Mathies *et al.* 2011). Recently however it has been shown by resonance Raman and DFT calculations that in the RC of *Rb. sphaeroides* WT the Car is in a 15,15'-cis configuration (Mathies *et al.* 2011). A quantitative comparison of the yields of triplet formation in wild-type (WT) and R26 with reconstituted Car is yet to be performed. This could give information on how critical the 15,15'-cis configuration of the Car is and thereby on the triplet quenching mechanism.

Solid state photo-CIDNP NMR studies have shown that the asymmetric ET in the bacterial RC is supported by symmetry breaking in the electronic groundstate (Schulten *et al.* 2002; Prakash *et al.* 2007; Alia *et al.* 2009). Although the exact origin has remained unclear, electrostatic interactions within the BChl *a* of the special pair, and conformational tuning of the cofactors by the protein environment are suggested to play an important role in determining the structure and electronic distribution of the special pair (Alia *et al.* 2009; Daviso *et al.* 2009; Ganapathy *et al.* 2009). ^{1}H-^{13}C heteronuclear dipolar correlation studies on [$^{13}C_6$,$^{15}N_3$]-His-labeled bacterial RCs and DFT calculations, indicated that especially the differential charge polarization of the axial histidine, His-L173, which is coordinated to the Mg^{2+} of the P_L BChl *a* cofactor, balances the asymmetry of the special pair for the bacterial RC in its groundstate (Alia *et al.* 2009).

1.1.4 Photosystem II

The PSII complex, which is depicted in Figure 1.4A, is the only protein complex capable of oxidative water splitting. Its biophysical processes have been the subject of many studies using a wide variety of techniques including: spectral hole-burning (Tang *et*

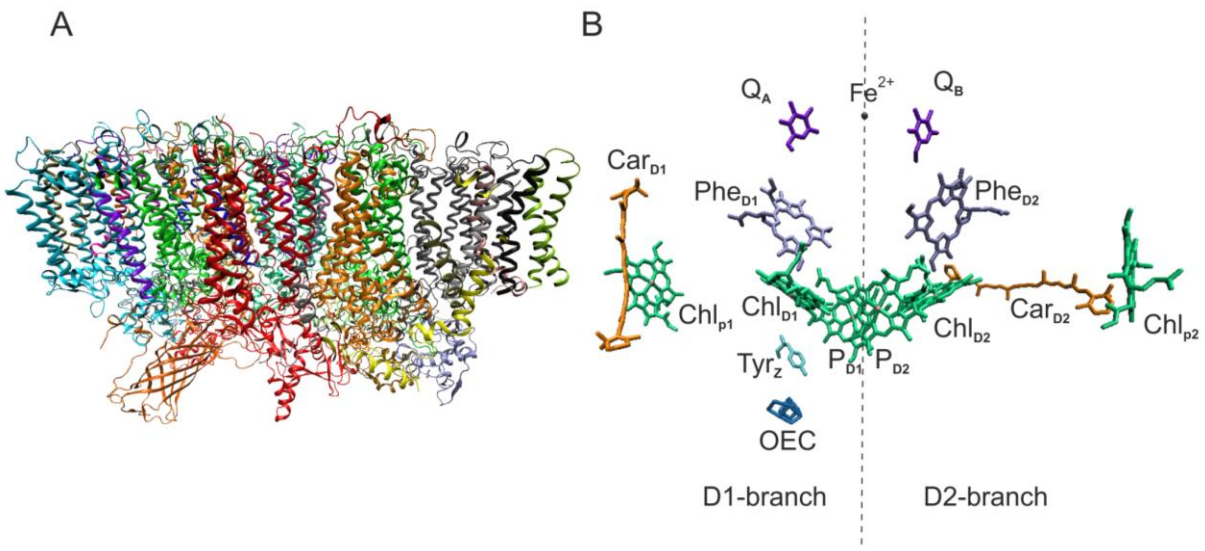

Figure 1.4: (A) The complex arrangement of homodimeric PSII with the polypeptide subunits represented in different colors with a ribbon representation. The D1 and D2 polypeptide subunits surrounding the PSII RC are depicted in orange and green, respectively. (B) The arrangement of cofactors in the PSII RC. The PSII RC consists of two central Chls (P_{D1} and P_{D2}), two accessory Chl *a* (Chl_{D1} and Chl_{D2}), two pheophytins (Phe_{D1} and Phe_{D2}), two Quinone's (Q_A and Q_B), and two peripheral Chl a (Chl_{p1} and Chl_{p2}) The cofactors are arranged in two symmetric branches, an active D1 branch (left) and an inactive D2 branch (right). Two β-carotenoids (Car_{D2} and Car_{D1}) are associated with the PSII core complex. At the P_{D1} donor side a Tyrosine residue Tyr_Z is bridging in ET between the P_{D1} and the Oxygen evolving complex (OEC). [PDB entry 3ARC (Umena *et al.* 2011)]

al. 1990; Tang *et al.* 1991; Jankowiak *et al.* 2003; Zazubovich *et al.* 2003; Riley *et al.* 2004), stark spectroscopy (Frese *et al.* 2003), photon echo (Prokhorenko and Holzwarth 2000), time-resolved-fluorescence (Novoderezhkin *et al.* 2005), visible pump-probe (Groot *et al.* 1997), 2D spectroscopy (Myers *et al.* 2010), photo-CIDNP (Matysik 2000; Diller *et al.* 2005; Diller *et al.* 2007; Diller *et al.* 2007), mutagenesis studies (Alizadeh *et al.* 1995; Diner *et al.* 2001; Wang *et al.* 2002; Schlodder *et al.* 2008) and theoretical calculations (Raszewski *et al.* 2005; Novoderezhkin *et al.* 2007; Raszewski *et al.* 2008; Kitagawa *et al.* 2011). PSII is a multiprotein complex found in higher plants, algae and cyanobacteria. Recently a high resolution X-ray structure of a dimeric PSII core complex from cyanobacteria *Thermococcus vulcanus* has been solved (Umena *et al.* 2011). Based on the available X-ray structures PSII was believed to function predominantly as a homodimer *in vivo*, but recent studies suggested that cyanobacteria might contain monomeric PSII (Zouni *et al.* 2001; Kamiya and Shen 2003; Biesiadka *et al.* 2004; Loll *et al.* 2005). The entire homodimeric PSII supercomplex consists of about 20 subunits, but variations are possible between PSII from different organisms. The PSII monomeric 'core complex' (~350 kDa) includes the PSII RC with the associated RC cofactors and a total of

12 β-carotenes. In addition the PSII core contains two integral antennae proteins CP43 and CP47, the α and β subunits of the cytochrome b559 complex (Cytb559), and a variable number of extrinsic proteins needed for the stabilization of the oxygen evolving complex (OEC) (Bricker *et al.* 2012).

The OEC is the water-oxidizing enzyme which catalyses the splitting of water and is bound to residues of the D1 protein and the integral antennae protein CP43. The OEC core consists of a cluster of four manganese ions, a calcium ion and five oxygens (Mn_4CaO_5), and is surrounded by amino acid chains. It is generally accepted that the OEC can exist in 5 states; S0 to S4, as was first described in 1970 by the Kok model (Kok *et al.* 1970). Many attempts to copy the catalytic power of the OEC by a stable artificial system have been made by either molecular mimicking of the OEC structural and functional features or by constructing artificial photocatalytic systems based on inorganic semiconductor materials and modular molecular assemblies (Boghossian *et al.* 2011; Li and Fan 2011). However, a truly biomimetic catalytic system that matches the performance of photosystem-II for efficient water splitting, operating with four consecutive proton coupled electron transfer steps to generate oxygen and hydrogen for hundred thousands of cycles at high rate is yet to be achieved. Recently a robust mono-iridium complex was presented for electrocatalytic water splitting (Joya *et al.* 2012). This iridium complex had a catalytic turn over number of more than 210 000 and an oxygen generation current densities of over 1.70 mA cm^{-2}. This is an example of a complex that could help to pave the way for photoelectrocatalytic devices with immobilized mono-site molecular complexes for future fuel generation from water splitting.

1.1.4.1 The Photosystem II RC

The PSII RC was first isolated in 1987 by Nanba and Satoh (Nanba and Satoh 1987). Figure 1.4B shows the arrangement of the cofactors inside the PSII RC which, in contrast to the several differences in the composition of the minor subunits of the PSII supercomplex, is highly conserved among different species. The reaction center contains two inner Chl *a* molecules (P_{D1} and P_{D2}, together denoted as P680), two accessory Chls (Chl_{D1} and Chl_{D2}, two pheophytins (Phe_{D1} and Phe_{D2}) and two quinones (Q_A and Q_B) bound to the D1 and D2 polypeptides. The arrangement of the cofactors inside PSII is similar to that known from RCs of purple bacteria, and the high resolution X-ray data

confirmed a homology between the amino acid sequences of the D1 and D2 subunits and their bacterial counterparts L and M (Deisenhofer *et al.* 1985). The P_{D1} and P_{D2} chlorophylls are the structural analogues of P_L and P_M, while the Chl_{D1} and Chl_{D2} and Phe_{D1} and Phe_{D2} correspond to respectively the $BChl_{L,M}$ and $\Phi_{L,M}$ cofactors in bacterial RC.

Two carotenoids, β-carotenes, are associated to the PSII RC with the Car_{D1} at a distance of ~20 Å from the Chl_{D1}, while Car_{D2} is ~13.2 Å away from Chl_{D2} (Loll *et al.* 2005). The bacterial RC on the other hand, contains one spheroidene Car, located within van der Waals distance, d_{vdW} ~3.6 Å, from the accessory $BChl_M$ (Camara-Artigas *et al.* 2002). In the PSII RC the Car cannot be in close proximity to the Chls, since the Car would be oxidized as a consequence of the high redox potential of PSII (Tracewell *et al.* 2011). Hence, efficient Chl triplet quenching by the Dexter mechanism, as is observed in the bacterial RC, is not possible for PSII. The Car in PSII do scavenge singlet oxygen species and transfer electrons to the $P680^{\bullet+}$ in case of over-reduction on the acceptor side (Hanley *et al.* 1999). In the antennae carotenoids protect against over-excitation in a range of mechanisms called "non-photochemical quenching" (NPQ) (Holt *et al.* 2004). Besides their photo-protective role, carotenoids in PSII are essential for the assembly of the D1 and D2 (Herrin *et al.* 1992) and function as light harvesting pigments (Frank and Cogdell 1996).

Only one branch of cofactors, that is the one associated to the D1 protein, is believed to be active in charge separation in PSII, as is also observed in purple bacteria (Trebst 1986). However recent studies suggest the participation of the D2 branch in ET in closed RCs, with Q_A singly reduced and in high light conditions. In this case a photoprotection mechanism involving the participation of the Car of the D2 branch (Car_{D2}) is activated (Martinez-Junza *et al.* 2008). In addition to the four inner Chls discussed above, the isolated D1D2 PSII complex contains two additional loosely coupled peripheral chlorophylls that are not found in bacterial RC (Xiong *et al.* 1998). These Chl's are most probably bound to the exterior of the PSII RC by histidine residues of D1 and D2.

Figure 1.5 A depicts the electron transfer steps occurring inside the PSII RC and the midpoint redox potentials of the involved centers. In PSII systems containing the Q_A secondary electron acceptor, charge separation in the $P_{D1}^{+}Phe_{D1}^{-}$ radical pair is stabilized by the formation of $P_{D1}^{+}Q_A^{-}$. The lifetime of the $P_{D1}^{+}Phe_{D1}^{-}$ radical pair is strongly influenced by the redox state of Q_A ranging from 20 to 250 ns when Q_A is either in the Q_A^{-}

or Q_AH_2 state, respectively, while the P680 triplet (^{3}P680) lifetime increases from 2 µs to 1 ms (van Mieghem *et al.* 1995). From Q_A the electrons are transferred to the more loosely associated quinone Q_B. After taking up two electrons and two protons, Q_B dissociates from the RC as Q_BH_2 and is replaced by a quinone from the surrounding quinone pool. Q_BH_2 delivers the electrons to the cytochrome complex cyt. b_{6f} (Stroebel *et al.* 2003). Through the lumenal space the electrons are subsequently transferred to PSI by the small water-soluble protein named plastocyanin (PC) (Xue *et al.* 1998). In parallel the protons are released to the lumen space, establishing a proton gradient that drives the synthesis of ATP. Upon isolation of the smallest photochemically active PSII complex, namely the ~34kDa D1D2 complex containing only the D1 and D2 proteins, the inner Chl and Phe cofactors remain bound but the OEC as well as Q_B and Q_A are lost (Madjet *et al.* 2009) and ET past the Phe_{D1} acceptor is blocked. This causes a long donor triplet state, as is also observed upon double reduction of Q_A by chemical treatment (Hillmann *et al.* 1995; van Mieghem *et al.* 1995).

1.1.4.2 The electronic structure of the PSII electron donor

The electronic coupling between the two inner chlorophylls P_{D1} and P_{D2} in PSII is much less than for the primary electron donor in the bacterial RC that is also known as the special pair. While the average coupling between the bacterial special pair and the other cofactors is 100 cm^{-1}, the electronic coupling between P_M and P_L is in the range of 500 to 1000 cm^{-1} due to an almost perfect overlap of ring I of P_L with ring I of P_M (Woodbury and Allen 1995). Because of their strong coupling both BChls carry electron spin density (with 68 ± 4 % of the electron density being located on P_L (Daviso 2008)). In contrast, P_{D1} and P_{D2} show a different geometry with P_{D2} being rotated in the plane of the ring I with respect to P_{D1}, causing a dramatic decrease in overlap (Madjet *et al.* 2009; Umena *et al.* 2011). The maximum electronic coupling between P_{D1} and P_{D2} is therefore estimated between 85 cm^{-1} and 150 cm^{-1} (Tetenkin *et al.* 1989; Braun *et al.* 1990; van Kan *et al.* 1990). This renders the inner chlorophyll pair far less ‘special’ among the other cofactors than for the special pair in the bacterial RC, based on their electronic coupling. The individual couplings of P_{D1} and P_{D2} with the accessory Chls and Phe’s are in the range of 50 cm^{-1} (Cardona *et al.* 2012). Whether the PSII donor should be considered monomeric, dimeric or even multimeric, including all six central pigments, is still under discussion. It is

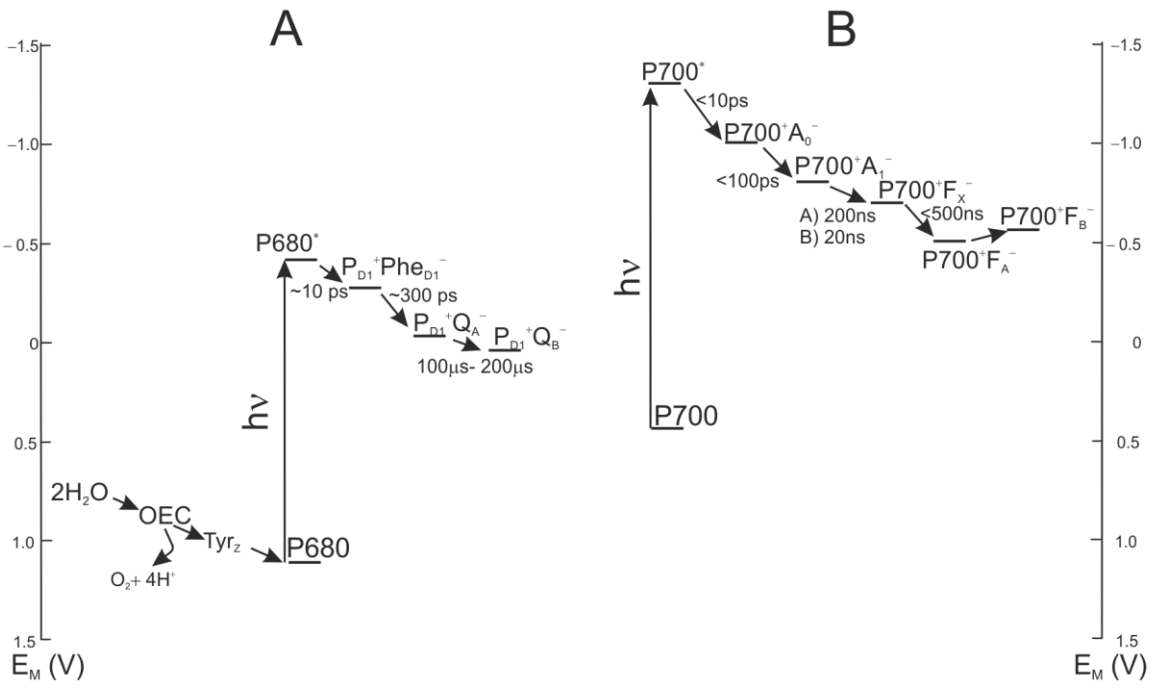

Figure 1.5: Midpoint redox potentials of the components involved in linear electron transfer in PSII (A) and PSI (B) with the rates of forward electron transfer (schematic). Adapted from (Cardona *et al.* 2012; Muh *et al.* 2012, Golbeck 2004). (A) The capacity to generate a potential up to +1.2V (van Gorkom and Schelvis 1993) renders the P680 in PSII capable to extract an electron from a neighboring tyrosine residue. This Tyr_Z amino acid side chain in PSII functions as a bridge between the OEC and P680. The highly reactive tyrosine radical, which is formed upon reduction of $P680^{\bullet+}$, is capable of fully oxidizing the OEC. After 4 successive oxidation steps and the release of 4 protons, two water molecules are split and one oxygen molecule is released by the active site of the OEC (Gorkom and Schelvis 1993; Najafpour and Govindjee 2011). (B) Midpoint redox potentials of centers involved in linear electron transfer in PSI with the rates of forward electron transfer. After excitation of the heterodimer P700, fast ET to the Chl *a* acceptor (A_0) occurs. From A_0 the charge separation is further stabilized by ET to the quinone acceptor A_1 and the three iron-sulphur, [4Fe-3S], clusters F_X, F_A, F_B that function as terminal intrinsic electron acceptors. Adapted from Golbeck 2004.

becoming generally accepted that $P_{D1}P_{D2}$ forms a loosely coupled pair, for which the coupling is unique, both in character and in strength, among the other interactions between the pigments of PSII (Durrant *et al.* 1995; Barter and Klug 2005; Raszewski *et al.* 2008). In this work $P_{D1}P_{D2}$ will be denoted as P680. Due to differences in the direct environment of the two Chl's, most of the dimer HOMO is located on P_{D1} (Nilsson Lill 2011). The cationic state is predominantly located on the P_{D1}, with a $P_{D1}^{\bullet+}/P_{D2}^{\bullet+}$ ratio of ~80:20 (Rigby *et al.* 1994; Diner *et al.* 2001). One reason for this strong asymmetry is the recent finding that if a one electron oxidation is considered, the redox potential of P_{D1} is lower than for P_{D2}, thus favoring the location of the cationic charge on P_{D1} (Saito *et al.* 2012).

PSII can generate a potential up to +1.2V (Gorkom and Schelvis 1993) which is much higher than the potential of 0.5V observed for the special pair electron donor P840 of bacterial photosynthetic RCs (Lin *et al.* 1994). This makes the oxidized electron donor

of PSII, $P680^{\bullet+}$, the strongest oxidizing agent known in nature. Factors that contribute to the high redox potential include;

- differences in the intrinsic electronic and structural properties between Chl *a* and BChl *a* leading to an +160 mV increase (Fajer *et al.* 1975),
- the cation being mainly located on P_{D1} generating a higher charge localization (+140 mV) (Takahashi *et al.* 2008) and asymmetry in the electron spin density (ρ_i) distribution (Diller *et al.* 2005),
- several electrostatic effects with, according to calculations, the highest increase resulting from;
    I. the close proximity of the OEC,
    II. the accumulated effect of the dipoles from the protein backbone and
    III. the atomic charges on the peripheral proteins surrounding the D1/D2 proteins (Ishikita *et al.* 2006).

In addition theoretical calculations suggest an increase (-135 mV) in the oxidative power of P680 due to the amino acid side chains surrounding P_{D1} (Ishikita *et al.* 2006). Previous photo-CIDNP studies on isolated D1D2 particles of spinach suggested a hinge model of the PSII donor involving the axial histidine, His-198, to explain the stabilization of the HOMO on P_{D1} and subsequent increase in the redox potential (Diller *et al.* 2007).

To summarise, the stronger oxidising nature of the cation of PSII opposed to the bacterial RC cation, is in addition to the molecular differences between Chl *a* and BChl *a*, in part due to structural differences, with PSII providing a chlorophyll monomer in a large multiprotein complex that is in the right position to experience a large effect from the backbone dipoles from the trans-membrane helices. This inference fits to the idea that PSII has evolved from a large homodimeric chlorophyll containing a Type I reaction centre ancestor, rather than from the small purple bacterial-type reaction centre (Rutherford and Nitschke 1996, Rutherford and Faller 2003).

Due to the strong overlap of the absorption spectra of the six central pigments in the PSII RC (P_{D1}, P_{D2}, Chl_{D1} and Chl_{D2}, Phe_{D1} and Phe_{D2}), the excitation energy is initially not localized on a single cofactor (Raszewski *et al.* 2008; Shibata *et al.* 2013). Transient absorption experiments on isolated PSII preparations from spinach indicated the existence of two different pathways for ultrafast charge separation with either the P680 or the

accessory Chl_{D1} pigment acting as the primary electron donor at 77 K (Romero *et al.* 2010 and 2012). The latter option results in the formation of the charge separated state $Chl_{D1}^{+}Phe_{D1}^{-}$ prior to the more stable $P680^{+}Phe_{D1}^{-}$ radical pair. In these first picosecond after light absorption even the $P_{D1}^{+}P_{D2}^{-}$ radical pair can occur (Novoderezhkin *et al.* 2011). In contrast to the highly delocalized excited state, the triplet appears to be highly localized on a single Chl (Saito *et al.* 2011). At low temperatures this is the accessory Chl_{D1}, while at higher temperatures, towards physiological conditions, the location of the triplet alternates between Chl_{D1} and P_{D1} (van Mieghem *et al.* 1991; Raszewski *et al.* 2005).

Recently it has been suggested by Acharya *et al.* that isolating the D1D2 complex from its natural environment, (*i.e.* the PSII core complex and surrounding thylakoid membrane), could destabilize the PSII RC and affect the electronic structure of the P680 donor (Acharya *et al.* 2012). Indeed the PSII RC is known to be considerably more fragile upon isolation and interrogation procedures in comparison to PSI and the bacterial RC (Seibert 1993; Cox *et al.* 2010). Detergents commonly used in D1D2 preparations, such as Triton X-100, appear to affect the electron transfer from the Chl_{D1} to the Phe_{D1} acceptor (Tang *et al.* 1991). In addition it was suggested that isolation of the D1D2 PSII RC affects the P680 donor (Hillmann and Schlodder 1995; Riley *et al.* 2004) and leads to a weakening of the coupling between the P_{D1} and P_{D2} cofactors (Acharya *et al.* 2012). These findings question if the isolated D1D2 complex could be used as a proper model for the PSII RC in intact systems.

1.1.5 Photosystem I

In the process of oxygenic photosynthesis electrons flow from PSII to PSI, while the nomenclature follows the order in which the photosystems have been discovered (Emerson and Chalmers 1958; Govindjee and Rabinowitch 1960). The X-ray structure of PSI has been solved in the prokaryotic system of cyanobacteria *Thermosynechococcus elongatus* with 2.5 Å resolution as a trimeric supercomplex, which is depicted in Figure 1.6A (Jordan *et al.* 2001). In the eucaryotic plant system of *Pisum sativum* (Pea) the PSI-LHCI complex has been resolved up to 3.4 Å resolution (Ben-Shem *et al.* 2003). The cyanobacterial PSI core complex consists of 12 subunits containing a total of 96 chlorophylls, while the corresponding plant complex consists of at least 17 subunits harboring over 170 Chls. In cyanobacteria the PSI is mostly observed as a trimer of

monomeric PSI cores (Kruip *et al.* 1994; Fromme *et al.* 2001) while PSI in plants, red algae and green algae is monomeric (Scheller *et al.* 2001; Jensen *et al.* 2003; Kouril *et al.* 2005). Two functional moieties can be distinguished in the PSI supercomplex: the photosystem I core, including the redox active cofactors, and the peripheral light-harvesting complex (LHCI), which serves to increase the light absorption capacity (Schmid *et al.* 1997; Amunts *et al.* 2010). While the structural organization of the redox centers is virtually identical in the structures obtained from Pea and *Thermosynechococcus elongates* (Jordan *et al.* 2001; Amunts *et al.* 2007), the LHCI complex shows a high degree of variability in size, subunit composition and bound pigments. This variation allows each organism to adjust to its specific natural habitat (Boekema *et al.* 2001; Croce *et al.* 2007; Wientjes *et al.* 2009). The PSI core complex is sometimes also denoted as PSI-110 particle referring roughly to the total number (~110) of bound Chls (Mullet *et al.* 1980), and has a molecular weight of ~300 kDa.

1.1.5.1 The Photosystem I reaction center

Figure 1.6B shows the arrangement of the cofactors inside the PSI RC. As in PSII and the bacterial RC, the cofactors in PSI are symmetrically arranged in two parallel chains relative to a pseudo-C_2 symmetry axis perpendicular to the membrane plane in which PSI is embedded in *vivo.* Like Type I bacterial RCs, PSI consists of six chlorophyll molecules, two quinones, and three iron-sulphur [4Fe-3S] clusters (F_X, F_A, F_B), which function as terminal intrinsic electron acceptors. The F_A and F_B clusters operate in series, and are bound by the PsaC subunit. The F_X cluster is located at the interface of the PsaA/PsaB subunits, while the accessory Chls (A_{-1A} and A_{-1B}), the Chl acceptors (A_{0A} and A_{0B}), and the quinone acceptors (A_{1A} and A_{1B}) are bound to either the PsaA (A-branch) or PsaB (B-branch). In comparison to their PSII quinone counterparts, A_{1A} and A_{1B} in PSI are more tightly associated with the protein backbone and not as readily accessible for chemical reducing agents (Srinivasan *et al.* 2009). With distances ranging between 15 and 40 Å, the cofactors in the PSI RC are relatively isolated from the surrounding antenna pigments compared to their PSII and bacterial RC counterparts. The core antenna consists of ~100 tightly packed Chls and 20 β-carotene molecules (Fromme *et al.* 2001).

In addition, the PSI RC contains the heterodimer P700 that consists of one Chl *a* (P_B) and one Chl *a′* (P_A), which is the 13^2-epimer of Chl *a*. Similar to the F_X cluster, P700

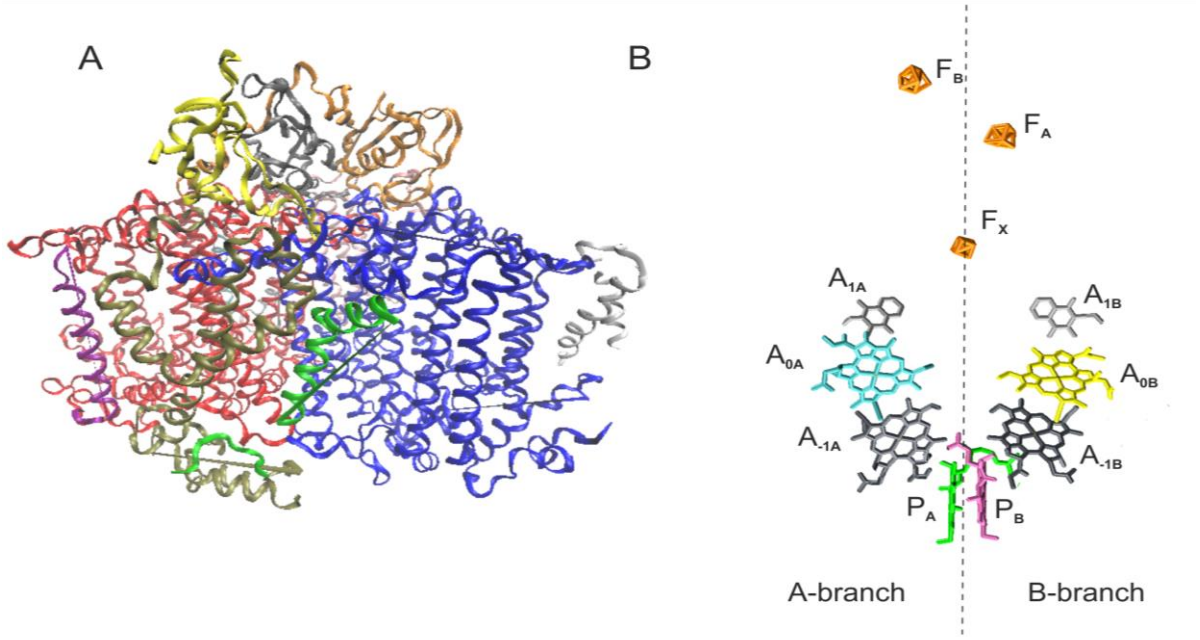

Figure 1.6: (A) The complex arrangement of the trimeric PSI supercomplex with the polypeptide subunits represented in different colors with a ribbon representation. (B) The arrangement of cofactors in the PSI RC. Depicted in pink and green are the two central Chls, P_B and P_A of the Chl *a*/Chl *a'* dimer. In addition the RC contains two accessory Chl *a* (A_{-1A} and A_{-1B}), two donor Chl *a* (A_{0B} and A_{0A}), and two tightly associated phylloquinone's (A_{1A} and A_{1B}). Finally there are three iron-sulphur [4Fe-3S] clusters (F_X, F_A, F_B) which function as terminal intrinsic electron acceptors. Both the A and B branch participate in electron transfer with the relative activity depending mainly on the organism and the reduction conditions. [PDB entry 2WSC (Jordan *et al.* 2001).

is located at the interface of the two branches. While the P_A forms hydrogen bonds to its protein environment, no hydrogen bonds are found on the P_B side (Watanabe *et al.* 1985). The ratio of the spin-density distribution over the P_A/P_B dimer shows strong differences among different species and conditions (Webber and Lubitz 2001): Fourier transform infrared spectroscopy and EPR studies on PSI from *Synechocystis* sp. PCC 6803 cyanobacteria indicated a ratio in the range of 50:50 - 33:67 in favor of the P_B (Breton *et al.* 1999). On the other hand, in spinach and *Thermosynechococcus elongatus* (*T. elongatus*) ratios in the range of respectively 25:75–20:80 and 15:85 have been estimated (Davis *et al.* 1993; Käss *et al.* 2001). Recent theoretical calculations suggested a ratio of 27.9:72.1 based on the coordinates taken from the high resolution X-ray data of *T. elongatus* (Saito and Ishikita 2011). The hydrogen bond of the P_A Chl, the asymmetry in molecular geometry (Chl *a*/Chl *a'*) and minor differences in the protein environment were indicated to be the strongest influences on the relative spin density distribution over P_A and P_B. While P680 in PSII is the strongest oxidizing agent known in nature, P700 is optimized to provide a strong reducing potential. With a potential of approximately -1.2 V,

$P700^{\bullet+}$ is probably the most reducing compound found in natural systems (Ishikita *et al.* 2006).

1.1.5.2 Functional heterogeneity of the Photosystem I RC

Over the past decade intensive investigations of the electron transfer reactions have revealed some unique characteristics of PSI. After the initial suggestions made in 1993 and 1995 by Brettel, Golbeck, Setif and co-workers (Setif and Brettel 1993; Brettel and Golbeck 1995), evidence has been accumulated that, whereas in PSII and bacterial RC the ET proceeds down only one of the cofactor branches, in PSI both branches participate in ET. This process is generally referred to as a 'bidirectional ET' (see for review; (Santabarbara *et al.* 2010)).

Figure 1.5 B (see page 24) depicts the electron transfer steps that occur during linear ET in the PSI RC, and the midpoint redox potentials of the involved centers. Initially it was thought that the electron arriving in PSI was absorbed by the P700 donor, but recent kinetic studies by flash absorption-spectroscopy have questioned if P700 can be rightfully appointed as the primary donor (Holzwarth *et al.* 2006; Müller *et al.* 2010). These studies indicated the accessory chlorophyll A_{-1} as the primary electron donor, resulting in the formation of the radical pair $A_{-1}^{\bullet+}A_0^{\bullet-}$ (with a lifetime of <18 ps) prior to the formation of $P700^{\bullet+}$ $A_0^{\bullet-}$. The identification of the accessory Chl A_{-1} as the primary electron donor in PSI discarded the structural asymmetry of the P700 Chl *a*/Chl *a*' heterodimer as a valid argument against the participation of both branches in ET. A possible explanation for the presence of bidirectional ET in PSI could be the function of the PSI phylloquinone A_1: In Type II RCs (*e.g.* PSII and bacterial RC) the Q_A functions as a 'two electron gate', with a mobile quinone on the inactive branch (Q_B) being used as a terminal acceptor (Müh *et al.* 2012). The quinones present in PSI on the other hand function as single electron carriers facilitating electron transfer to the F_X iron-sulfur cluster. The fact that the quinones of the two branches in PSI function independent of each other, and serve only as intermediates in electron transfer, supports the feasibility of bidirectional ET.

In data obtained from transient optical studies (Holzwarth *et al.* 2006; Müller *et al.* 2010), but also by transient EPR studies (Guergova-Kuras *et al.* 2001), a biphasic forward electron transfers from P700 to A_1 and from A_1 to F_X has been observed. The biphasic

kinetics indicated the presence of two different lifetimes of ~250 and ~20 ns that have been assigned to the oxidation of the quinones A_{1A} and A_{1B}, respectively. The latter was concluded based on site-directed mutagenesis studies showing an increase in the 'slow' 250 ns phase by mutations of residues involved in the coordination of A_{1A}, whereas mutations near A_{1B} influenced the 20 ns phase (Brettel 1997; Joliot and Joliot 1999). Mutations targeting the axial ligands of the A_0 Chl acceptors further confirmed the assignment of the 'fast' phase to the B branch (Guergova-Kuras *et al.* 2001).

The relative activity of the two branches is usually in favor of the A-branch, but seems to vary strongly among different organisms ranging from ~3:2 in green algae (Holzwarth *et al.* 2006; Li *et al.* 2006) to ~3-4 : 1 in cyanobacteria (Ramesh *et al.* 2004; Dashdorj *et al.* 2005). The nature of the strong asymmetry regarding the electron transfer rates to F_X via A_{1A} or A_{1B}, with ET from A_{1B} to F_X occurring 10 times faster than the corresponding ET step on the dominant A branch, is still under discussion. A possible explanation could be the differences in the orientation of A_{1A} and A_{1B} in their respective protein pockets, facilitating a strong H-bond between the A_{1A} cofactor and the protein backbone, which is absent on the A_{1B} side (Berthold *et al.* 2012). Another explanation is the effect of the relative redox potentials of the A and B side phylloquinones on the transfer rate as is described by Marcus theory (Ptushenko *et al.* 2008). Past the phylloquinones cofactors the two branches merge in the F_X cluster from where electrons are passed via the F_A and F_B clusters to ferredoxin in 500 ns, driving ultimately the formation of NADPH by Ferredoxin-NADP reductase (FNR, see Figure 1.1 on page 14).

While consensus on the bidirectional nature of ET in both prokaryotic and eukaryotic PSI has been reached (Fairclough *et al.* 2003; Cohen *et al.* 2004; Redding *et al.* 2007), the molecular details of the mechanism have not yet been elucidated (Berthold *et al.* 2012). Since the first observations of the biphasic nature of the A_1^- oxidation were obtained from isolated PSI particles (Setif and Brettel 1993; Brettel and Golbeck 1995), the presence of the 'fast' lifetime was initially suggested to result from purification artifacts. Although the conservation of the biphasic nature in whole cells of green algae (Joliot and Joliot 1999) ruled out this possibility, the isolation level and subsequent presence of detergents did seem to influence the relative branch activity (Brettel and Golbeck 1995). In addition the oxidation state of the quinones seems to affect the relative branch activity with *e.g.* ET in *Synechococcus lividus* occurring solemnly along the B branch at low temperature (100K) and strong reducing conditions (Poluektov *et al.* 2005).

Thus the mechanistic nature of bidirectional electron transfer in PSI across different species and sample preparation remains unresolved.

1.2 PHOTO-CIDNP

1.2.1 The Solid State Photo-CIDNP effect

Nuclear spin hyperpolarization, *i.e*. the creation of large, non-equilibrium population differences between nuclear spin states, allows for a significant enhancement of signal intensities in NMR experiments. This signal increase is crucial for NMR investigations where sensitivity represents a limiting factor, such as the characterization of large (bio)molecular systems as photosystems. Similar to other hyperpolarization methods, including spin-exchange optical pumping and dynamic nuclear polarization (DNP), photochemically induced dynamic nuclear polarization (photo-CIDNP) realizes this process via a polarization transfer from electron spins to nuclear spins.

Photo-CIDNP is a well-known phenomenon in liquid NMR. In the liquid state it was discovered in 1967 and explained by the radical pair mechanism (RPM) (for review see: Bargon and Fischer 1967; Ward and Lawler 1967; Cocivera 1968; Closs and Closs 1969; Kaptein and Oosterhoff 1969; Hore and Broadhurst 1993; Roth 1996; Goez 1997). In 1994, Zysmilich and McDermott observed the photo-CIDNP effects in solids for the first time in frozen and quinone-blocked RCs of purple bacteria of *Rb. sphaeroides* R26 by ^{15}N magic-angle spinning NMR (Zysmilich and McDermott 1994). Since the RPM depends also on diffusion, it could not provide the complete explanation for the solid-state photo-CIDNP. Meanwhile much progress has been made in resolving the spin-chemical mechanisms of the solid-state photo-CIDNP effect (for reviews see: (Jeschke and Matysik 2003; Roy *et al.* 2007), and in particular for RCs of *Rb. sphaeroides* it is now well understood and will be discussed in more detail in section 1.2.2 (Daviso *et al.* 2009).

Up to this point the solid-state photo-CIDNP effect has been observed in a wide variety of photosynthetic RCs; purple bacteria *Rb. sphaeroides* WT (Prakash *et al.* 2005), its Car lacking mutant R26 (Prakash *et al.* 2006), *Rhodopseudomonas acidophila* (Diller *et al.* 2008), *Heliobacillus mobilis* (Roy *et al.* 2008; Thamarath *et al.* 2012), green sulfur bacteria *Chlorobium tepidum* (Roy *et al.* 2007), and isolated higher plant photosystems I and II from *Spinacias oleracea* (Matysik 2000; Alia *et al.* 2004; Diller *et al.* 2007; Diller *et al.* 2007). The detection of the effect across a range of otherwise rather different

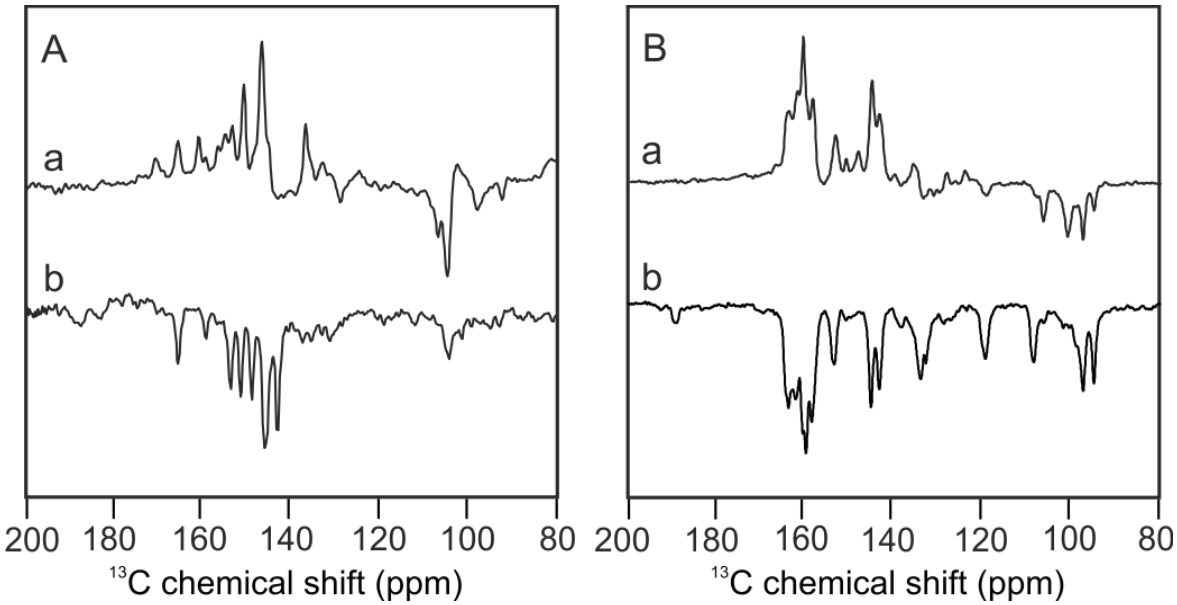

Figure 1.7: ^{13}C photo-CIDNP MAS NMR spectra collected from (A) isolated D1D2 (a) and PSI-110 (b) from spinach and (B) RCs of *Rb. sphaeroides* R26 (a) and WT (b). The data were obtained by continuous illumination with white light at 223 K. The sign pattern of the photo-CIDNP spectrum obtained from PSII (A,a) is similar to the sign pattern observed for the R26 mutant (B,a), due to the relatively long triplet lifetimes (~1ms and 100 µs, respectively, opposed to 10 µs in *Rb. sphaeroides* WT). The similarity between the sign patterns observed in PSI and *Rb. sphaeroides* WT is less straightforward and will be further discussed in Chapter 5.

photosynthetic RCs suggests that the occurrence of photo-CIDNP is related to an optimization of the first ET step and may thus be a guide for the improvement of artificial systems.

Photo-CIDNP has been observed for intact bacterial RC-LH core complexes embedded in the chromatophore membrane of selectively ^{13}C isotope labeled whole cells of purple bacteria (Prakash *et al.* 2003). Addition of detergent, causing dissociation of the bacterial RC-LH complexes from the membrane, resulted in a dramatic decrease in the intensity of the light induced signals. The pronounced differences between intact membrane-bound and detergent solubilized bacterial RC-LH complexes were tentatively explained by the loss of self-orientation upon solubilization. Photo-CIDNP MAS NMR studies of whole cells of heliobacteria (*Heliobacillus mobilis*) (Thamarath *et al.* 2012) indicated the occurrence of symmetric electron transfer via both branches of cofactors in this organism.

^{13}C-Photo-CIDNP experiments on PSII and PSI were restricted to isolated PSII D1D2 and PSI-110 complexes due to the difficulty to incorporate selective labels in plants. Previous experiments on isolated natural abundance samples of PSII and PSI

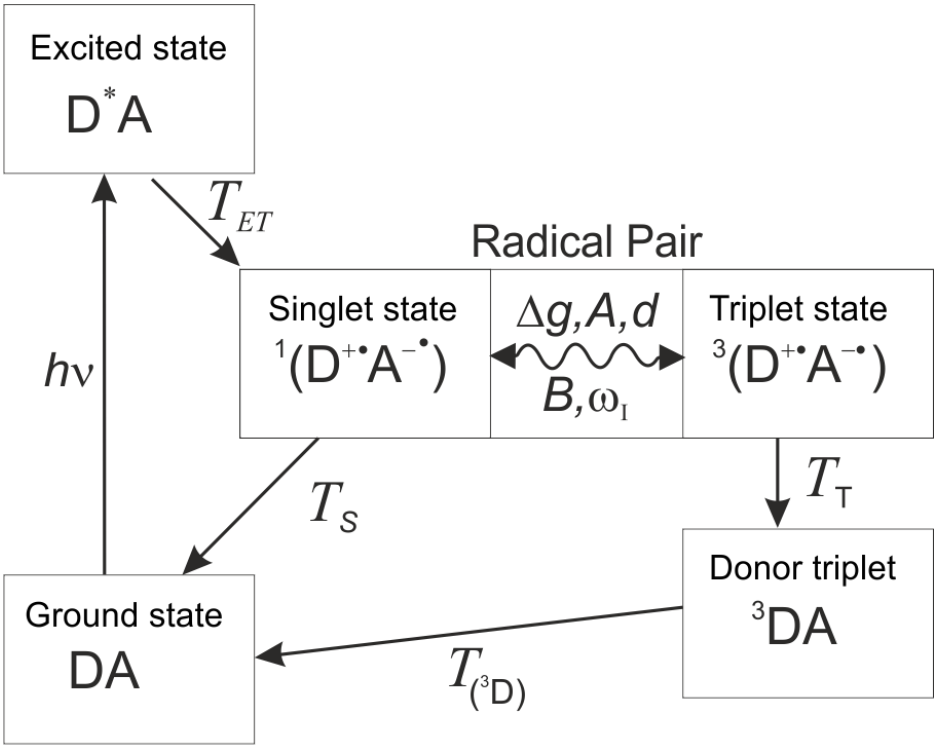

Figure 1.8: Schematic representation of the photocycle in photosynthetic RCs. After absorption of a photon, electron transfer occurs from the donor (D), (*e.g.* P_MP_L in purple bacteria, P_{D1} in PSII or P_B in PSI), to the primary acceptor (A), (*e.g.* Φ_L in purple bacteria, Phe_{D1} in PSII and A_0 in PSI). The initial excited state D*A is followed by electron transfer to form the correlated radical pair in its non-stationary singlet state. The radical pair can decay via its singlet state $^1(D^{+\bullet}A^{-\bullet})$ or convert its electronic zero quantum coherence into double quantum coherence in the triplet state $^3(D^{+\bullet}A^{-\bullet})$ by coherent electron-nuclear spin evolution. This TSM process depends on the difference of the *g* value between the two electrons, Δg, the secular part of the hyperfine interaction, *A*, the coupling between the two electrons, *d*, the pseudo-secular hyperfine coupling, *B*, and the nuclear Zeeman frequency, ω_I. The triplet state can decay back to the ground state via the triplet donor state, ^{3}DA.

rendered spectra with different sign patterns (Figure 1.7). Spectra obtained from isolated PSI showed only emissive signals, as has also been observed in spectra obtained from *Rb. sphaeroides* WT. Isolated PSII D1D2 on the other hand provided a spectrum with both emissive and absorptive signals in a pattern similar to those observed from the R26 mutant of *Rb sphaeroides*. This similarity is in line with a long distance (20 Å) of the P_{D1} donor to the Car in PSII and correspondingly slow triplet quenching for the P_{D1} donor (Matysik 2000; Diller *et al.* 2005). The signal doubling observed in spectra obtained from *Rb sphaeroides*, indicating a dimeric donor, is absent for both PSII and PSI.

1.2.2 The Mechanism of Solid State Photo-CIDNP

Based on experimental data from *Rb. sphaeroides* and corresponding computational work, the mechanism of photo-CIDNP in bacteria has been well established

(Daviso *et al.* 2009). Figure 1.8 depicts the photocycle occurring in photosynthetic RCs and the radical pairs produced upon illumination are shown. Initially, the spin-correlated radical pair is formed in a pure singlet state and and has, therefore, a high electron spin order. Three different mechanisms, which run in parallel, build up photo-CIDNP under continuous illumination; electron-electron-nuclear three-spin mixing (TSM), differential decay (DD) and differential relaxation (DR).

Electron-electron-nuclear three-spin mixing (TSM) breaks the antisymmetry of the population of the nuclear states by coherent spin evolution in the correlated radical pair and depends on the signs of the electron-electron and of the electron nuclear interactions (Jeschke 1997; 1998). The symmetry breaking is driven by the off-diagonal, pseudosecular, part of the hyperfine interaction. The contribution of TSM through spin mixing is maximized when the difference of the electron Zeeman frequencies ($\Delta\Omega$), the nuclear Zeeman frequency (ω_I), and the secular part of the hyperfine interaction (A) match. This is reflected in the double matching condition: $2|\Delta\Omega| = 2|\omega_I| = 2|A|$.

In the differential decay (DD) mechanism (Polenova and McDermott 1999), the symmetry between the two decay channels is broken by the different lifetimes of the singlet and triplet state and by the pseudosecular part of the hyperfine interaction. The result is an additional imbalance between the fractions of nuclei in spin-up and spin-down states in the two decay channels. To maximize the symmetry breaking caused by the DD mechanism only a single matching of interactions, that is $2|\omega_I| = 2|A|$, is required and the difference of the singlet and triplet radical pair lifetimes should be of the order of the inverse hyperfine coupling.

In samples of RCs with a long lifetime of the triplet donor (^{3}P), such as in RCs of the R26 mutant of *Rb. sphaeroides* which lack the carotenoid, a third mechanism creating nuclear polarization may occur in addition to the two polarization transfer mechanisms TSM and DD. In this differential relaxation (DR) mechanism, which is called 'Cyclic reactions' in the liquid-CIDNP language, the breaking of antisymmetry of the polarization in the singlet and triplet branches occurs in a non-coherent way. The enhanced relaxation of nuclear spins in the proximity of the high-spin donor partially cancels the nuclear polarization in the donor cofactor. Hence, when the ^{3}P lifetime is comparable to or exceeds the paramagnetically enhanced longitudinal relaxation time, net polarization occurs due to partial extinction of nuclear polarization of the triplet state of the radical pair (Goldstein and Boxer 1987; McDermott *et al.* 1998). A strong contribution of the DR mechanism is also observed in PSII (spectrum 1.7Aa, page 30) where the long distance

between the Car and P680 causes a long-lived triplet (^{3}P680) and subsequent buildup of nuclear polarization by DR. The similarity of the signal pattern of the spectrum obtained from PSI (spectrum 1.7Ab) to that obtained from WT *Rb. sphaeroides* (spectrum 1.7Bb) suggests the absence of DR contribution in these samples.

1.3 SCOPE OF THIS THESIS

In this thesis the advantages of photo-CIDNP MAS NMR in combination with isotope labeling are demonstrated. The main aim is to show how the combination of photo-CIDNP signal enhancement with the increased selectivity and sensitivity obtained by isotope labeling, can be applied to study the electronic structure of the electron donor in PSI and PSII RCs with atomic resolution, even directly in intact systems. In this way pending questions can be addressed regarding: 1) The conservation of the photo-CIDNP effect in whole cells of cyanobacteria. 2) The conservation of the electronic ground state of the PSI electron donor and its functional heterogeneity in different plant species and under different sample conditions. 3) The conservation of the electronic structure of the P_{D1} electron donor upon PSII isolation. In addition to the obtained refinements in the photo-CIDNP signal assignments and the application of time-resolved photo-CIDNP to plant systems, a model for the mechanism of photo-CIDNP buildup in intact PSII systems that contain the OEC is constructed and the mechanism of photo-CIDNP buildup in PSI is discussed (Chapter 4).

Photo-CIDNP has been observed for selectively ^{13}C isotope labeled whole cells of purple- and heliobacteria (Prakash *et al.* 2003; Thamarath *et al.* 2012), while previous attempts to selectively label plants failed, limiting photo-CIDNP studies of PSII and PSI to the fully isolated systems, namely PSII D1D2 complexes and PSI-110 particles (Matysik 2000; Alia *et al.* 2004; Diller *et al.* 2005).

In **chapter 2** photo-CIDNP ^{13}C MAS NMR data of PSI obtained directly from selective ^{13}C- isotope labeled whole cells of cyanobacteria *Synechocystis* sp. PCC 6803 are presented, showing photo-CIDNP signals from cyanobacterial PSI in its natural membrane environment. In the growing list of natural RCs proven to show the solid-state photo-CIDNP effect, RCs of cyanobacteria (blue-green algae) remained to be a blank spot. Cyanobacteria are model microorganisms for the study of plant photosynthesis having a photosynthetic apparatus very similar to the one found in plants while being suitable for mutagenesis studies.

Chapter 3 adresses the question whether variations associated with different organisms affect P700 with its highly optimized redox properties. Data obtained from ^{15}N-labeled PSI-110 particles from spinach and duckweed are presented in order to compare these two organisms. The data demonstrate that the ratio of activity of both branches is modified between different species.

In **chapter 4** data of selectively ^{13}C labeled duckweed at different stages of isolation are presented, all the way from isolated D1D2 particles to entire plants. The main question addressed in this chapter is whether the electronic structure of the non-stationary correlated radical pair state observed in the isolated D1D2 complex is different compared to the electronic structure observed in intact RC in the PSII core in higher preparations. In addition we will compare the electronic structure of the PSII electron donor in spinach and duckweed.

In **chapter 5** the first time-resolved photo-CIDNP data sets obtained from plant photosystems will be presented. It includes a discussion of the results obtained upon applying ns laser flash photo-CIDNP MAS NMR to uniformly ^{15}N and selectively ^{13}C labeled PSI and natural abundance D1D2 PSII complex and compares the experimental data with theoretical calculations.

Chapter 6 provides an outlook on future applications of photo-CIDNP to selectively labeled PSII and PSI. In addition the apparent strong field dependence of PSI photo-CIDNP will be discussed and illustrated by prelimenairy results obtained by ^{13}C photo-CIDNP MAS NMR data obtained from selectively ^{13}C labeled PSI-110 particles of duckweed. Finally it includes the first results obtained from selectively ^{15}N-ALA labeled PSII.

Chapter 2

Observation of the solid-state photo-CIDNP effect in whole cells of cyanobacteria *Synechocystis* sp. PCC 6803

Cyanobacteria, also known as blue green algae, are widely used as model organisms for oxygenic photosynthesis since they represent the simplest photosynthetic organisms containing both PSI and PSII. In this chapter the first photo-CIDNP observed in whole cells of the cyanobacterium *Synechocystis* sp. PCC 6803 is presented. Photo-CIDNP ^{13}C MAS NMR is a powerful tool for understanding the photosynthesis machinery at the cofactor level with atomic selectivity. Combined with selective isotope enrichment, this technique has now opened the door to the study of primary charge separation in whole living cells. This implies that photo-CIDNP MAS NMR studies on oxygenic photosystems are no longer limited to isolated plant photosystems. The results show that the solid-state photo-CIDNP effect is highly conserved in photosynthetic systems as proposed earlier (Matysik *et al.* 2009). In addition, the photo-CIDNP features of PSI and PSII appear to be very similar in plant and cyanobacterial systems, suggesting remarkable conservation of the electronic properties of their photochemical machineries.

The content of this chapter has been published in *Photosynthesis Research* (2010) 104: 275-282

2.1 INTRODUCTION

Natural photosynthesis in plants, algae and several types of bacteria, is initiated by highly efficient light-induced electron transfer, occurring in reaction center (RC) proteins and having a quantum yield close to unity. It has been proposed that this remarkable efficiency is related to the occurrence of correlated radical pairs (Thurnauer and Norris 1980) and the solid-state photo-CIDNP effect (Matysik *et al.* 2009).

Photochemical induced dynamic nuclear polarization (photo-CIDNP) is a well-known phenomenon in liquid NMR (for review see: Hore and Broadhurst 1993; Roth 1996; Goez 1997). It was discovered in 1967 and explained by the radical pair mechanism (RPM) (Bargon and Fischer 1967; Ward and Lawler 1967; Cocivera 1968; Closs and Closs 1969; Kaptein and Oosterhoff 1969). In 1994, Zysmilich and McDermott observed for the first time this new type of photo-CIDNP in frozen and quinone-blocked RCs of purple bacteria *Rb. sphaeroides* R26 by ^{15}N magic-angle spinning NMR (Zysmilich and McDermott 1994). Meanwhile, the exact spin-chemical mechanism of the solid-state photo-CIDNP effect (for reviews see Jeschke 1997; Jeschke and Matysik 2003) in *Rb. sphaeroides* is understood (Daviso *et al.* 2009). Initially, the spin-correlated radical pair is formed in a pure singlet state (Figure 1.8, chapter 1, page 31) and it is, therefore, highly electron correlated. Three mechanisms occur to build up photo-CIDNP under continuous illumination, which run in parallel. In all mechanisms the breaking of the balance of the opposite nuclear spin populations in the two decay branches of the radical pair states leads to *net* steady-state nuclear polarization, which is detected in the NMR experiment: (I) Electron-electron-nuclear three-spin mixing (TSM) breaks the balance of the two radical-pair decay channels by coherent spin evolution within the correlated radical pair state depending of the signs of the electron-electron and of the electron nuclear interactions (Jeschke 1997; 1998). The symmetry breaking is driven by the pseudosecular, off-diagonal, part *B* of the hyperfine interaction. (II) In the differential decay (DD) mechanism (Polenova and McDermott 1999), the symmetry between the two decay channels is broken by the different lifetimes of the states of the correlated radical pair. This means that in the two radical pair spin states different fractions of polarization flow from the electrons to the nuclei. The result is an additional imbalance between the fractions of nuclei in spin-up and spin-down states in the two decay channels. (III) In addition to the two polarization transfer mechanisms TSM and DD, in samples as R26-RCs of *Rb. sphaeroides* having a long lifetime of the triplet donor (^{3}P), a third mechanism may occur that selects nuclear

polarization. In this differential relaxation (DR) mechanism the breaking of antisymmetry of the polarization in the singlet and triplet branch occurs in a non-coherent way. The enhanced relaxation of nuclear spins in the proximity of the high-spin donor partially cancels the nuclear polarization in the donor cofactor. Hence, when the ^{3}P lifetime is comparable to or exceeds the paramagnetically enhanced longitudinal relaxation time, net polarization occurs due to partial extinction of nuclear polarization of the triplet state of the radical pair (Goldstein and Boxer 1987; McDermott *et al.* 1998).

The number of RC species that show the solid-state photo-CIDNP effect is growing. The list contains systems from various bacteria as well as from plants, such as bacterial RCs of *Rb. sphaeroides* WT (Prakash *et al.* 2005) and R26 (Prakash *et al.* 2006), *Rhodopseudomonas acidophila* (Diller *et al.* 2008), *Chlorobium tepidum* (Roy *et al.* 2007) and *Heliobacillus mobilis* (Roy *et al.* 2008) as well as in RCs of plant photosystems I and II (Matysik 2000; Alia *et al.* 2004; Diller *et al.* 2007). It appears that the occurrence of the solid-state photo-CIDNP effect is an intrinsic property of photosynthetic RCs (Roy *et al.* 2008; Matysik *et al.* 2009), although the window of occurrence of this effect is rather limited by kinetic and magnetic parameters (Allen 1968; Jeschke and Matysik 2003). Initially, photo-CIDNP MAS NMR experiments were performed on isolated RCs. Later it became evident that the strong enhancement effect also allows for investigations directly on cells (Prakash *et al.* 2006) or photosynthetic membranes (Roy *et al.* 2008).

In the growing list of natural RCs proven to show the solid-state photo-CIDNP effect, RCs of cyanobacteria remained to be a blank spot. Cyanobacteria are model microorganisms for the study of plant photosynthesis having a photosynthetic apparatus very similar to the one found in plants. In particular, cyanobacterium *Synechocystis* sp. PCC 6803 is of interest, which can grow both autotrophically or heterotrophically in the absence of light and is easily transformed by exogenous DNA. In this chapter we present photo-CIDNP ^{13}C MAS NMR data obtained directly from ^{13}C- isotope labeled whole cells of the cyanobacterium *Synechocystis* sp. PCC 6803.

2.2 MATERIALS AND METHODS

2.2.1 Strains and culture conditions

Wild-type cyanobacterium *Synechocystis* sp. PCC 6803 strain was kindly provided by A.H.M. de Wit of the Biophysics group of Leiden University. Cultures were grown at

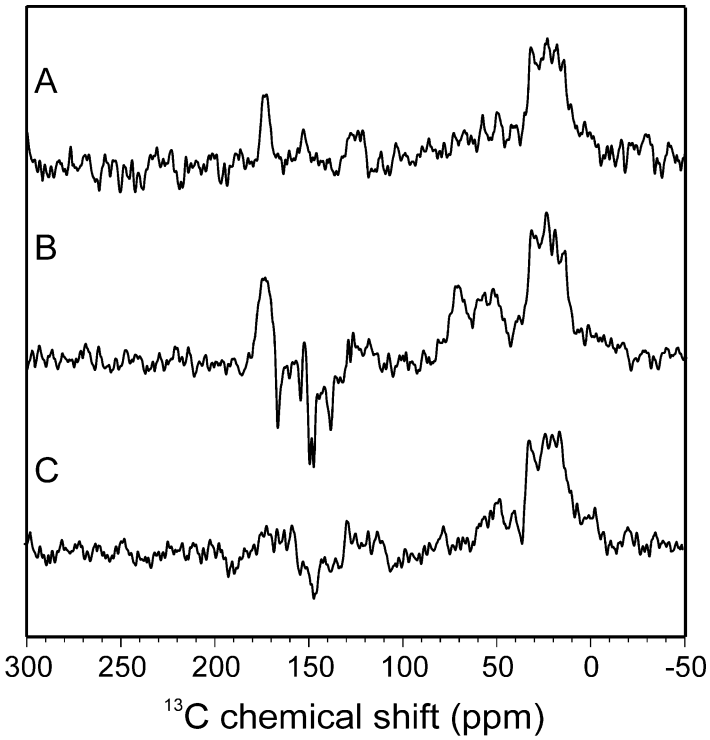

Figure 2.3: ^{13}C MAS NMR spectra of fresh *Synechocystis* sp. PCC 6803 cells obtained in the dark (A), and upon continuous illumination with white light (B). The cells were grown in [4-^{13}C]-ALA supplemented BG-11 medium. Spectrum C shows data obtained by continuous illumination of fresh *Synechocystis* sp. PCC 6803 cells grown in normal BG-11 medium. All spectra have been obtained at a temperature of 235K, in a magnetic field of 4.7 T and with a MAS frequency of 8 kHz.

25°C in standard BG-11 medium (Allen 1968) and illuminated by fluorescent white lamps giving a total intensity of 50 μE $m^{-2}s^{-1}$. Cultures were bubbled with 5% CO_2 enriched air to promote growth. Selective isotope enrichment of chlorophyll (Chl) in *Synechocystis* sp. PCC 6803 was done by growing the cyanobacterium in BG-11 medium supplemented with [4-^{13}C]-δ-aminolevulinic acid (4-ALA) purchased from Cambridge Isotope Laboratories (99% ^{13}C-enriched) to a final concentration of 53 mM.

2.2.2 Determination of the ^{13}C incorporation

Chl *a* was purified from cells grown in 4-ALA supplemented BG-11 medium (labeled sample) and from unlabeled cells (reference sample), according to the following procedure: Cells were harvested by centrifugation for 10 minutes at 13.2 krpm. The cell pellet was resuspended in 1 mL methanol, shaken and centrifuged for 5 min at 2 krpm after which the green supernatant was collected. This procedure was repeated until the pellet showed a white-bluish color. The solvent was evaporated under nitrogen (low light conditions were kept for the entire purification procedure) and the obtained pigments

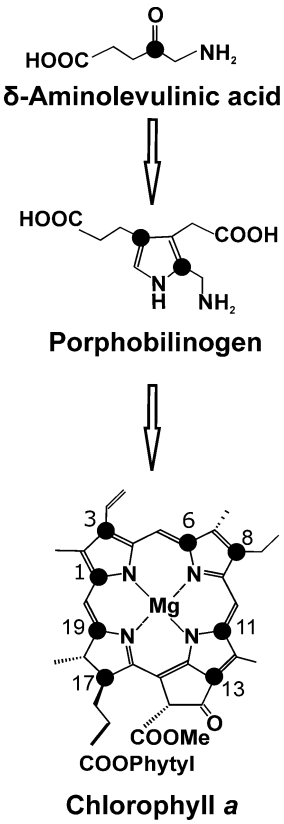

Figure 2.1: Incorporation of [4-^{13}C]-ALA into Chl *a*, black dots indicate the positions of the ^{13}C isotopes

resuspended in 2500 µL running solution, 70:30 (v/v) petroleum ether/acetone. This was loaded on a column filled with silica gel (particle size 40-63 µm, pore diameter ~60 Å) and washed with running solution. Fractions containing pure Chl *a* were identified using a Shimadzu UV-visible spectrophotometer, combined, dried under nitrogen and stored at -20 ˚C.

Mass spectra were measured on a Linear Trap Quadrupole Forier Transform (LTQ–FT) hybrid mass spectrometer (Thermo Fisher Waltham, MA, USA). Spectra were measured in ESI mode, with a source temperature of 200 °C, source voltage of 3.8 kV and tube lens voltage 150V. Chl *a* was dissolved in 90% EtOH and 10% 10 mM ammonium acetate to a final concentration of ~1 mg/mL. The sample was infused with a flow rate of 10 µL/min.

The level of 4-ALA incorporation was determined quantitatively by LC-MS analysis. Chl *a* pigments were extracted from *Synechocystis* cells grown in 4-ALA supplemented BG-11 (labeled sample), and normal BG-11 medium (reference sample). The total level of incorporation (P_{tot}) was determined via an iterative procedure as

described earlier in Schulten *et. al*. (Schulten *et al.* 2002) making use of a weighted sum according to the formula:

$$P_{tot} = \sum_{n=0}^{8} \frac{n}{8} \times P_n \qquad (1)$$

Where n stands for the number of labels present in an isotopomer and P_0 is the corresponding fraction of unlabeled Chl *a* estimated from the isotopic labeling pattern detected from the reference sample (Figure 2.2A). The mass pattern of the unlabeled sample was used to calculate the true intensities (I_t) of the labeled Chl *a*. Thus for example, the true intensity of the n=2 peak at m/z = 895.5 in the labeled Chl *a* spectrum ($^{L}I_t$ (n=2)) was calculated using the true intensities in the labeled spectrum ($^{L}I_t$) and the relative intensities in the unlabeled spectrum ($^{U}I_{\%}$) of the n = 0 and n=1 peaks according to the formula:

$$^{L}I_t(n=2) = {}^{L}I(n=2) - ({}^{U}I_{\%}(n=2) \times {}^{L}I_t(n=0)) - ({}^{U}I_{\%}(n=1) \times {}^{L}I_t(n=1)) \quad (2)$$

Based on the true intensities the Pn could then be calculated according to the formula:

$$P_n = {}^{L}I_t(n) \div \sum_{n=0}^{8} {}^{L}I_t(n) \qquad (3)$$

2.2.3 MAS NMR sample preparation

Selectively isotope enriched *Synechocystis* cells were harvested by centrifugation and washed once with standard BG-11 medium. The pellet was resuspended in a 100 µL of standard BG-11 with low light conditions. The sample was bubbled shortly with nitrogen to remove oxygen and quinone reduced by adding sodium dithionite to a final concentration of 100 mM with oxygen free and near dark conditions. After 30 minutes of incubation in the dark at room temperature (RT) the sample was loaded into an optically transparent 4-mm sapphire MAS rotor under oxygen free conditions. The sample was inserted into the NMR spectrometer right away. The isolated samples of PSI and PSII from spinach at natural abundance have been prepared following the procedures described in refs (Matysik 2000; Alia *et al.* 2004).

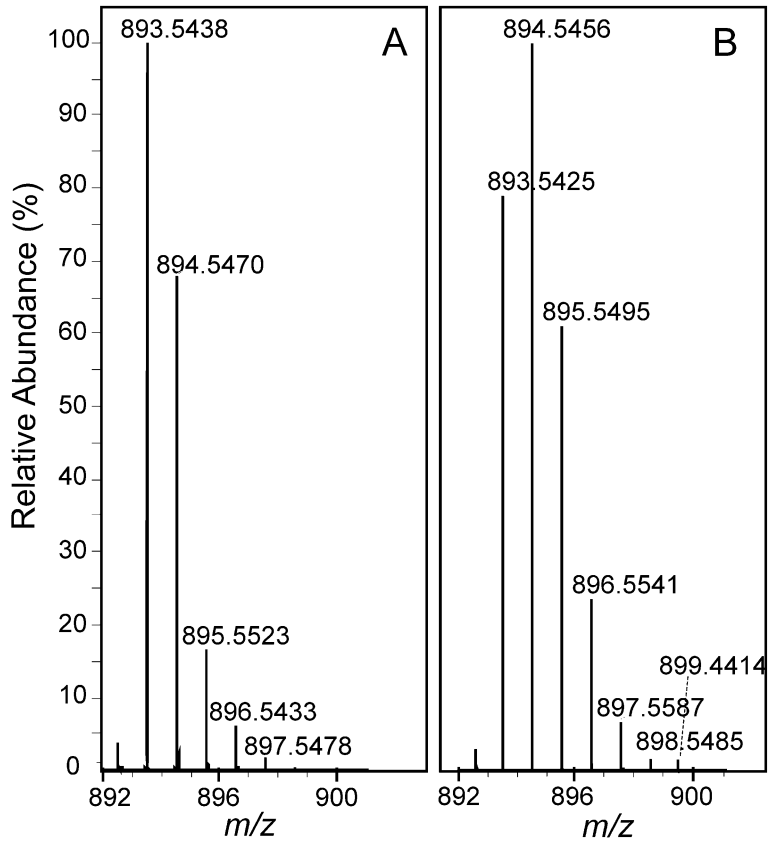

Figure 2.2: Patterns observed with LC-MS spectroscopy around *m/z* = 893 from natural abundance Chl *a* (A) and $^{13}C_{0\text{-}8}$ Chl *a* (B)

2.2.4 Photo-CIDNP MAS NMR experiments

^{13}C-MAS NMR experiments were performed on a DMX-200 NMR spectrometer (Bruker Biospin GmbH, Karlsruhe, Germany). All spectra have been obtained at a sample temperature of 235 K and with a spinning frequency of 8 kHz. The spectra were collected with a spin echo pulse sequence with the CYCLOPS phase cycle of (π/2) pulse under TPPM carbon-proton decoupling. Photo-CIDNP MAS NMR spectra have been obtained under continuous illumination with a 1000-Watt xenon arc lamp.

2.3 RESULTS AND DISCUSSION

2.3.1 Determination of the ^{13}C label incorporation

The biosynthetic route from 4-ALA to Chl *a* is depicted in Figure 2.1. Two molecules of 4-ALA are asymmetrically condensed to form the pyrrole porphobilinogen (PBG). Four molecules of PBG tetramerize, and prior to macrocycle ring closure, the last pyrrole ring is inverted via a spiro-intermediate (Schulten *et al.* 2002). Upon incorporation

of 4-ALA, a maximum of eight ^{13}C can be pairwise incorporated into each Chl *a* molecule, resulting into the specific labeling pattern shown in Figure 2.1 with ^{13}C isotopes incorporated on position C-1/C-3, C-6/C-8, C-11/C-13 and C-17/C-19. Figure 2.2 shows the LC-MS spectra observed in the region of m/z = 893.5 ([M]•+; $C_{55}H_{72}O_5N_4Mg$) from the reference- (A) and the labeled sample (B). Analysis of the isotopic patterns and relative abundances depicted in Figure 2.2 reveal a total incorporation ^{13}C isotope labels (P_{tot}) of 8% (see Table A1 in Appendix A).

2.3.2 Occurrence of the solid-state photo-CIDNP effect in Synechocystis

Spectrum A in Figure 2.3 shows a ^{13}C MAS NMR spectrum of *Synechocystis* cells containing 4-ALA labeled Chl *a* and Phe *a* cofactors obtained in the dark. The spectrum shows, as expected, signals in the aliphatic region between 0 and 50 ppm, in the aromatic region as well as in the region of the amide carbonyls. Probably some of the aromatic ^{13}C response is due to the isotope labelling. Upon illumination with continuous white light (spectrum 2.3B), additional signals occur between 170 and 120 ppm that are predominantly emissive (negative). It is also possible that light-induced signals occur in the aliphatic region between 50-80 ppm, obscured by overlap with dark signals and a high noise level.

Spectrum C in Figure 2.3 shows a ^{13}C MAS NMR spectrum of another preparation of *Synechocystis* cells with ^{13}C at natural abundance, obtained with continuous illumination. In these conditions, it is difficult to identify light-induced signals, although there may be some weakly emissive signal at ~150 ppm chemical shift.

Until now, in two other whole cell systems, for the purple bacterium *Rb. sphaeroides* R26 (Prakash *et al.* 2006; Thamarath *et al.* 2012) and for *Heliobacillus* (*Hb*.) *mobilis* (Thamarath *et al.* 2012) the observation of the solid-state photo-CIDNP effect has been reported. However, for those systems, only one type of RC is present and no isotope labelling was required. Here we show that the solid-state photo-CIDNP effect can also be observed in intact cyanobacterial cells containing both PSI and PSII. In order to recognise the light-induced signals in *Synechocystis*, however, specific isotope labelling was necessary. The necessity to use labels for *Synechocystis* suggests that the intensity of the light-induced signals is about of a factor of 30 weaker than for RCs of *Rb. sphaeroides* R26. Assuming that the solid-state photo-CIDNP mechanisms are similar across species

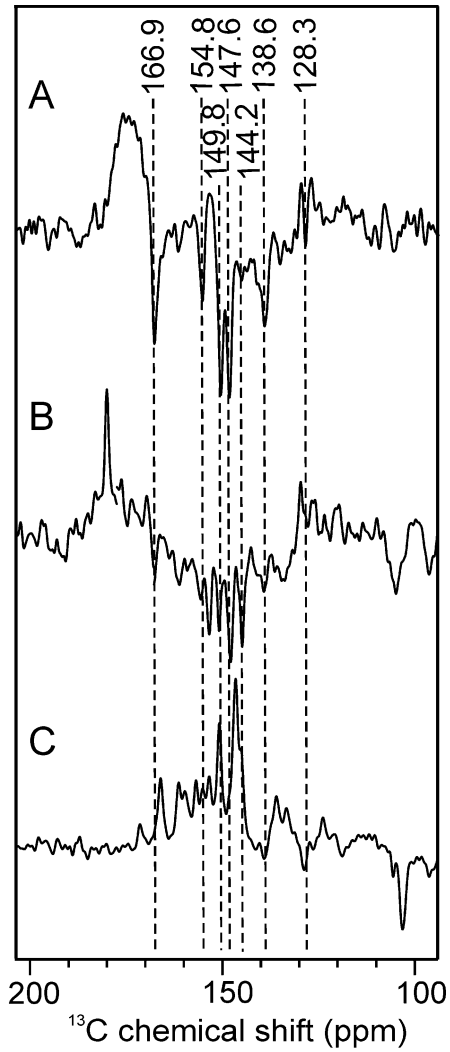

Figure 2.4: (A) Aromatic and carbonyl regions of the ^{13}C MAS NMR photo-CIDNP data collected from fresh [4-^{13}C]-ALA labeled *Synechocystis* sp. PCC 6803 cells shown in Figure 4A are reproduced in the upper trace. The two lower traces show the corresponding ^{13}C regions from photo-CIDNP spectra collected,from isolated PSI (B) and PSII (C) particles from spinach containing ^{13}C at natural abundance. MAS centerband assignments are indicated with vertical dashed lines. The spectra were obtained by continuous illumination with white light at a temperature of 235 K, in a magnetic field of 4.7 Tesla and with a MAS frequency of 8 kHz

and protein complexes, the weak intensity for *Synechocystis* sp. PCC 6803 may be due to (i) incomplete reduction of the acceptor site, (ii) lower concentration of the photosystems caused by the presence of other cellular units, or (iii) destructive interference of photo-CIDNP signals from PSI and PSII.

2.3.3 Assignment of light-induced signals

Trace A in Figure 2.4 shows the aromatic and carbonyl regions of spectrum 2.3B. The light-induced signals are indicated with dashed lines and originate from the 4-ALA labeled Chl *a* and Phe *a* cofactors. Table 2.1 shows the chemical shifts of the observed

Table 2.1: ^{13}C chemical shifts of the photo-CIDNP signals obtained at 4.7 T compared with data from the literature. Abbreviations: σ = chemical shift, a = absorptive signal, e = emissive signal.

Chemical shifts				
Chl *a*	assignment (tentative)	PSI	PSII	PSI+PSII
σ_{ss} [a]		σ [b]	σ [c]	σ [d]
170.0	19	167.1 e	166.8 a	166.9 e
162.0	14	160.4 e	162.2 a	
155.9	1	154.8 e	156.0 a	154.8 e
154.4	6		154.3 a	149.8 e
154.0	16	152.6 e	151.6 a	
150.7	4	149.9 e	149.2 a	
147.2	11	147.2 e	147.7 a	147.6 e
147.2	9			
146.2	8	144.2 e	146.0 a	144.2 e
138.0	3	138.6 e	137.4 a	138.6 e
136.1	2	~136 e	136.0 a	
134.0	12		133.9 a	
133.4	7	~ 132 e	~ 132.0 a	
126.2	13			128.3 e
108.2	10	105.4 e	106.9 e	~104.5 e
102.8	15		104.7 e	
98.1	5		97.9 e	
93.3	20		92.2 e	
51.4	17			

[a] (Schulten *et al.* 2002), data obtained from solid aggregates of Chl *a*.
[b] (Alia *et al.* 2004), data obtained from isolated PSI particles from spinach.
[c] (Diller *et al.* 2007), data obtained from D1D2 particles of spinach.
[d] This work, data obtained from whole cells *Synechocystis* sp. PCC 6803.

signals and summarizes literature values for Chl *a* aggregates and light-induced signals for isolated PSI and D1D2 particles (Boender *et al.* 1995; Alia *et al.* 2004; Diller *et al.* 2005). With the possible exception of the absorptive feature at 153.4 ppm (see below), all light induced signals are of emissive nature.

As suggested by Table 2.1, most of the light-induced signals observed in *Synechocystis* sp. PCC 6803 cells appear at frequencies matching very well with those observed in isolated photosystems of spinach. For example, the signals at 166.9, 154.8, 147.6, 144.2 and 138.6 ppm are observed in isolated PSI at very similar frequencies. This similarity suggests that photosystems are highly conserved even between different families. We also conclude that the isolation of the photosystems from plants does not significantly affect

the electronic properties of the photochemical machinery. Spectra B and C in Figure 2.4 show ^{13}C photo-CIDNP MAS NMR data obtained from isolated PSI and PSII obtained

from spinach with ^{13}C at natural abundance. The spectrum of PSI is entirely emissive in the aromatic region (spectrum B). In contrast, the spectrum of PSII shows in the region from 180 to 130 ppm only absorptive signals (spectrum C). Hence, most probably all emissive signals in spectrum 2.4A arise from PSI. Three possible reasons may explain the absence of PSII resonances: (i) The PSI/PSII ratio in *Synechocystis* sp. PCC 6803 is known to be strongly in favour of PSI with PSII being up to 9 times less abundant (Rögner *et al.* 1990), (ii) PSII proteins may degrade following intense illumination, (iii) If the chemical shifts of the signals from PSI and PSII are very similar at the isotope labeled positions (cf. Table 2.1), absorptive PSII signals may be cancelled by dominant emissive PSI signals. The emissive photo-CIDNP signals in the aromatic region can thus be attributed to the specifically isotope labeled carbons C-1, C-3, C-6, C-8, C-11, C-13, and C-19 (Figure 2.1) of PSI.

Two absorptive signals may be light-induced, at ~170 and 153.4 ppm (spectrum 2.4B). At these positions positive signals can arise from PSII that are not cancelled by emissive PSI signals (see spectrum 2.4C). In addition, two broad absorptive resonances occur with maxima around 70 and 50 ppm in spectrum 2.4B. During continuous illumination of selectively enriched RCs, labeled aliphatic carbons may gain intensity indirectly by spin diffusion from labeled aromatic carbons nearby which can explain the origin of the enhanced aliphatic response in spectrum 2.4B (Matysik *et al*. 2001). A possible explanation may be that these positive light-induced signals indeed originate from PSII, while the light-induced signals in the aromatic region originate from PSI. In that case, the PSII signal would be suppressed in the aromatic region and dominate the aliphatic region due to different relaxation properties. This would imply an almost complete destructive interference of PSI and PSII signals. Investigations on systems with a different ratio between PSI and PSII may provide further insight.

2.3.4 Activity of sample upon storage

Photo-CIDNP signals have been observed exclusively in samples prepared from *freshly* harvested cells. Samples prepared from previously frozen 4-ALA labeled cells, which were otherwise treated identically, did not show the solid-state photo-CIDNP effect (data not shown). Likewise, samples prepared from freshly harvested cells quickly lost activity upon storage at -20^{o}C, to about 70% of the photo-CIDNP intensity after two

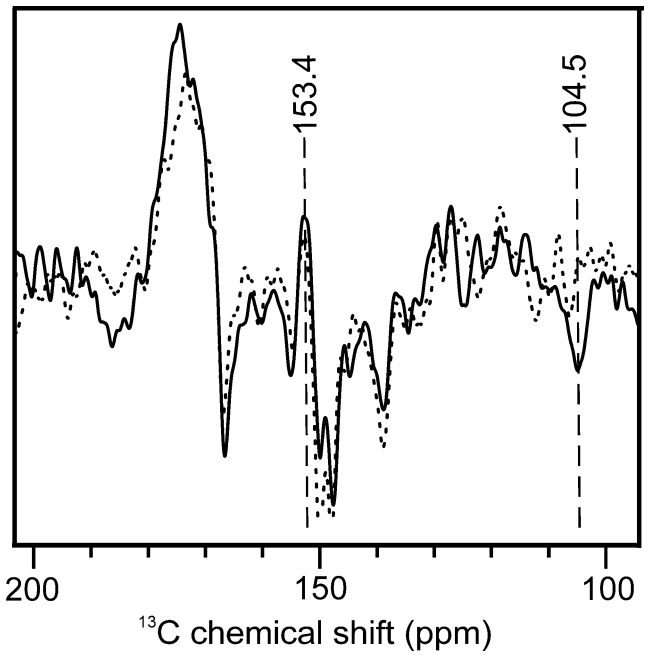

Figure 2.5: ^{13}C MAS NMR spectra of fresh [4-^{13}C]-ALA labeled *Synechocystis* cells obtained by continuous illumination with white light from hour 0 to 25 (solid trace) and hour 50 to 75 (dashed trace). The 104.5 and 153.4 ppm centerbands are visualized by dashed lines.

weeks of storage. In contrast, samples of isolated PSI or D1D2-PSII particles of spinach (Alia *et al.* 2004; Diller *et al.* 2005) did not show a significant loss of activity after storage at -20 ˚C for up to several years.

2.3.5 Light-induced changes in the sample

Using a freshly harvested sample, signals started to appear after 12 hours of measurement. In contrast, in a sample already exposed for 50 hours to white light before, photo-CIDNP signals arose after 4 hours (data not shown). Figure 2.5 shows the aromatic region of two ^{13}C MAS NMR spectra collected from fresh 4-ALA labeled *Synechocystis* sp. PCC 6803 cells obtained under continuous illumination with white light from hour 0 to 25 (solid line) and hour 50 to 75 (dashed line). It seems that signals that can be considered characteristic for PSII (spectrum 2.4C), diminish upon extended illumination. In particular the positive features at 170 and 153.4 ppm, as well as the emissive signal at 104.5 ppm are significantly weakened in the second data set.

A possible explanation could rely on the fact that PSI is, compared to PSII, known to be very difficult to reduce (Feldman *et al.* 2007) and its reduction might be ongoing during the measurement at 235K. This is in agreement with the observation that upon

decreasing the incubation time after reduction with sodium dithionite from 30 to 10 minutes, the emissive signals assigned to PSI are weakened significantly. It may be that the absorptive resonances of more efficiently reduced PSII initially slow down the build-up of emissive PSI signals while upon full reduction of PSI the PSII signals, having opposite signs with respect to the PSI signals, are fully cancelled. This is consistent with the fact that the PSI/PSII ratio in *Synechocystis* sp. PCC 6803 is known to be strongly in favour of PSI (Rögner *et al.* 1990). In addition, since PSI is much more robust than PSII after several hours of illumination PSII may be degraded (Mattoo *et al.* 1984), allowing for a faster build-up of PSI signals. Indeed the typical marker of the PSII spectrum, the emissive signal at ~104.5 ppm, diminishes upon prolonged illumination while the PSI signals remain.

2.3.6 Summary and Conclusion

The occurence of the solid-state photo-CIDNP effect, which appears to be highly conserved in photosynthetic systems, has been demonstrated in cyanobacteria. In addition, the photo-CIDNP features of PSI and PSII appear to be similar in plant and cyanobacterial systems, suggesting conservation of the electronic properties of their photochemical machineries. The occurrence of the effect also in cyanobacterial photosystems directly in prokaryotic cells demonstrates that photo-CIDNP MAS NMR studies on oxygenic photosystems are not limited to isolated photosystems from higher plants but can also be conducted on whole cells. This opens the possibility to apply this method in the analysis of systems in which a further isolation has not yet been established or is too expensive.

Chapter 3

^{15}N Photo-CIDNP MAS NMR reveals functional heterogeneity in the electron donor of PSI across plant species

In plants and cyanobacteria two light-driven electron pumps, PSI and PSII, facilitate electron transfer from water to ferredoxin with quantum efficiency close to unity. While similar in structure and function, the reaction centers of PSI and PSII operate at widely different potentials with PSI being the strongest reducing agent known in living nature. Photochemically induced dynamic nuclear polarization (photo-CIDNP) in magic-angle spinning (MAS) NMR measurements provides direct access to the heart of large photosynthetic complexes (Alia *et al.* 2004; Diller *et al.* 2005). By combining the dramatic signal increase obtained from the solid-state photo-CIDNP effect with ^{15}N isotope labeling of PSI, we were able to map the electron spin density (ρ_i) in the active cofactors of PSI and study primary charge separation at the atomic level. We compare data obtained from two different PSI proteins, one from spinach (*Spinacia oleracea*) and other from the aquatic plant duckweed (*Spirodela oligorrhiza*). Results demonstrate a large flexibility of the PSI in terms of its electronic architecture while their electronic ground states are strictly conserved.

The content of this chapter has been published in *Applied magnetic resonance* (2011) 42: 57-67.

3.1 INTRODUCTION

Photosynthesis in cyanobacteria, algae and plants involves the participation of two reaction centers (RCs), PSI and PSII, located in the thylakoid membrane of chloroplasts. The coupling of these two photosystems allows for pumping of electrons across the photosynthetic membrane from water molecules finally into CO_2 in order to achieve the buildup of organic material. The oxidized primary electron donor of PSII, $P680^{\bullet+}$ is the strongest oxidizing agent known in living nature, with a redox potential of at least 1.2 V (Gorkom and Schelvis 1993). On the other hand, the electronically excited electron donor of PSI, P700, is a strongly reducing agent, at a potential of approximately -1.2 V. Thus, P700* probably is the most reducing compound found in natural systems (Webber and Lubitz 2001). The redox properties of PSI are highly optimized in order to provide a strongly reducing species.

The X-ray structure of cyanobacterial PSI has been solved with 2.5 Å resolution and shows high resemblance to plant PSI (Fromme *et al.* 2001; Jordan *et al.* 2001). From plant PSI currently only X-ray structures at a resolution down to 3.4 Å are available (Amunts *et al.* 2010), leaving the exact electronic structure of plant P700 a matter of debate (Webber and Lubitz 2001, Amunts *et al.* 2010). All PSI systems, as in other RCs, have two symmetric branches of chlorophyll-type cofactor molecules, and two quinones (Figure 3.1). In addition, PSI contains three iron-sulphur [4Fe-4S] clusters as terminal intrinsic electron acceptors (Romberger and Golbeck 2010). The primary electron donor P700 is a heterodimer consisting of one chlorophyll *a* (Chl *a*, P_B) and one Chl *a′* (P_A) which is the 13^2-epimer of Chl *a*. While P_A forms hydrogen bonds to its protein environment, no hydrogen bonds are found on the P_B side (Jordan *et al.* 2001). EPR studies showed most of the positive charge to be localized on the Chl *a* (the P_B donor) molecule (Käss *et al.* 1995; Holzwarth *et al.* 2006), however a consensus about the extent of asymmetry has not yet been reached (Alia *et al.* 2004; Santabarbara *et al.* 2010).

In contrast to PSII, where electron transfer (ET) is known to be primarily on a single branch, data from transient EPR indicate that both branches are active in PSI (Setif and Brettel 1993; Poluektov *et al.* 2005; Müller *et al.* 2010). However, the conservation of the occurrence of bidirectional ET among different species and varying experimental conditions remains under discussion (Santabarbara *et al.* 2010). The biological significance of bidirectional ET in PSI is also not yet understood. Hence, despite the

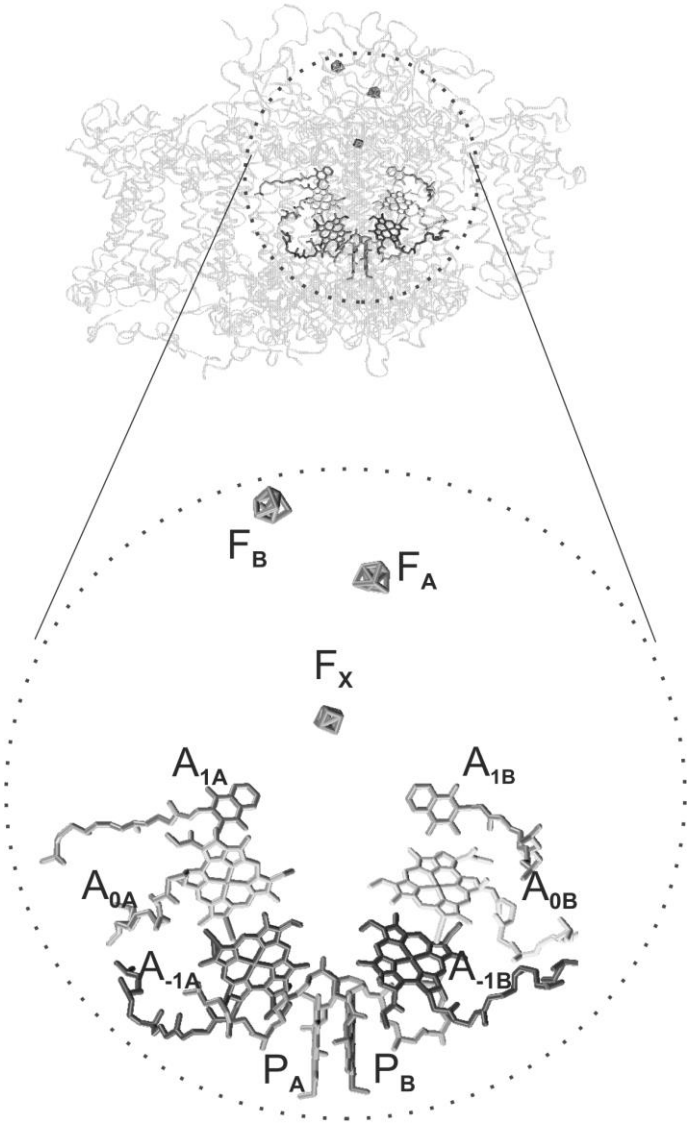

Figure 3.1: Arrangement of the cofactors in the RC of PSI (bottom) located in the heart of the PSI protein (top). Based on the X-ray crystal structure of cyanobacterial PSI (Jordan *et al.* 2001), visualized using VMD (Beckman Institute, University of Illinois at Urbana-Champaign).

highly optimized redox properties of P700, PSI appears to be functionally heterogeneous, *e.g.* in terms of the relative participation of the two branches in ET. The question addressed here is whether these variations affect P700 in different plant systems from different habitats, containing the highest evolved photosystems.

Photochemically induced dynamic nuclear polarization (Photo-CIDNP) is well known in liquid NMR as a method that increases NMR intensities (Hore and Broadhurst 1993; Goez 1997). In solid-state NMR upon illumination with continuous white light, photo-CIDNP has been observed by applying ^{15}N magic-angle spinning (MAS) NMR to four photosynthetic RCs: (i) *Rhodobacter (Rb.) sphaeroides* R26 (Zysmilich and

McDermott 1994; Zysmilich and McDermott 1996; Prakash *et al.* 2006) and wild type (WT) (Matysik 2000; Schulten *et al.* 2002; Prakash *et al.* 2005), PSI (Alia *et al.* 2004) and PSII (Diller *et al.* 2007). Photo-CIDNP is caused by the strong electron polarization in the initial radical pair and subsequently transferred to nuclei, where it is detected by NMR as signal enhancement up to a factor of about 10,000 (Prakash *et al.* 2005; Prakash 2006).

The origin of photo-CIDNP in bacterial RCs is now understood (Jeschke and Matysik 2003; Daviso *et al.* 2009). Two coherent mechanisms running in parallel, called 'three spin mixing' and 'differential decay', transfer electron spin order to nuclear spin order. A third mechanism, called 'cyclic reaction' or 'differential decay', requires a long lifetime of the donor triplet state and is not expected to be relevant in PSI (Jeschke 1998). Since the appearance of the photo-CIDNP signals improves sensitivity and selectivity of NMR dramatically, this method allows the study of small changes in the photochemically active region of the RCs in great detail and is therefore particularly suitable for the study of packing effects on P700. In this study we compare PSI proteins of spinach (*Spinacia oleracea*) and of the aquatic plant duckweed (*Spirodela oligorhizza*), using ^{15}N photo-CIDNP MAS NMR. Our results demonstrate that the electronic ground state of the donor cofactor is highly conserved and reveal differences in the overall electronic architecture in the two different plant systems, which may represent a common denominator across species (Santabarbara *et al.* 2010).

3.2 MATERIALS AND METHODS

3.2.1 Photosystem I Particle Preparation

^{15}N-labeled spinach plants were grown as described by Diller et al 2007 (Diller *et al.* 2007). ^{15}N-labeled duckweed plants were grown under aseptic conditions on half-strength Hunter's medium (Posner 1967) under continuous light (20 $\mu Em^{-2}s^{-1}$) at 25 °C. The medium was continuously bubbled with sterile air containing 5% CO_2. As a source of isotope labeled nitrogen KNO_3 was substituted by 5.5 mM of $^{15}NH_4{}^{15}NO_3$, and in addition $Ca(NO_3)\bullet 4H_2O$ was replaced by 4 mM $CaCl_2$. After 7 days plants were harvested, frozen in liquid nitrogen and stored at -80 °C until use. The PSI complex containing ~110 Chl/P700 (PSI-110 particles) was prepared according the method described by Alia *et al.* 2004.

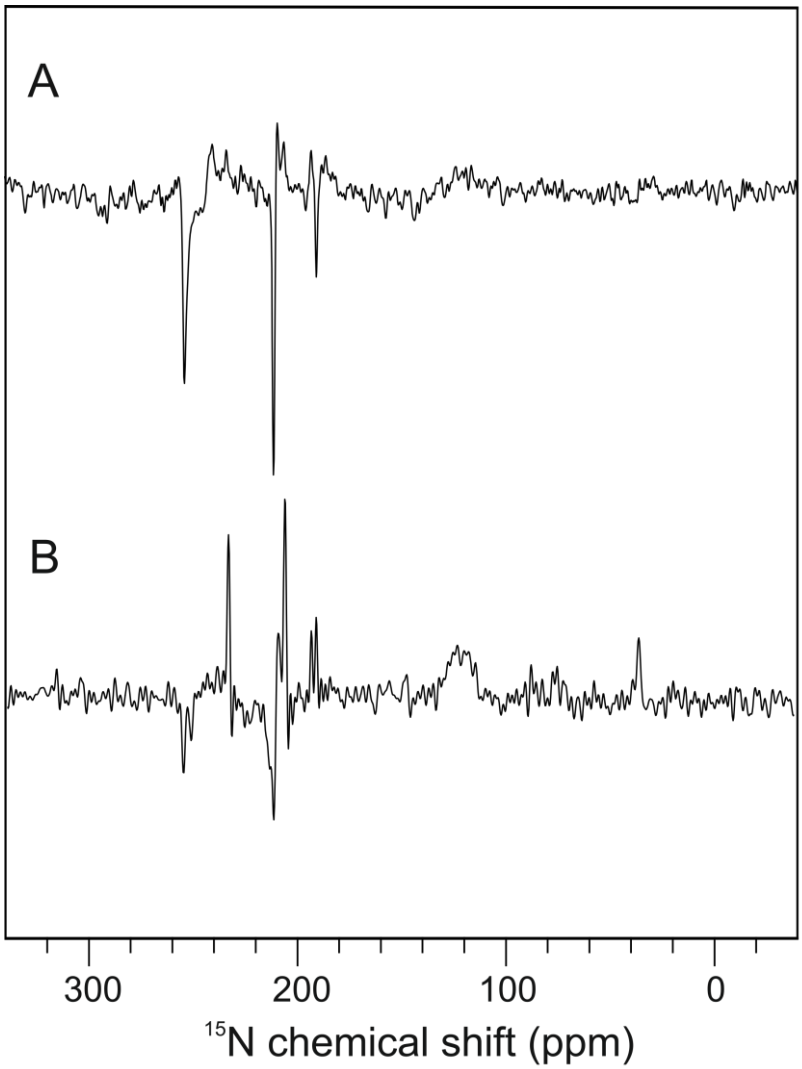

Figure 3.2: ^{15}N photo-CIDNP MAS NMR spectra of PSI of duckweed (A) and spinach (B), obtained by continuous illumination at 4.7 T, with a cycle delay of 4 s, a spinning frequency of 8 kHz and at a temperature of 240 K.

3.2.2 Photo-CIDNP MAS NMR experiments

The NMR experiments were performed using a DMX-200 NMR spectrometer (Bruker GmbH, Karlsruhe, Germany). The samples were loaded into optically transparent 4-mm sapphire rotors. The PSI samples were reduced by the addition of an aqueous solution of 10 mM sodium dithionite solution and 40 mM glycine buffer (pH 9.5) in an oxygen free atmosphere. Immediately following the reduction, slow freezing of the sample was performed directly in the NMR probe inside the magnet with liquid nitrogen-cooled gas under continuous illumination with white light. The temperature was kept at 235 K. The used illumination set-up was specially designed for the Bruker MAS probe (Matysik 2000). The light and dark spectra were collected with a CPMG-echo pulse sequence and two pulse phase modulation (TPPM) proton decoupling. The number of scans was 20 k,

unless stated differently. Fitting of the spectra was performed with Igor Pro 6.01, based on the relative intensity of the signals the electron spin density was calculated for the nitrogen assigned to the donor.

3.3 RESULTS AND DISCUSSION

3.3.1 The occurrence of photo-CIDNP in different PSI preparations from duckweed and spinach

Figure 3.2A shows the ^{15}N MAS NMR spectrum of uniformly ^{15}N labeled PSI of duckweed obtained under continuous illumination. The very weak and broad positive signals arising at about 120 ppm originate from the amide nitrogen of the protein backbone and are also present in spectra obtained in the (data not shown). Upon illumination six absorptive, positive, and five emissive, negative, photo-CIDNP signals can be resolved in the spectrum. No spinning side bands are observed at the applied magnetic field of 4.7 T and with a spinning frequency of 8 kHz. The narrow linewidth of the photo-CIDNP signals reveal a highly defined packing of the cofactors in the RC that are involved in the light-induced NMR response. The photo-CIDNP effect in PSI has been observed previously for another plant species, spinach (Alia *et al.* 2004; Diller *et al.* 2005; Roy *et al.* 2007) as well as for *Synechocystis* sp. PCC 6803 (chapter 2, (Janssen *et al.* 2010)). Here, we demonstrate that the solid-state photo-CIDNP effect on PSI can also be observed in duckweed. Hence most likely the effect occurs in all natural photosynthetic systems (Matysik *et al.* 2009). Being an aquatic plant, duckweed has the advantage over spinach that it is easier to introduce isotope labels, which allows for more detailed and selective ^{15}N and ^{13}C solid state photo-CIDNP studies (chapters 4 and 5). Duckweed previously has shown to successfully incorporate isotope labeled amino acids into its RC (Alia 2003).

Spectra A and B in Figure 3.2 compare the ^{15}N MAS NMR spectra of uniformly ^{15}N-labeled PSI of duckweed and spinach obtained by continuous illumination, with light induced signals occurring between 180 and 280 ppm. Figure 3.3 shows detailed spectra of duckweed (spectrum 3.3A) and spinach (spectrum 3.3B) PSI. Both the linewidth and the chemical shift of the photo-CIDNP signals observed for the two plant systems are very similar. However the intensity and sign of the signals are different for the two species.

Table 3.1 ^{15}N chemical shifts of the photo-CIDNP signals observed in duckweed in comparison with published chemical shift data

Assignment	Solution data	PSI spinach	PSI duckweed
atom	σ_{LS} [a]	σ_{SS} [b]	σ_{SS} [c]
N-I	186.0	**186.2** e	**186.3** a
		190.9 a	188.6 a
N-II	206.5	206.1 a	206.3 a
			210.0 a
		211.5 e	**211.4** e
N-III	189.4		**191.0** e
		193.2 a	193.3 a
N-IV	247.0	233.3 a	233.6 a
		250.3 e	250.1 e
			253.0 e
		254.9 e	**254.3 e**

All shifts are referenced to liquid ammonia with use of an external standard of solid $^{15}NH_4NO_3$ (δ = 23.5).
Bold printed shifts are assigned to the primary Chl *a* donor of the B-branch (P_B)
a, Absorptive (positive); *e*, emissive (negative).
[a] Chemical shift in ppm. Free Chl *a* measured in $CDCl_3$. Source: Boxer 1974.
[b] Chemical shift in ppm. PSI-110 complex from spinach. Source: Diller 2007
[c] Chemical shift in ppm. PSI-110 complex from duckweed Source: this work.

3.3.2 Signal assignment and electron spin density distribution in the donor P_B

The ^{15}N chemical shift assignments of the photo-CIDNP signals observed in duckweed PSI are summarized in Table 3.1, and are compared with ^{15}N chemical shifts assignments for spinach PSI (Diller *et al.* 2007) and liquid NMR data of monomeric Chl *a* in solution (Boxer *et al.* 1974) . If both branches participate in the ET, photo-CIDNP signals from up to three active Chl *a*, and one active Chl *a´* cofactors can be expected from PSI with a total maximum of sixteen nitrogens. In photo-CIDNP spectra of PSI in duckweed, a total of eleven signals has been observed, as opposed to eight signals assigned previously based on data obtained from spinach PSI (Diller *et al.* 2005). In duckweed PSI the four signals with chemical shifts between 242 ppm and 255 ppm have been assigned to the N-IV nitrogens of four different cofactors. In addition, the observation of three signals within the chemical shift range expected for the N-II nitrogens indicate that both branches may be active in PSI of duckweed. Based on the expectation

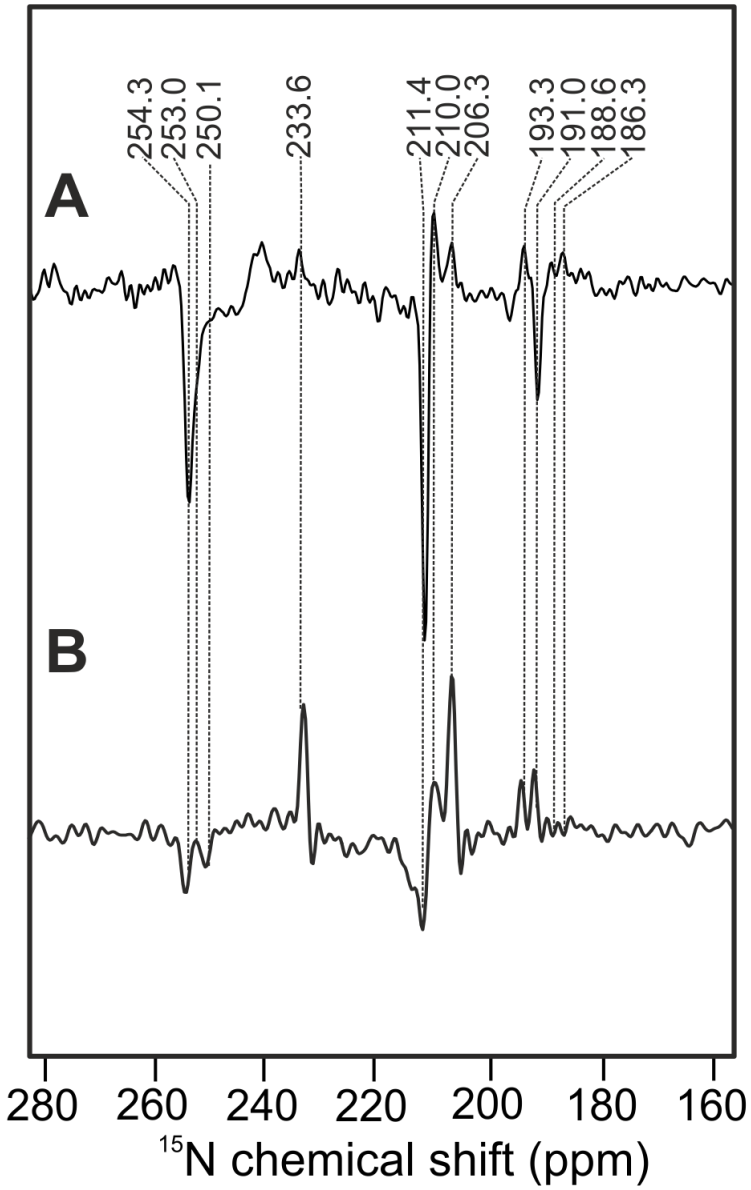

Figure 3.3: Detailed ^{15}N photo-CIDNP MAS NMR spectra of the light induced signals obtained from PSI of duckweed (A) and spinach (B). Spectra were obtained by continuous illumination at 4.7 T, with a cycle delay of 4 s, at a temperature of 240 K.

that most electron spin density (ρ_i) is located on the primary Chl *a* donor of the B-branch (P_B) (Plato *et al.* 2003), four signals in the spectrum obtained from duckweed PSI have been assigned to the nitrogen of P_B; N-I at 188.6 ppm, N-II at 211.4 ppm, N-III at 191.0 ppm and N-IV at 254.3 ppm (bold printed in Table 3.1). The signal at 186.3 ppm, which is assigned to the N-I of P_B (see Figure. 3.3 and Table 3.1) is absorptive in duckweed and emissive in spinach while in general the absorptive signals observed in the spinach PSI spectrum are much more pronounced. The relative intensities of the emissive signals assigned to the P_B cofactor are stronger in duckweed compared to the corresponding signals observed in spinach.

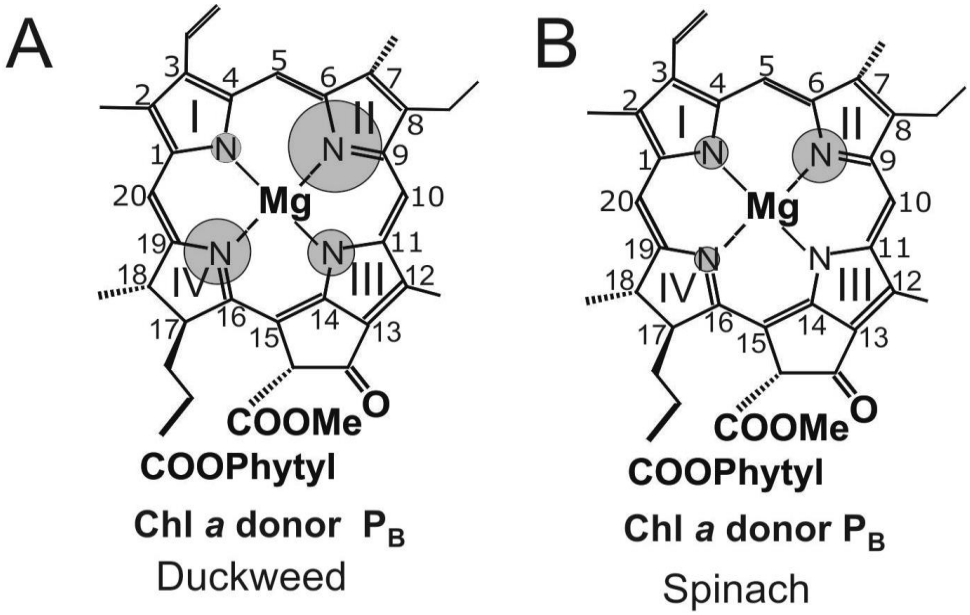

Figure 3.4: Estimated electron spin density (ρ_i) patterns in the steady state based on the integrated ^{15}N photo-CIDNP signal intensities for the primary donor of the B branch (P_B) of PSI of duckweed (A) and spinach (B).

The chemical shifts observed for duckweed appear very similar to those observed for spinach (see Table 3.1 on page 57). For both PSI systems the donor and primary acceptor cofactors, are plant Chl *a* or Chl *a′*. Hence, the ^{15}N shift data indicate that for the RCs of duckweed and spinach, the packing effects on the cofactors and their electronic ground states are quite comparable for both species, while the signal intensities reveal differences at a higher level in the protein machinery.

Based on the intensities of the observed photo-CIDNP signals, the distribution of ρ_i in the $2p_z$ orbitals can be estimated (for details, see Diller *et al.* 2005). In Figure 3.4 the steady-state electron spin density map of the P_B cofactor of duckweed (Figure 3.4A) is compared to the relative ρ_i distribution observed for the primary donor of spinach PSI (Figure 3.4B). Both for the duckweed and for the spinach PSI most of the ρ_i is located on the ring II nitrogens, which is in line with the electron spin distribution observed for free Chl *a* in solution (Käss *et al.* 1995; Käss *et al.* 1996; Käss *et al.* 1998). Likewise, similar to undisturbed Chl *a* in solution, a small ρ_i is observed on the N-I for both spinach and duckweed PSI. A prominent difference is that the signal assigned to the ring I nitrogen of P_B of spinach, with a chemical shift of 186.2 ppm, is emissive in nature while in duckweed it is observed as an absorptive signal with almost the same chemical shift (186.3 ppm, see

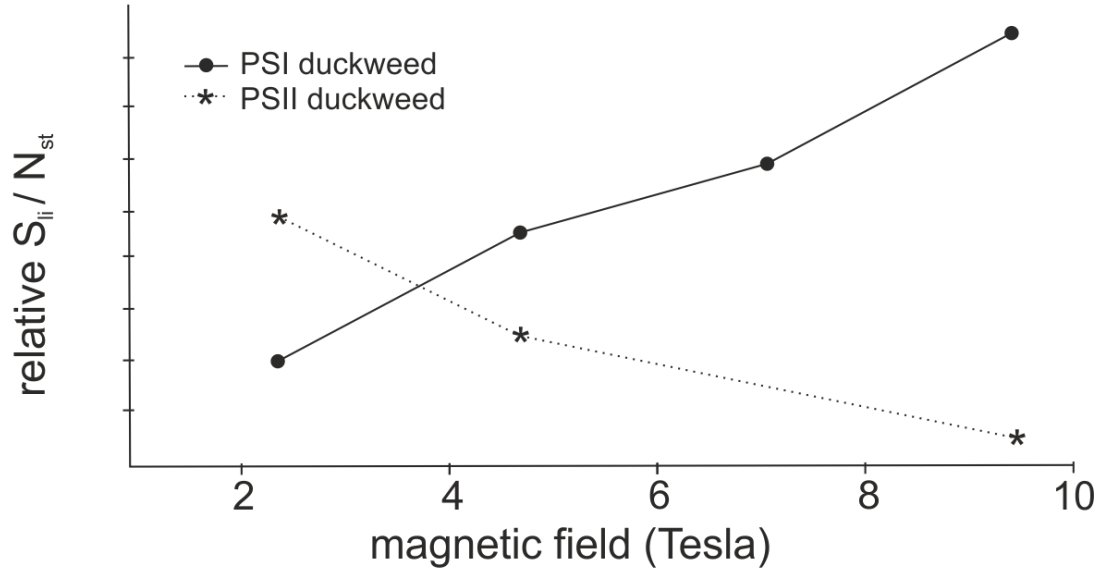

Figure 3.5: The relative magnitude of the ratio of the light-induced signal (S_{li}) to the standardized noise (N_{st}) for PSI and PSII of duckweed.

Table 3.1 and Figure 3.3). Compared to spinach PSI, a much higher ρ_i on the ring IV nitrogen is observed in the duckweed PSI preparation (Figure 3.4A), while a moderate ρ_i is found to be located on N-III. None of the signals in the spectrum obtained from spinach PSI (Table 3.1, Figure 3.3B) was assigned to the N-III of the primary donor P_B which is expected to procduce an emissive signal around 190 ppm (Table 3.1) (Diller *et al.* 2007).

In contrast with the similar chemical shifts, the intensity patterns between duckweed and spinach appear substantially different. Such changes in the intensity pattern suggest fundamental differences between the radical pairs and electron delocalization in both plant systems. It is possible that this difference is related to a different balance of the photo-CIDNP enhancement mechanisms. This would imply that parameters ruling dynamics, or the architecture of the radical pair, are also different. Such an interpretation implies that there is a large flexibility in PSI systems as proposed earlier (Santabarbara *et al.* 2010). The differences in the electronic architecture may be due to different patterns of activation of two branches in two systems leading to more asymmetric radical pair architectures having other coupling parameters. The question then remains if (i) the functionality of PSI differs between species or (ii) if functional flexibility is an inherent property of the PSI system itself, independent of the species or (iii) a combination of both options. This will be discussed further in chapter 6 of this thesis.

3.3.3 The magnetic field effect of photo-CIDNP in different plant PSI

The field dependence of the solid state photo CIDNP effect in PSI from spinach has been measured previously and it was shown that the signal strength increases from 2.4T to 9.4 T (Roy *et al.* 2007). Figure 3.5 shows the relative signal to noise intensity of the photo-CIDNP signals obtained from uniformly ^{15}N-labeled PSI and PSII of duckweed at different magnetic field strengths. In line with previous observations in spinach PSI (Roy *et al.* 2007), the light induced signals of duckweed PSI increase in intensity with an increasing magnetic field strength from 2.4 T up to 9.4 T. PSII on the other hand seems to show the opposite trend with signal intensity decresing upon increasing the field from 2.4 T to 9.4 T. Within the lower range of observed fields, the field dependence of the solid state photo-CIDNP effect in duckweed thus appears to be similar to the signal enhancement for spinach. This observation contrasts with the significant differences in the intensity patterns of the light induced signals, which suggest different electronic architecture of the radical pairs, while the field dependence appears to be similar in the two systems.

3.3.4 Outlook

To explain the differences between the radical pairs for the two PSI systems and determine if the functionality of PSI differs between species or functional flexibility is an inherent property of the PSI system itself, further experimental and theoretical studies have been performed. In chapter 5 time-resolved experiments on ^{13}C and ^{15}N labeled PSI and theoretical simulations will be discussed. In chapter 6 preliminary data obtained from selectively ^{13}C- labeled PSI from duckweed at different fields will be presented and the discussion about the functional flexibility of PSI will be continued.

Chapter 4

Photochemically induced dynamic nuclear polarization NMR on photosystem II obtained directly from plants reveals remarkable similarity and robustness of the radical pair across species.

The solid-state photo-CIDNP (photochemically induced dynamic nuclear polarization) effect allows for dramatic signal enhancement of the photochemically active machinery in solid-state magic-angle spinning (MAS) NMR spectroscopy. Here we present photo-CIDNP MAS NMR data from photosystem II of *Spirodela oligorrhiza* (duckweed), using biosynthetic sparse ^{13}C isotope labeling of PSII. Extending our earlier data collected from D1D2 preparations, it is shown that photo-CIDNP signals from selected ^{13}C nuclei within the heart of the large PSII protein can be obtained directly from entire plants, BBY, thylakoid membranes and core particles as well. Despite the presence of both PSI and PSII, the photo-CIDNP signals arise selectively from the PSII radical pair within the plants. The coherent evolution of the radical pair is enabled by a combination of blocking of electron transfer from the $P680^-$ to the Tyr_Z and the OEC and blocking or loss of the Q_A plastoquinone. The source of the photo-CIDNP response is remarkably robust, remains essentially unaffected by the various preparation procedures, and is similar for duckweed and *Spinacia oleracea* (spinach). Both in the electronic ground state and in the radical cation state the electronic structure of $P^+_{D1}Phe^-_{D1}$ is highly conserved between different plant species. The radical pair is formed by a single Chl *a* donor and a single Phe *a* acceptor. Thus, according to the photo-CIDNP the P^+_{680} donor, assigned to P^+_{D1}, is monomeric and only weakly coupled to the neighboring P_{D2}. In contrast, strong evidence for a matrix involvement, probably a histidine sidechain, in the radical pair is found.

4.1 INTRODUCTION

The photosynthetic machinery found in plants converts energy from the sun into chemical energy by oxidizing water and reducing carbon dioxide, while releasing oxygen as a side product. To achieve this, two large trans-membrane protein complexes, PSII and PSI, operate in tandem (for a review see *e.g.* Blankenship *et al.* 2002). While PSII has the highest oxidation power known in living nature, +1.2 V, PSI has the strongest reductive power (ca.-0.5 V) (Gorkom and Schelvis 1993; Witt 1996; Holzwarth *et al.* 2006; Nakamura *et al.* 2011). How PSII is able to produce and maintain such high potential within a 'soft' protein environment, has been the subject of extensive research by optical-kinetic (Hughes *et al.* 2010; Romero *et al.* 2010; Novoderezhkin *et al.* 2011) and magnetic resonance techniques (Kammel *et al.* 2003; Lendzian *et al.* 2003; Lubitz 2003; Diller *et al.* 2007). The strong oxidising nature of the cation of PSII has been attributed to a monomeric chlorophyll species that is in the right position within the large PSII multiprotein complex to experience a strong effect from the backbone dipoles of the trans-membrane helices (for a review see Cardona et *al.* 2012). Recently a high resolution X-ray structure, of a dimeric PSII core complex from cyanobacteria *Thermococcus vulcanus* has been resolved down to 1.9 Å resolution (Umena *et al.* 2011). The PSII reaction center, or D1D2 complex, consists of the D1 and D2 polypeptides in which two branches of cofactors are symmetrically arranged (Figure 4.1C). The cofactors consist of two inner Chlorphyll *a* (Chl *a*) molecules (P_{D1} and P_{D2}), two accessory Chl *a* (Chl $_{D1}$ and Chl $_{D2}$) two Pheophytins *a* (Phe *a*) and two quinones (Q) arranged in two symmetric branches. In addition the PSII RC contains two β-carotenes and two peripheral Chl *a* (Chl_{p1} and Chl_{p2}) (Figure 4.1C).

Excited state dynamics investigations have shown that the initial charge separation in oxygenic photosynthesis is provided by a multimer of four chlorophyll *a* (Chl_{D1}, P_{D1}, P_{D2}, Chl_{D2}) and two pheophytin *a* (Phe_{D1} and Phe_{D2}) pigments embedded in the PSII membrane protein complex (Kamlowski *et al.* 1996; Holzwarth *et al.* 2006; Raszewski *et al.* 2008; Novoderezhkin *et al.* 2011). Using the optical transition energies and the X-ray data as a basis, the energy levels of the various pigments were calculated. It was found that the energies of the components in the multimer are different, and that the energies of Chl_{D1} and P_{D1} depend on the temperature (Raszewski *et al.* 2008). At cryogenic temperatures the excited state is strongly localized on the accessory Chl_{D1}, while at physiological temperatures there are contributions from all chlorophyll pigments to the primary excited state (Raszewski *et al.* 2008). Charge separation is thought to involve at least two different pathways, with

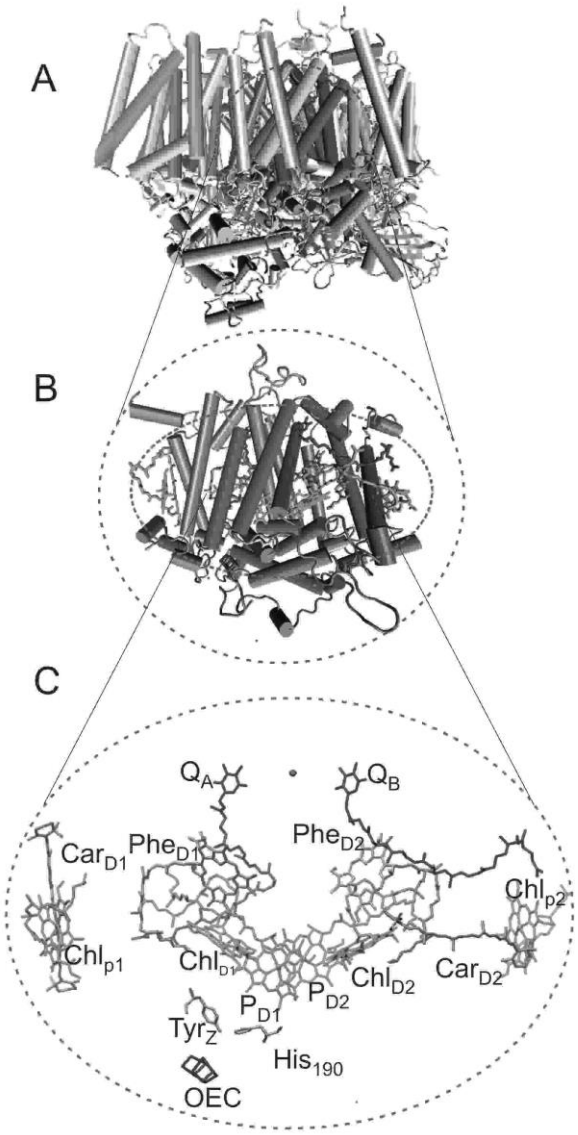

Figure 4.1: (A) PSII core complex. (B) D1D2 reaction center complex. (C) The arrangement of cofactors of electron transfer chain located in D1D2 complex consists of two central Chl *a* (P_{D1} and P_{D2}), two accessory Chl *a* (Chl_{D1} and Chl_{D2}), two pheophytins (Phe_{D1} and Phe_{D2}), two Quinone's (Q_A and Q_B), two peripheral Chl *a* (Chl_{p1} and $Chlp_2$) and two β-carotenoids (Car_{D2} and Car_{D1}). At the P_{D1} side a Tyrosine residue Tyr_Z is bridging between the P_{D1} and the Oxygen evolving system (OEC).

electron transfer from the Chl_{D1} to the Phe_{D1} or from the $P_{D1}P_{D2}$ excitonically coupled dimer to the Phe_{D1} (Raszewski *et al.* 2008; Novoderezhkin *et al.* 2011). Within ~20 ps the complex charge separation processes have occurred, and the hole stabilizes on P_{D1} to produce the $P^+_{D1}Phe^-_{D1}$ in its non-stationary correlated radical pair state (Raszewski *et al.* 2008).

The photo-CIDNP magic-angle spinning (MAS) NMR is an optical solid-state NMR method exploiting the coherent evolution in the spin-correlated electron pair. The conversion of electron spin zero quantum coherence into T_0 double quantum coherence by coupling to the nuclear spins leads to nuclear polarization and allows for a strong increase of sensitivity

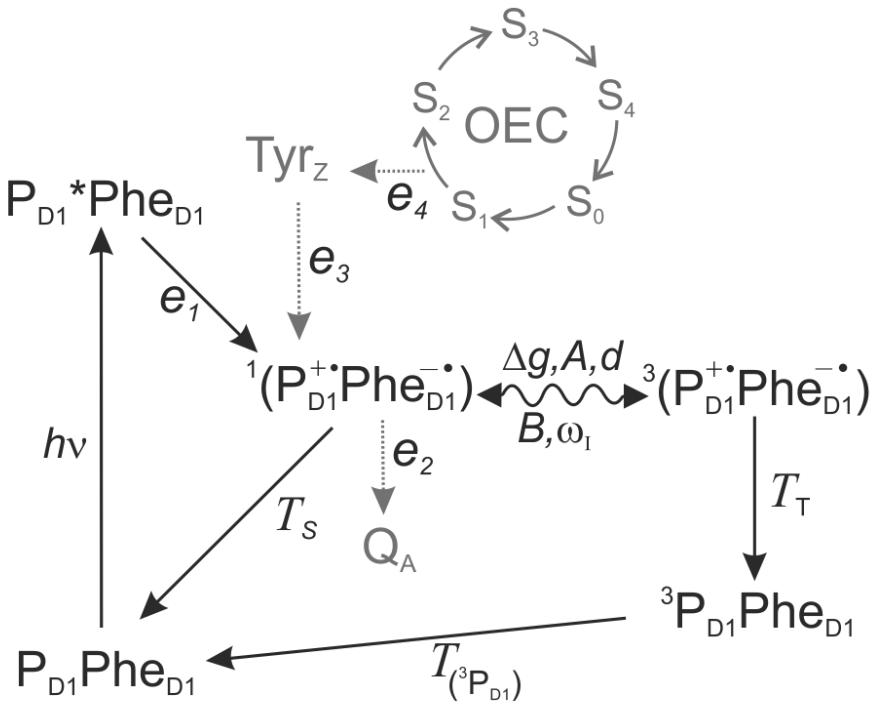

Figure 4.2: Reaction cycle in PSII D1D2 particles. After absorption of a photon ET occurs from the Chl donor P_{D1} to the primary acceptor Phe_{D1}. The oscillating arrow represents coherent evolution of the initial zero quantum coherence of the pure singlet state into double quantum coherence of the triplet radical pair and back. This process is driven by the difference of the *g* value between the two electrons Δg, the secular part of the hyperfine interaction *A*, the coupling between the two electrons *d*, the pseudo-secular hyperfine coupling *B*, and the nuclear Zeeman frequency ω_I. T_S, T_T and $T(^3P_{D1})$ refer to the lifetimes of the singlet and the triplet radical pairs, and the triplet donor state, respectively. The direction of the excitation and decay after light induced electron transfer from the electron donor (P_{D1}) to the Phe_{D1} acceptor, are shown in solid arrows. Depicted in grey are the S-cycle of the OEC, the Tyr_Z residue bridging between the OEC and the P_{D1} chlorophyll donor and the secondary electron acceptor Q_A. In PSII systems larger than D1D2 (*i.e.* the PSII core, BBY, thylakoid and plants) both the OEC and the Q_A are present and ET steps e_2 to e_4 cause fast quenching of the singlet radical pair $1(P_{D1}^{\bullet+}Phe_{D1}^{\bullet-})$ avoiding ISC and subsequent triplet state buildup.

and selectivity of NMR signals. This makes it possible to study the electronic structure of photosynthetic cofactors in great detail (Zysmilich and McDermott 1994; Jeschke and Matysik 2003; Daviso *et al.* 2009). The spin-chemical origin of the photo-CIDNP effect is based on the contribution of different mechanisms, TSM (Jeschke 1998), DD (Polenova and McDermott 1999) and DR (Zysmilich and McDermott 1994). While the observed chemical shift refers to the electronic ground state obtained after the photocycle, the photo-CIDNP intensity is related in a non-trivial manner to the local electron spin density in the radical pair state (Daviso *et al.* 2009). Until recently the solid-state photo-CIDNP effect has been observed only in natural photosynthetic RCs (Matysik *et al.* 2009). Observation of solid-state photo-CIDNP in a blue-light photoreceptor (Thamarath *et al.* 2010) as well as the prediction that it occurs at earth fields (Jeschke *et al.* 2011) suggest that the phenomenon is rather common in electron transfer systems.

Photo-CIDNP MAS NMR has been successfully applied to various photosynthetic RCs from bacteria and plants (Alia *et al.* 2004; Roy *et al.* 2007; Roy *et al.* 2008) and a strong increase in sensitivity and selectivity by the solid-state photo-CIDNP effect has been observed. In combination with selective isotope labeling the photo-CIDNP allows for direct observation of the primary radical pair in entire cells of selectively ^{13}C labeled purple bacteria (Prakash *et al.* 2003) and cyanobacteria *Synechocystis* sp. PCC 6803 (chapter 2; Janssen *et al.* 2010). In PSII the relatively stable $P_{D1}^{+}Phe_{D1}^{-}$ radical pair can contribute to photo-CIDNP via the TSM and DD mechanisms on the ns timescale, while charge recombination triplets that can possibly contribute to the photo-CIDNP via the DR mechanism are expected to equilibrate between Chl_{D1} and P_{D1} (Figure 4.2).

For PSII the Photo-CIDNP effect has been detected for D1D2 preparations only (Matysik *et al.* 2000; Diller *et al.* 2005). Based on the PSII photo-CIDNP data, the donor was identified to be a single Chl *a* cofactor with little interaction with other pigments (Matysik 2000; Diller *et al.* 2005). This is in line with theoretical studies (Durrant *et al.* 1990; Raszewski *et al.* 2008) and ADMR experiments (van der Vos *et al.* 1992) concluding the P_{D1} donor to be only weakly coupled to the neighboring P_{D2} and functioning as a monomer. It has been proposed that the high oxidation power of PSII, +1.2 V, relative to the closely related RC of purple bacteria, + 0.7 to 0.9 V, may be due to the localization of the cation on a single Chl *a* pigment rather than being distributed over a strongly coupled bacterial chlorophyll (BChl) pair (Groot *et al.* 2005; Holzwarth *et al.* 2006; Saito *et al.* 2011). Photo-CIDNP data also reveal a pronounced asymmetry of the electronic spin density (ρ_i) distribution within the Chl *a* donor (Käss *et al.* 1995; Matysik 2000; Diller *et al.* 2005). The pattern of electron spin density distribution was found to be inverted in the oxidized radical state relative to Chl $a^{+\bullet}$ in solution with a much lower redox potential of -0.5 V compared to the Chl *a* donor inside the PSII RC. While monomeric Chl *a* in solution has the highest ρ_i located at ring II (Käss *et al.* 1995), the Chl *a* cation radical in the D1D2 complex shows a shift of ρ_i towards ring III and IV (Matysik 2000; Diller *et al.* 2005; Diller *et al.* 2007). A possible explanation of the ρ_i inversion was suggested to be the presence of a local electrostatic field close to ring III, illustrated in a computational model by the protonation of the keto group of ring IV (Matysik 2000). However improved assignment of ^{13}C resonances of Chl *a* is still demanding for confirming the source of ρ_i sign inversion. Based on data obtained from uniformly ^{15}N labeled D1D2, the inversion of electron spin density observed in the oxidized radical state of the Chl *a* donor was proposed to originate from a tilting of the

axial histidine toward pyrrole ring IV causing π-π overlap of both aromatic systems (Diller *et al.* 2005).

Until now photo-CIDNP MAS NMR studies on plant PSII have been restricted to experiments on isolated D1D2, which is prepared following a harsh biochemical procedure (Matysik 2000; Diller *et al.* 2005). First thylakoid membrane containing PSI and PSII are isolated and then PSI is removed to obtain PSII enriched membranes (so-called BBY preparations) (Novoderezhkin *et al.* 2011). Next the removal of peripheral light harvesting complex 2 (LHC2) leads to PSII core complex (van Leeuwen *et al.* 1991). Finally removal of core antenna proteins CP43 and CP47 leads to the PSII reaction center or D1D2 complex (Figure 4.1B).

The question arises whether the electronic structure of the non-stationary correlated radical pair state ($P^{+}_{D1}Phe^{-}_{D1}$) is influenced in isolated D1D2 complex as compared to intact RC in PSII core or in higher preparations. Previously a novel application of photo-CIDNP MAS NMR has been recognized where the radical pair in the photosynthetic bacterial reaction center was studied directly in intact cells (Prakash *et al.* 2003). However, Photo-CIDNP buildup in large PSII systems (*i.e.* PSII core complex, BBY complex or thylakoid membrane) is challenging because of sensitivity issues and previous attempts of ^{13}C isotope labeling of PSII in plants have not been successful. In addition, the presence of quinones and the oxygen evolving complex, which cause fast quenching of the singlet radical pair avoiding intersystem crossing (ISC) and subsequent triplet state buildup, will cause additional problems for Photo-CIDNP buildup in larger PSII systems (Figure 4.2). In order to observe photo-CIDNP, the nonstationary singlet state that is generated by photoexcitation and charge separation, $P^{+}_{D1}Phe^{-}_{D1,}$ has to evolve coherently for ~ 10-100 ns. An essential difference between higher PSII preparations on the one hand, and D1D2 or bacterial RCs on the other hand, is the presence of an "upstream" depletion mechanism by hole transfer from the radical cation P^{+}_{D1} to the Tyr_Z and the OEC, in addition to the "downstream" depletion from electron transfer from the Phe^{-}_{D1} to the quinone acceptor (Figure 4.2). Thus, in order to observe photo-CIDNP in higher PSII preparations, the removal or blocking by intense illumination of quinones that was successfully exploited in photo-CIDNP studies of the D1D2 and bacterial RC preparations to block the downstream transfer is insufficient.

In this work we successfully incorporate selective ^{13}C labels in PSII of duckweed and report photo-CIDNP signals of PSII directly from core particles, thylakoid membranes and entire plants. The coherent evolution of the radical pair is enabled by a combination of pH-

induced blocking of electron transfer from the $P680^-$ to the Tyr_Z and the OEC and blocking or loss of the Q_A plastoquinone. Despite the presence of both PSI and PSII, the photo-CIDNP signals arise selectively from the PSII radical pair within the plants. The electronic structure of $P^+_{D1}Phe^-_{D1}$ is presented and compared at various steps of PSII isolation, from the entire plant to the D1D2 complex. The results show that the photochemical machinery of PSII is remarkably robust and that the electronic structure of the non-stationary correlated radical pair state, the source of the photo-CIDNP response, remains essentially unaffected by the various preparation procedures. Finally the data reveal and contribute to converging evidence that the P^+_{680} donor is, also at higher temperature, P^+_{D1}, and only loosely coupled to the neighboring P_{D2} functioning as a monomer.

4.2 MATERIALS AND METHODS

4.2.1 Strains and culture conditions

Duckweed plants were grown under aseptic conditions on half-strength Hunter's medium (Posner 1967) under continuous light (20 $\mu Em^{-2}s^{-1}$) at 25 °C. The medium was continuously bubbled with sterile air containing 5% CO_2. For selective ^{13}C labeling fully grown plants were exposed to δ-aminolevulinic acid (ALA, purchased from Cambridge Isotope Laboratories), isotopically ^{13}C labeled at carbon position 3, (3-ALA), 4, (4-ALA) or 5, (5-ALA), to a final concentration of 1.4 mM in half-strength Hunter's medium at pH 4.8. After 7 day's plants were harvested and used directly for sample preparation or frozen in liquid nitrogen and stored at -80 °C until further use.

4.2.2 Determination of the ^{13}C-label incorporation

Chl *a* was extracted from plants grown in half-strength Hunter's medium (labeled sample) supplemented with labeled ALA and from unlabeled plants (reference sample), according to the following procedure (Moran and Porath 1980): Plants were homogenized in half-strength Hunter's medium and centrifuged for 10 min at 16000 × *g*. The supernatant was removed and the residue was dissolved in 1 ml MeOH. The methanolic solution was centrifuged for 5 min at 300 × *g*. The green supernatant was separated from the blue and white residue and dried under a gentle stream of N_2. The sample was resuspended in acetone, loaded on a cellulose column and pure Chl *a* fractions were eluted with petroleum

ether/acetone (7/3 v/v). The solvent was evaporated under N_2 flow and the pure Chl *a* was stored at -20 °C in a dry nitrogen atmosphere.

Mass spectra were measured with a Linear Trap Quadrupole Forier Transform (LTQ–FT) hybrid mass spectrometer (Thermo Fisher Waltham, MA, USA). Spectra were measured in the ESI mode, with a source temperature of 200°C, a source voltage of 3.8 kV and a tube lens voltage of 150 V. Chl *a* was dissolved in 90% EtOH and 10% 10 mM ammonium acetate to a final concentration of ~1 mg/mL. The sample was infused with a flow rate of 10 $\mu Lmin^{-1}$. In the biosynthetic route from ALA to Chl *a* and Phe *a*, two molecules of 5-, 4-, or 3-ALA are asymmetrically condensed to form the pyrrole porphobilinogen (PBG). Four molecules of PBG tetramerize, and prior to macrocycle ring closure, the last pyrrole ring is inverted via a spiro-intermediate (Schulten *et al.* 2002). Upon incorporation of 5-, 4-, or 3-ALA a maximum of 8 ^{13}C can be incorporated into each Chl *a* or Phe *a* molecule, which leads to the sparse labeling patterns shown in Figure A1 in Appendix 1. Based on the LC-MS spectra observed in the region of m/z = 893.5 ([M]•+; $C_{55}H_{72}O_5N_4Mg$) to m/z +8 (maximum ^{13}C incorporation) the total level of incorporation (P_{tot}) was determined via an iterative procedure as described earlier by Schulten *et al.* (Schulten *et al.* 2002) and in section 2.3.1 of this thesis. Since ALA is a precursor of both Chl *a* and Phe *a*, it is assumed that the level of label incorporation into Phe *a* and Chl *a* is identical (Beale and Weinstein 1991). Figure A1 shows a characteristic mass spectrum of Chl *a* isolated from *S. oligorrhiza* grown under standard conditions (see Appendix A, Figure A1 and Table A2) and in the presence of ^{13}C labeled ALA precursor (Figure A1B). An average of 30% isotope enrichment was accomplished.

4.2.3 Isolation of PSII D1D2, BBY and Core complex

The natural abundance samples of isolated D1D2 from spinach were prepared as described earlier in Matysik *et al*. (Matysik 2000) The PSII core complexes from duckweed were isolated according to the procedures described by van Leeuwen *et al*. (van Leeuwen *et al.* 1991)

Selectively ^{13}C labeled BBY membranes were isolated according to the methods described in (Berthold *et al.* 1981). This procedure was adjusted for micro scale preparation using 10 g of 4-ALA labeled duckweed plants as a starting material. After solubilization in MES buffer (20 mM MES, 15 mM $NaCl_2$, 5 mM $MgCl_2$, pH 6.0), starch was removed by 5

minutes of slow centrifugation (Sorvall SS34) at 80 × *g*. The Chl *a* concentration of the reaction mixture was determined using a Moran Assay and adjusted to 1 mg/mL. Triton-100 was added to a final concentration of 5% (w/v). After incubation on ice while stirring for 20 minutes the sample was centrifuged for 20 minutes at 25,000 × *g*. The pellet was resuspended in MES buffer to remove the Triton-100 and again centrifuged for 20 minutes at 25,000 × *g*. The product, 1.5 mL of 1.7 mg/mL Chl *a*, was stored at -80°C in BTS-200 buffer (20 mM Tricine, 10 mM $MgCl_2$, 5 mM $CaCl_2$,10 mM $MgSO_4$, 0.2 M Sucrose and 0.03% (w/v) n-dodecyl-β-D-maltoside, pH 6.5).

4.2.4 NMR sample preparation

D1D2 was directly loaded into an optically transparent 4-mm NMR sapphire rotor. All other samples were previously reduced by the addition of sodium dithionite to a final concentration of 100 mM under oxygen free and low light conditions and loaded into NMR sapphire rotors. For experiments on BBY, 200 µL of BBY product (Chl *a* concentration of 1.7 mg/mL) was washed twice with sucrose free BTS-200 buffer (BTS-0) and resuspended in 70 µL of BTS-0 before reduction. For preparation of thylakoid samples ~200 mg isotope labeled plants were homogenized in a minimal amount of half-strength Hunter's medium at pH 5.8 under near dark conditions. Starch was removed with slow centrifugation at 60 × *g* for 3 minutes (Eppendorf 5415D). The supernatant was collected and centrifuged for 10 min at 16000 × *g*, and the pellet was resuspended in half strength Hunters medium. For experiments on entire plants, ~100 mg duckweed plants was incubated for 15 minutes in a solution containing 100 mM sodium dithionite in complete darkness in a nitrogen atmosphere. Plants were carefully stacked inside an optically transparent 4-mm NMR sapphire rotor and half-strength Hunter's medium was added to fill the rotor. In all cases the filled rotor was directly loaded into the NMR-probe and cooled to 235 K with slow sample spinning at 800 Hz.

For a high triplet yield and subsequent photo-CIDNP buildup it is necessary to doubly reduce the quinones (Q, Figure 4.1C). Only in D1D2 preparations reduction is not required because the quinones are already lost during D1D2 preparation. Double reduction of both Q_A and Q_B was realized by the addition of sodium dithionite to a final concentration of 100 µM. Membrane and plant samples were always freshly prepared and directly frozen inside the NMR apparatus.

4.2.5 Photo-CIDNP MAS NMR experiments and data processing

^{13}C-MAS NMR experiments were performed with a DMX-200 NMR spectrometer (Bruker Biospin GmbH, Karlsruhe, Germany). All spectra have been obtained at a sample temperature of 235 K and with a spinning frequency of 8 kHz. The spectra were collected with a spin echo pulse sequence with phase cycling of (π/2) pulses under two-pulse phase modulation carbon-proton decoupling (Bennett *et al*.). Photo-CIDNP MAS NMR spectra have been obtained using continuous illumination with a 1000-Watt Xenon arc lamp (Matysik *et al.* 2000).

The fitting of the light induced signals obtained by MAS NMR photo-CIDNP has been performed using Igor Pro version 6.01 (Lake Oswego, Oregon).

4.3 RESULTS AND DISCUSSION

4.3.1 Comparison of ^{13}C Photo-CIDNP MAS NMR spectra of isolated PSII systems from spinach and duckweed.

In Figure 4.4A, Spectra a and b were obtained by continuous illumination of D1D2 from spinach and core particles from unlabeled duckweed. Spectra a′ and b′ show the corresponding dark spectra. The dark spectra show signals in the aliphatic region between 0 and 50 ppm, as well as a broad signal between 60 and 80 ppm. These dark signals are due to the C-α of the amino acids of the protein backbone. In the photo-CIDNP spectra in Figure 4.4A (a,b), absorptive (positive) light-induced signals occur in the region between 120 and 170 ppm. These signals have been assigned to the aromatic ring carbons of the Chl *a* donor based on our previous study (Diller *et al.* 2005) (Table 4.1). Emissive signals between 90 and 130 ppm were identified as four methine carbons. Figure 4.4B shows the aromatic regions of Spectra a and b in Figure 4.4A. A total of 23 light-induced signals previously assigned to the Chl *a* donor (Table 4.1) are visualized by dashed lines. The broad negative response observed at 142.5 and 146 ppm and the emissive signal at 129.2 ppm can be sttributed to a response from aromatic amino acids in the vicinity of the Chl *a* donor (Diller *et al.* 2005; Holzwarth *et al.* 2006).

The photo-CIDNP signals obtained by illumination of a spinach D1D2 preparation (a) and duckweed PSII core particles (b) are similar, both with respect to the chemical shifts and in terms of the overall intensity pattern. These data corroborate earlier work by

femtosecond transient absorption spectroscopy, which revealed a conservation of the efficient electron transfer rate constants upon isolation of the D1D2 complex from PSII core (Holzwarth *et al.* 2006). Also the mechanism of electron transfer, with Chl_{D1} acting as the primary electron donor and Phe_{D1} as the primary acceptor, was found to be the same in both D1D2 and PSII core systems (Holzwarth *et al.* 2006).

The data obtained from the core complex show a lower signal to noise ratio compared to data obtained from the fully isolated system, due to less PSII RCs per unit area in PSII core complex preparations, compared to isolated RCs. A ratio ~1:5 is estimated based on the 80% drop in relative OD_{675} absorption upon isolation of D1D2 from PSII core. Based on these numbers and the observation of a single Chl component with narrow signals, the presence of different RC subpopulations or a substantial inactive PSII fraction is highly unlikely. For the preparation of both the D1D2 and PS2 core, treatment with Triton-X detergent is used (Leeuwen *et al.* 1991). Triton-X has been found to affect the absorption and hole burning spectra of PSII, disrupting the charge transfer from the Chl_{D1} to Phe_{D1} in the first picoseconds after excitation (Tang *et al.* 1991). In addition it has been suggested that D1D2 preparations contain two subpopulations of fully intact and destabilized (blue shifted) PSII with a distorted P_{D1}-P_{D2} coupling (Hillmann *et al.* 1995; Riley *et al.* 2004; Acharya *et al.* 2012).

In the current work the PS2 core complex is studied when embedded in its natural membrane environment, in the thylakoid membrane. Observation of photo-CIDNP from thylakoid membranes is difficult without the additional sensitivity that can be obtained by specific isotope labeling. To compare the radical-pair structure of PSII in isolated D1D2 particles with that of PSII embedded in native thylakoid membrane or in intact leaves, site specific ^{13}C labeling in Chl *a* and Phe *a* of PSII in duckweed were performed.

4.3.2 Observation of ^{13}C photo-CIDNP from site-specific ^{13}C labeled PSII in native thylakoid membrane

Figure 4.4C shows ^{13}C photo-CIDNP spectra from PSII in native thylakoid membrane from duckweed plants that were specifically ^{13}C labeled at different carbon positions by feeding plants with ^{13}C labeled precursors of chlorophylls. The isotope label patterns for the Chl *a* donor and Phe *a* acceptor, obtained by feeding with ^{13}C 5-ALA, 4-ALA and 3-ALA are indicated in Figure 4.3. By using specifically labeled samples it was

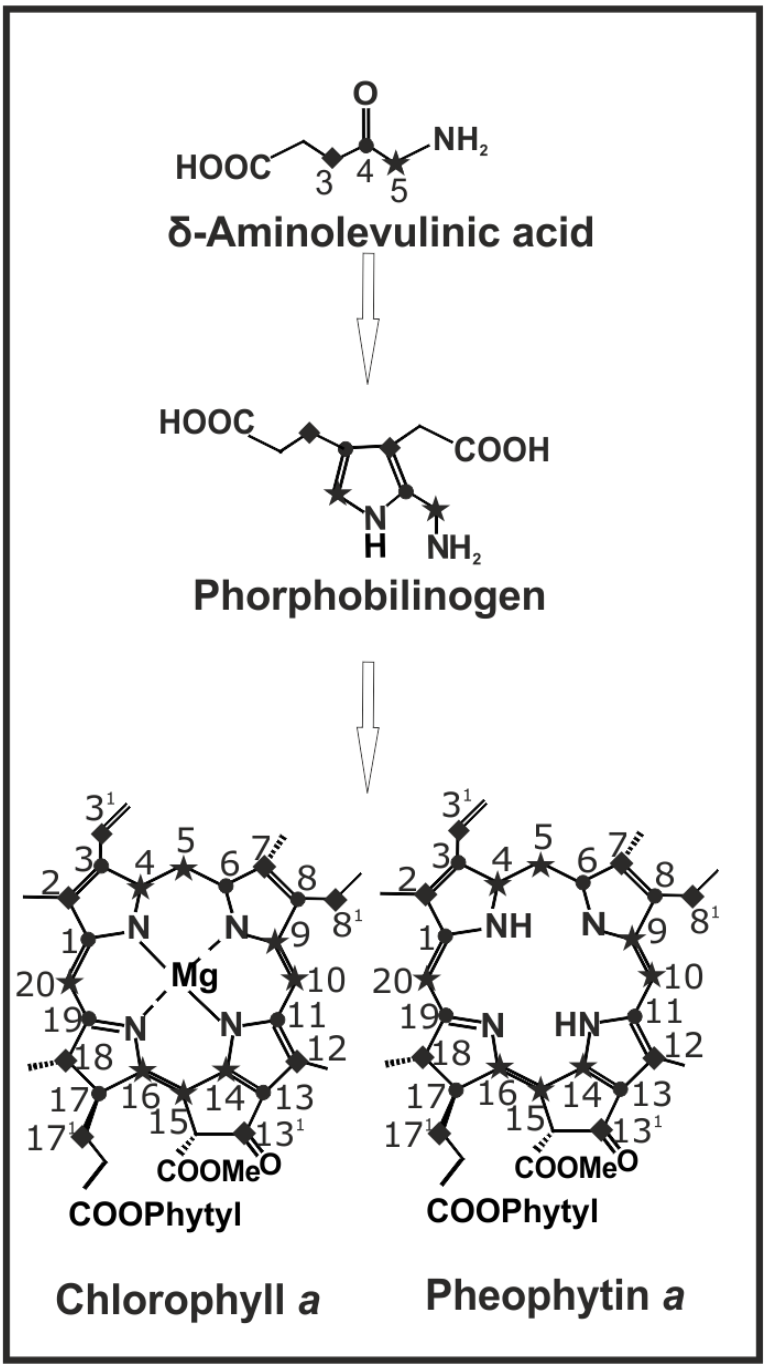

Figure 4.3: Incorporation of ^{13}C labels by feeding 5-aminolevulinic acid (ALA), 4-ALA or 3-ALA precursors to the growing plants. Depending on the placement of the ^{13}C isotope within the precursor (at position 5, 4 or 3) the Chl *a* and Phe *a* molecules are labeled during the natural biosynthesis pathway at the positions visualized by the different symbols. With the stars, circles and diamonds referring to the pattern obtained by the addition of 5-, 4- or 3-ALA precursors, respectively. The numbering of Chl *a* and Phe *a* is according to the IUPAC nomenclature.

possible to selectively highlight eight carbons in each active Chl *a* or Phe *a* cofactor (Figure 4.3).

From the 23 light induced signals obtained from unlabeled PSII core and D1D2 systems (Figure 4.4B), 19 signals can be traced back in the data obtained from selectively

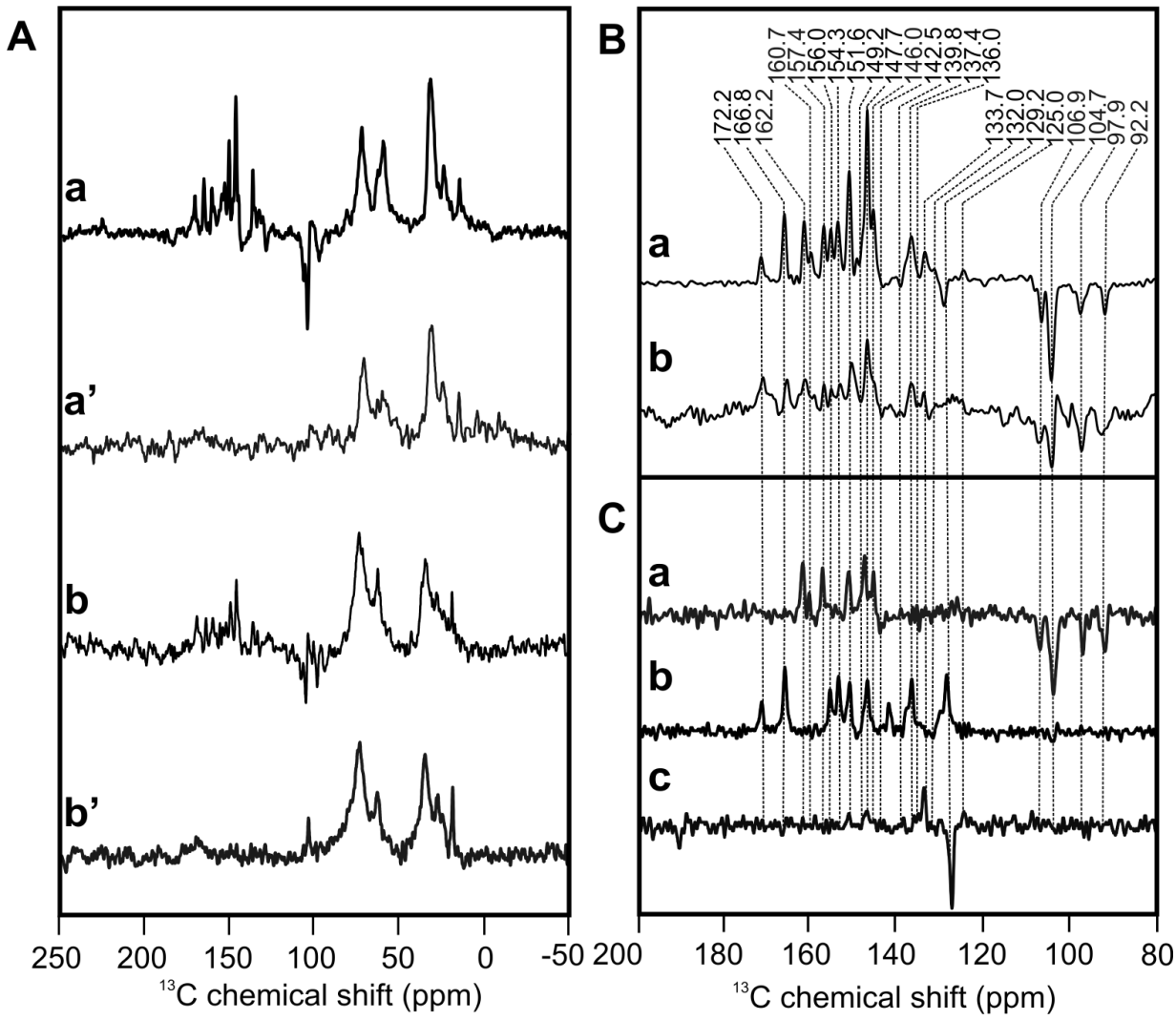

Figure 4.4: (A) ^{13}C photo-CIDNP MAS NMR spectra obtained by continuous illumination of D1D2 particles of spinach with ^{13}C at natural abundance (a) and unlabeled core complexes of duckweed (b). Spectra a′ and b′ depict the corresponding spectra obtained in the dark. (B) Aromatic region of the continuous illumination spectra of Figure 4.3A. (C) ^{13}C photo-CIDNP spectra from PSII in native thylakoid membrane from duckweed plants labeled with ^{13}C 5-ALA (a), 4-ALA (b) or 3-ALA (c).

labeled thylakoid membranes (Figure 4.4C). Upon comparison of the spectrum obtained from unlabeled isolated PSII (Figure 4.4B) with data collected from selectively labeled thylakoid membranes (Figure 4.4C) a remarkable conservation of the relative signal intensities emerges, if the signal overlap at 129.2, 147.7 and 151.6 ppm is taken into account. The chemical shift pattern is the same for the various samples. This clearly demonstrates the conservation of the electronic structure of the PSII Chl *a* donor upon isolation of core particles from thylakoid membranes.

In Table 4.1, the ^{13}C chemical shifts of the photo-CIDNP signals obtained from selectively ^{13}C-labeled thylakoid membranes from duckweed are compared with the signals observed for D1D2 samples of spinach with ^{13}C at natural abundance, literature values of

Table 4.1: ^{13}C chemical shifts of the photo-CIDNP signals of sparsely ^{13}C-labeled PSII embedded in thylakoid membranes from duckweed in comparison with literature data for unlabeled isolated spinach D1D2 and solid state NMR chemical shifts of Chl *a* and Phe *a* molecules or aggregates.

Chl *a*	Phe *a*	Carbon atom	PSII D1D2	PSII Thylakoid
σ_{ss} [a]	σ_{ss} [b]		σ_{ss} [c]	σ_{ss} [d]
190.6	190	13[1]		190.4 e
170.0	171	19	166.8 a 172.2 a	166.6 a 171.9 e
162.0	151	14	162.2 a 151.6 a	162.1 a 151.5 a
155.9	142	1	156.0 a 142.5 e	156.0 a 142.3 a
154.4	156	6	154.3 a	155.0 a 153.9 a
154.0	161	16	157.4 a 160.7 a	157.5 a 160.6 a
150.7	137	4	149.2 a	148.8 a 145.7 a
147.2	138	11	147.7 a	147.2 a
147.2	150	9	146.0 a	147.8 a 146.6 a
146.2	145	8		151.4 a 148.1 a
138.0	136	3	139.8 e 137.4 a	138.2 a 136.9 a
136.1	131	2	136.0 a	-
134.0	128	12	133.9 a	134.2 a?
133.4	136	7	~ 132 a	-
126.2	133	13		130.2 a 128.8 a
126.2	129	3[1]	~ 125 a	127.8 e 124.7 a
108.2	105	10	106.9 e	107.2 e
102.8	107	15	104.7 e	103.9 e 104.8 e
98.1	97	5	97.9 e	97.9 e
93.3	93	20	92.2 e	93.0 e 92.0 e
51.4	52	17		48.9 a 51.0 a
32.5	32	17[1]		29.3 a
20.2	19.8	8[1]		19.6 a

[a] Boender (1995), data obtained from solid aggregates of Chl a (Boender *et al.* 1995).

[b] Egorova (1997) solid state data obtained from plant pheophytin a recomstituted in *Rb. sphaeroides* R26 RCs (Egorova Zachernyuk *et al.* 1997).

[c] Diller et al. (2005), data obtained from D1D2 particles of spinach (Diller *et al.* 2005).

[d] This work, solid state data obtained from specifically labeled thylakoid membranes of duckweed. Abbreviations: σ_{ss} = solid state chemical shift in ppm, a = absorptive signal, e = emissive signal.

signals obtained from Chl *a* aggregates (Boender *et al.* 1995) and the response from plant Phe *a* reconstituted in bacterial RCs (Egorova-Zachernyuk *et al.* 2008). Although all the Chl *a* and Phe *a* molecules that are present in the samples contain 5-, 4- or 3-ALA labeled cofactors, only carbons from cofactors forming the primary radical pair are expected to be enhanced upon illumination due to the solid-state photo-CIDNP effect. The ^{13}C-^{13}C spin diffusion between nearby isotope labels on the same cofactor allows for some equilibration of intensities of signals originating from labeled carbons in direct vicinity of each other (Matysik *et al.* 2001; Daviso *et al.* 2009).

In the spectrum obtained from 5-ALA labeled thylakoid samples, 14 light induced signals can be resolved. Based on a comparison with chemical shifts obtained from solid state data for aggregated Chl *a*, and Phe *a* reconstituted in *Rb*. *sphaeroides* RCs (Egorova-Zachernyuk *et al.* 2008), eight of the 14 signals can be assigned to the Chl *a* donor and 6 to the Phe *a* acceptor. The emissive signals between 90 and 130 ppm, which were assigned previously to the four methine carbons (Matysik 2000; Diller *et al.* 2005), appear in the spectrum obtained from 5-ALA labeled PSII (Figure 4.4C). Hence, the assignment based on selective isotope labelling contribute to converging and convincing evidence from MAS NMR photo-CIDNP studies for a monomeric donor and a monomeric acceptor forming the radical pair (Matysik 2000; Diller *et al.* 2005).

The spectrum obtained from 4-ALA labeled thylakoid membrane preparations shows 15 light-induced signals. Based on a comparison with chemical shifts obtained from solid state data of aggregated Chl *a* (Boender *et al.* 1995), eight of the 15 signals can be attributed to the Chl *a* donor. Interestingly, similar to the 5-ALA spectrum, the eight signals of the Chl *a* donor, in general, are stronger than the remaining seven. Based on their chemical shifts, the remaining seven are tentatively assigned to the Phe *a* acceptor (Egorova-Zachernyuk *et al.* 2008). The C-19 carbonyl of the Chl *a* donor is at rather high field of 166.6 ppm suggesting some local interaction (Diller *et al.* 2005).

The spectrum obtained from 3-ALA labeled thylakoid, which has the ^{13}C labels mostly positioned on aliphatic carbons (Figure 4.3), shows a limited number of light-induced signals compared to the data collected from the 5- and 4-ALA preparations with the ^{13}C isotopes in the macroaromatic cycle. Based on the literature data the strong emissive signal at 128.7 ppm is assigned to the C-3^1 of the Phe *a* acceptor, while the much weaker absorptive 124.7 ppm is assigned to the corresponding C-3^1 of the Chl *a* donor (See Table 4.1 and Figure 4.4 green trace; Boender *et al.* 1995; Egorova-Zachernyuk *et al.* 2008). The emissive

signal at 190.4 ppm is assigned to the C-13^1 carbonyl of the Chl *a* donor. This shift essentially rules out the possibility of the protonation of the C-13^1 carbonyl group in P_{D1} Chl *a* (Matysik 2000) as the possible source of an electric field polarizing the donor. In addition, since the chemical shift is close to the value observed for monomeric Chl *a*, a local chemical perturbation at this carbonyl is unlikely. The absorptive signal at 134.2 ppm is tentatively assigned to the C-12 of the Chl *a* donor and two weak absorptive features at 29.3 and 19.6 ppm (data not shown) match with the ^{13}C-17^1 and ^{13}C-8^1 responses observed for the models.

4.3.3 The involvement of the protein backbone and possible alternative electron spin carriers:

Two weak emissive signals at 142.5 and 139.8 ppm and two absorptive signals at 136.0 and 132.0 ppm that are observed in the spectra for the unlabeled PSII (Figure 4.4B) did not appear in the spectra obtained from PSII in thylakoid membrane that was sparsely ^{13}C labeled in the Chl *a* and Phe *a* and embedded in the thylakoid membrane (Figure 4.4C). While for the unlabeled species all carbons participating in primary charge separation events and carrying electron spin density can be observed by photo-CIDNP, the biosynthetic incorporation of ^{13}C highlights only the carbons of the Chl *a* and Phe *a* pigments, that are adressed by the labeling pathways. All carbons within the aromatic ring, C-1 to C-20, the C-13^1 carbonyl and the aliphatic carbons C-3^1, C-8^1 and C-17^1 are highlighted in either the 3-, 4- or 5-ALA ^{13}C-labeled preparations. The remaining aliphatic carbons of the Chl *a* and Phe *a* cofactors are not expected to carry electron spin density and, according to previous assignments, are not expected to resonate at the frequencies of the additional signals that are observed at 142.5, 139.8, 136.0 and 132.0 ppm. (Boender *et al.* 1995; Egorova-Zachernyuk *et al.* 2008). Therefore, our data strongly suggest that some electron spin density is attached to an amino acid, in addition to the electron spin density that is localized on the Chl *a* and Phe *a* cofactors.

The presence of the signals at 136.0 and 132.0 ppm in the unlabeled samples compared with the response from the set of labeled samples supports the proposal for a spin carrying histidine residue in close proximity of the Chl *a* donor P_{D1} (Matysik *et al.* 2001; Diller *et al.* 2005). Recently it has been suggested that a Chl$^{\delta-}$-His$^{\delta+}$ partial charge transfer motif is a common denominator across photosynthetic RC complexes in plants and bacteria and that this interaction lowers the energy barrier in photosynthetic complexes (Alia *et al.*

2013; Matysik *et al.* 2001; Alia *et al.* 2009). Experiments with selectively ^{15}N-ALA label patterns would be of great interest to arrive at a final conclusion regarding the involvement of electron spin carriers on the protein backbone (See chapter 6 for preliminary results).

It has been suggested that the emissive features at 139.8 and 142.5 ppm can be associated with a Schiff base or a carotenoid molecule (Diller *et al.* 2005, Breitmai and Voelter 1990). However, in contrast with bacterial systems, the carotenoids in PSII are not active as triplet quenchers when Q_A is doubly reduced or absent. If Q_A is singly reduced the carotenoid associated with the D_2 branch ($Car_{D2,}$ see Figure 4.1C) can act as a fast triplet quencher (Martinez-Junza *et al.* 2008). Possibly, a fraction of the PSII in our experiments remains in the singly reduced state providing the possibility for ρ_i buildup and quenching on the carotenoid.

4.3.4 Comparison of the data obtained from labeled BBY, Thylakoids and Plants:

Figure 4.5A compares the photo-CIDNP spectra from BBY (a), thylakoid membranes (b), and from entire plants (c) of selectively 4-ALA ^{13}C-isotope labeled duckweed. Figure 4.4B shows a detailed view of the light-induced spectra of Figure 4.5A. A total of 15 light induced signals can be distinguished and a comprehensive assignment of the Chl *a* donor and Phe *a* acceptor was deduced from the combination of spectra obtained from the sparsely labelled samples (Table 4.1). The pattern of isotope labels for the Chl *a* donor and Phe *a* acceptor, obtained by feeding with ^{13}C 4-ALA, is indicated by the black dots that are shown in the inset in Figure 4.5B. Interestingly, the comparison of the photo-CIDNP spectra of BBY particles, thylakoid membrane and intact leaves did not reveal any significant change. Minor changes in the relative intensities of the signals shifted to 51.0 and 147.2 ppm are observed. These can be attributed to a difference in concentration of RCs in various samples, which is, for example, limited by the small number of plants that fit inside the MAS NMR rotor. Hence both the chemical shifts and the overall intensity pattern are highly conserved among spectra obtained from BBY (spectrum 4.5a), thylakoid (spectrum 4.5b) and plant (spectrum 4.5c), demonstrating that the inner photochemical machinery forming the primary radical pair remains essentially unaffected upon extraction of thylakoid membrane from the plants and upon extraction of PSI from the thylakoid membrane, *e.g.* BBY isolation.

The dark spectra collected from BBY (spectrum a′), thylakoids (spectrum b′) or entire plants (spectrum c′) are very similar (Figure 4.5). The dark spectra show only a very weak

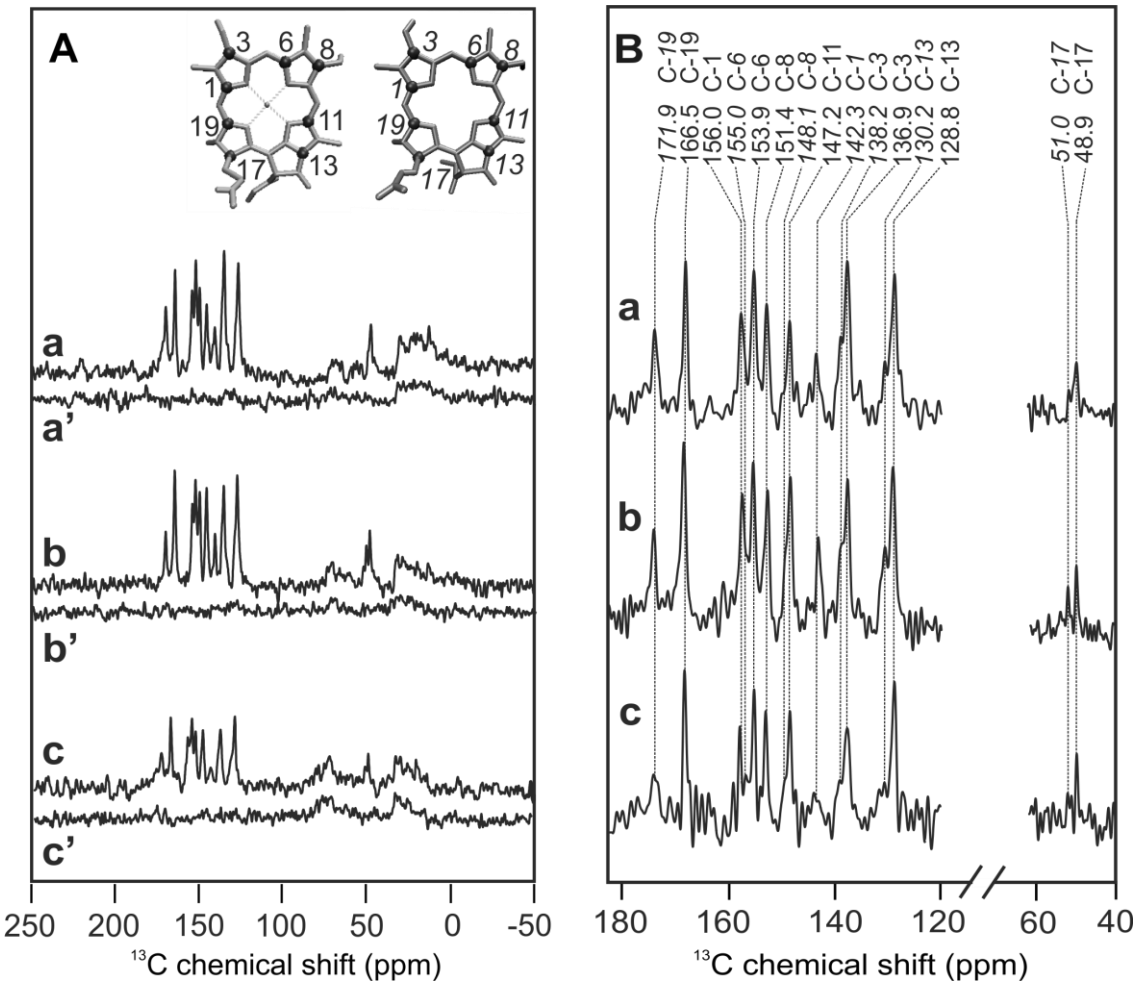

Figure 4.5: ^{13}C photo-CIDNP MAS NMR spectra obtained by continuous illumination of BBY (a) thylakoid membrane (b) and entire plants (c) obtained from selectively 4-ALA ^{13}C-isotope labeled duckweed. Spectra a′, b′ and c′ show the corresponding spectra obtained at dark conditions. B shows the signals occurring in the aromatic and aliphatic regions of the photo-CIDNP MAS NMR spectra. The Chl *a* donor (left) and the Phe *a* acceptor (right) with the positions of the ^{13}C-isotope labeled carbons (black dots) are depicted in upper right corner. The numbering follows the IUPAC nomenclature. Assigned centerbands are visualized by dashed lines. Signals assigned to the Phe *a* acceptor are written in italic.

broad positive signal in the aliphatic region between 0 and 50 ppm and between 60 and 80 ppm from to the ^{13}C-α nuclei at natural abundance in the the amino acids of the protein backbone, which matches the response from the unlabeled samples.

The data provide clear evidence for the same pattern of chemical shifts as well as photo-CIDNP intensities in the light-induced spectra of BBY, thylakoids and plants. Hence we conclude that the inner photochemical machinery is not modified or damaged by any of these isolation steps. While thylakoid and plant samples contain the full photosynthetic machinery, including both PSII and PSI, BBY contains PSII only. While the apparent absence of photochemically active PSI (Alia *et al.* 2004), can be due to several reasons, probably a selective reduction of quinone is most relevant. The quinones on PSII are easily

accessible and instantaneously reduced upon addition of sodium dithionite, which contrasts with the quinones in PSI that are difficult to reduce upon direct freezing and measurement (Feldman *et al.* 2007). To successfully reduce PSI, incubation at room temperature after addition of the reductant, and exposure to light at room temperature and during freezing are necessary (Janssen *et al.* 2010). In addition the pH of the sample environment favours observation of the photo-CIDNP effect in PSII. In *vivo* the active site of PSI is located at the alkaline stroma side of the thylakoid membrane that is in an alkaline environment with pH 8, while PSII functions at the acidic lumen side of the membrane with pH ~4.5 (Anderson *et al.* 2008). Acidic conditions strongly decrease PSI stability and activity (Yang *et al.* 2009) while the donor/acceptor side of PSII is known to remain intact under strong acidic conditions (Mathur *et al.* 2011). In any case, destructive interference of the emissive signals from PSI by the stronger absorptive signals of Chl *a* from PSII in the spectra of thylakoid membranes and plants is very unlikely due to the similarity between the data for the thylakoid preparations and the spectrum collected from BBY particles.

4.3.5 Photo-CIDNP buildup in BBY, Thylakoids and Plants

Since the OEC and the Tyr_Z are oxidized by hole transfer from the P680, the generation of a $P_{D1}^{+}Phe^{-}$ radical pair with sufficient lifetime to produce photo-CIDNP, *i.e.*, some ~10-100 ns, is an experimental challenge (Blankenship *et al.* 1975). In particular for larger PSII systems both the secondary electron acceptor Q_A and the OEC can become active and the electron transfer steps (e_2 to e_4) from the ($P_{D1}^{+}Phe^{-}$) radical pair can quench the photo-CIDNP effect (see Figure 4.2, page 66). The photo-CIDNP results presented here demonstrate that in higher preparations with the OEC the same radical species is present as for the D1D2 preparation without the OEC. The addition of $Na_2S_2O_3$ reductant lowers the pH and leads to slow electron transfer from the OEC to P_{D1}^{+} for higher sample preparations, thereby confining the radical pair for photo-CIDNP buildup. Previous studies have shown that the rate of re-reduction of P_{D1}^{+} (by Tyr_Z) decreases at low pH (Pulles *et al.* 1976). This was attributed to a distortion or breakage of the hydrogen bond between Tyr_Z and the nearby D1-His190, which has an estimated pKa of 4.5-5.3 (Rautter *et al.* 1995) (for a review see Styring *et al.* 2012). Such acidification of the lumen space down to a pH of 5.0 or slightly below also occurs *in vivo* under strong light conditions (Graber and Witt 1976). The pH dependence provides a natural mechanism for physiological regulation of electron transfer from the OEC, allowing for dissipation of excess excitation energy by the RC at high-light

conditions (Rochaix 2011). According to the Kok model, the mechanism for water oxidation is described by the S-cycle (Gorkom and Schelvis 1993). Here S0 to S4 refer to the intermediate redox states in the OEC and S1 is the state that is stable in the dark. After the oxidation of two water molecules and formation of an O-O bond, O_2 is released and the OEC returns from the S4 to the S0 state. The S-cycle is enabled for T > 250K and is strongly inhibited at ~ T = 230K (Styring and Rutherford 1988). In the temperature region of our experiment *T* ~ 235K, the S1 to S2 transition is allowed while the step to S3 and beyond is blocked. At low pH (<5.0) strong inhibition of the S2 to S3 transition occurs at T < 283K (Bernat *et al.* 2002; Suzuki *et al.* 2005). Hence with the experimental conditions employed in the current study the S2 intermediate of the OEC will most probably accumulate. When the OEC converts from the S1 to the S2 state, the reduction rate of P_{D1} slows down from 50 ns to 250 ns at pH 6-7.5 (Rappaport *et al.* 1994).

On the other side of the electron conversion chain, linear electron flow under natural conditions proceeds via the electron transfer step e_2 in Figure 4.2. This leads to depletion of the P_{D1}-Phe *a* radical pair state on a time scale of ~300 ps, which is very short compared to the time scale of the coherent buildup of the photo-CIDNP signal. Hence, for the fraction of the radical pairs that produce the light-induced nuclear polarization, the downstream electron transfer from the Phe *a* is blocked or slowed down considerably at the Q_A acceptor site. For D1D2 preparations quinone removal blocks the electron transfer and leads to radical pairs with sufficient long lifetimes for photo-CIDNP. In core preparations, however, Q_B is lost while Q_A remains bound to the protein pocket (Ghanotakis *et al.* 1987). In higher preparations, both quinones are, at least initially, present. Most likely the Q_B is lost upon reduction prior to the measurement.

To block the downstream electron transfer in core and higher preparations, double reduction of Q_A is necessary. It has been shown to occur under natural conditions at high light intensities, and leads to the release of up to 63% Q_A as Q_AH_2 in 80 min (Koivuniemi *et al.* 1993)). For core preparations, double reduction of Q_A can be significantly enhanced by the addition of a strong reductant and subsequent illumination (Feikema *et al.* 2005; Cox *et al.* 2009). In BBY preparations, illumination for ~10 min followed by 25 min of dark adaptation under reductive conditions at 40 mM sodium dithionite and 100 mM benzylviologen leads to 100% double reduction of Q_A (van Mieghem *et al.* 1995). In their early photo-CIDNP studies on RCs of *Rb. sphaeroides* R26, Zysmilich and McDermott reported significant and characteristic differences between the responses from Q-reduced and

Q-depleted samples (Zysmilich and McDermott 1996). In the photo-CIDNP data collected from PSII, the spectra for D1D2 and core preparations are very similar, which is in line with the converging evidence that Q_A is lost in reduced core preparations. Double reduction and release of Q_A is, in contrast to the release of reduced Q_B, irreversible, since it induces a change in the Q_A protein binding pocket (Vass *et al.* 1992). If oxygen is present, the blocking of ET by the absence of oxidized ('open') Q_A leads to the formation of singlet oxygen species and fast degradation of the D1 protein (minutes at room temperature) (Frank *et al.* 1989; Breitmai.E and Voelter 1990; Durrant *et al.* 1990; Vass *et al.* 1992; Ishikita *et al.* 2005). Under anaerobic conditions double reduction of Q_A increases the radical-pair lifetime from 20 to 250 ns which results in a high triplet yield (Frank *et al.* 1989; Lubitz *et al.* 2002) allowing photo-CIDNP build-up.

Recent data obtained by femtosecond transient absorption studies and theoretical calculations (Novoderezhkin *et al.* 2005; Holzwarth *et al.* 2006; Raszewski *et al.* 2008; Novoderezhkin *et al.* 2011) indicate a coexistence of at least two ET channels at early stages of charge separation (< 20 ns), with a single $P^+_{D1}Phe^-_{D1}$ species at later stages of the photochemistry. Our data reveal a homogeneous steady state at longer time scales. A partial or complete conversion into a photochemically active P^+_{D2} species that could not be excluded by the optical work (Raszewski *et al.* 2008) is unlikely in the steady state observed with photo-CIDNP. Specific shaping of the P_{D2} by the protein environment makes that a correlated radical pair state involving the P^+_{D2} is expected to give rise to a photo-CIDNP signal component with chemical shifts that are different from the P^+_{D1} and hence to signal doubling, while in all the CIDNP data collected from different PSII preparations the same and unique Chl *a* response is observed.

4.3.6 Conclusions

Here we demonstrate that the solid-state photo-CIDNP effect in conjunction with selective isotope incorporation allows for observation of NMR signals, of primary radical pair of PSII, directly from thylakoid membranes as well as from the entire plants (Figure 4.6). At the atomic resolution, it is demonstrated that the active photochemical machinery forming the primary radical pair of PSII is conserved between different higher plant species. In addition our results show that the photochemical machinery is remarkably robust and remains essentially unaffected by the various preparation procedures, since there are very

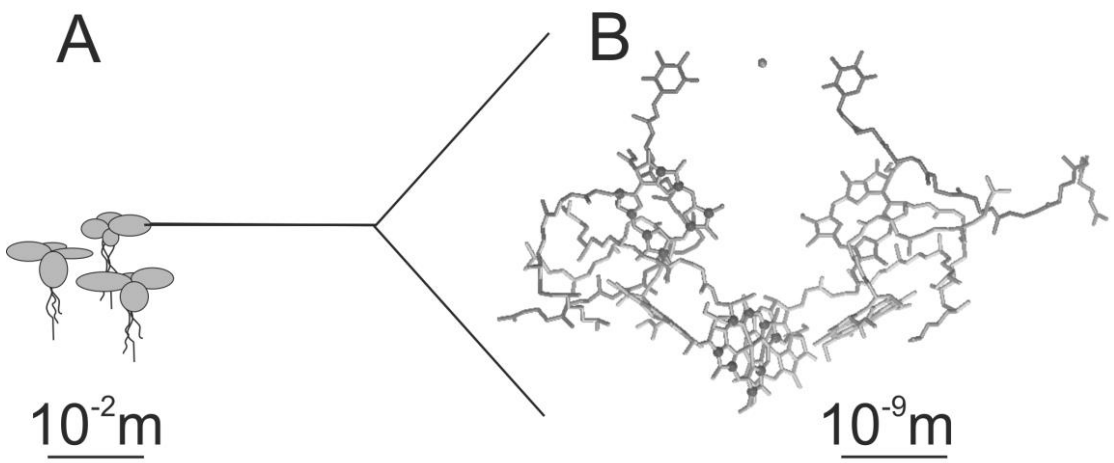

Figure 4.6: By combining specific isotope labeling with the photo-CIDNP technique signals from carbon atoms at labeled positions (B, dark grey balls) within the active Chl *a* and Phe *a* cofactors can be detected and it is possible to cover a range from the macroscopic plant scale of duckweed leaves (A) to the atomic scale of the PSII RC (B). The average adult leaf size of duckweed is 4 mm in length making it suitable to fit in an optically transparent 4-mm sapphire MAS NMR rotor.

little changes in the photo-CIDNP response across sample preparations from plant level to the D1D2 preparation. The data establish that the radical pair is clearly formed by a single Chl *a* and a single Phe *a*. In addition, there is significant empirical evidence for the involvement of the protein matrix. These observations can be explained by assuming the involvement of a histidine carrying a part of the electron spin density. In this chapter an explanation for the mechanism of photo-CIDNP buildup in larger PSII systems has been presented. The observation of photo-CIDNP MAS NMR directly from plants allows future application of this method for testing of the occurrence of radical pairs and the analysis of these in systems in which a further isolation has not yet been established or is too expensive.

Chapter 5

Time-resolved photo-CIDNP MAS NMR on PSI and PSII from plants

Excitation of the electronic states of photosynthetic RCs by nanosecond laser flashes allows for the visualization of transient polarization and provides insight into the mechanisms behind the buildup of polarization during repeated photo-cycles (Daviso *et al.* 2009). ns-flash photo-CIDNP MAS NMR can be applied to study the mechanism of photo-CIDNP buildup and the electronic structure of the active cofactors in PSI and PSII prior to spin diffusion. Up to this point, time-resolved photo-CIDNP MAS NMR experiments were restricted to bacterial systems (Daviso 2008; Daviso *et al*. 2009 and 2010b). In this chapter the first time-resolved photo-CIDNP data sets obtained from plant photosystems will be presented. ns-flash Photo-CIDNP has been applied to uniformly ^{15}N and selectively 4-ALA ^{13}C labeled PSI-110 particles. The experimental results and quantum chemical calculations suggest that the DD mechanism is the dominant mechanism in photo-CIDNP buildup in PSI and that mainly P_B acts as the electron donor. The results are in agreement with bidirectional electron transfer and the observed kinetics provides evidence for a high functional flexibility of PSI. In addition, this chapter discusses time-resolved photo-CIDNP data collected from D1D2 PSII particles of spinach. The results show that photo-CIDNP buildup in PSII resembles the buildup observed for *Rb. sphaeroides* R26 RCs. This can be explained by the relatively long lifetime of the triplet state in PSII and R26, which contrasts with the long triplet lifetime for WT *Rb. sphaeroides* bacterial RCs and PSI.

5.1 INTRODUCTION

5.1.1 Electron-Spin Echo Signals and Time-resolved Photo-CIDNP

In time-resolved photo-CIDNP experiments, excitation of the electronic states of the photosynthetic RC is achieved though illumination with nanosecond laser flashes. Each laser flash has a duration, τ_p ~ 8 ns and is followed by a variable delay time Δt between the laser pulse and the start of the NMR $\pi/2$ detection pulse, which has a duration of ~ 5 μs. This finite pulse length determines the time resolution for the detection of the polarization established by the coherence transfer and decay kinetics in a time-resolved photo-CIDNP experiment.

The buildup of photo-CIDNP occurs on the nanosecond time scale by coherent mixing of nuclear states with the non-stationary electron zero quantum state generated by photoexcitation and charge separation, and is revealed by the subsequent chemical decay kinetics (Figure 5.1). When radical pairs produced by continuous illumination are kept together for ~100 ns, by impairing the electron transfer from the acceptor to the quinone and from the cytochrome or OEC into the donor, the electronic zero quantum coherence of the singlet radical pair is converted into T_0 double quantum coherence by the electron-nuclear hyperfine interactions in what is called nowadays a "quantum biology" process. Net nuclear polarization accumulates from three mechanisms that break the antisymmetry of the population of nuclear spin states, TSM, DD and DR. Both TSM and DD require hyperfine anisotropy. The fully coherent TSM polarization buildup in addition requires a nonzero magnitude of the pseudosecular contribution to the hyperfine interaction, $B = \sqrt{\left(A_{zx}^2 + A_{zy}^2\right)}$. The TSM mechanism is strongest when $2\left|d\right| = 2\left|\omega_I\right| = \left|A\right|$, while the DD mechanism has its maximum when $2\left|\omega_I\right| = \left|A\right|$ (Jeschke and Matysik 2003). In RCs with a long lived triplet donor the DR relaxation mechanism occurs in addition to the TSM and the DD (Jeschke and Matysik 2003). For the DR mechanism, nuclear polarization of the donor in its triplet state is rapidly and selectively depleted by longitudinal paramagnetic relaxation of nuclear polarization during the ^{3}DA triplet lifetime. This exposes the opposite polarization generated via the $^1(D^{+\bullet}A^{-\bullet})$ singlet and $^3(D^{+\bullet}A^{-\bullet})$ triplet decay pathways. In ns-flash photo-CIDNP MAS NMR experiments, the τ_p of the laser pulse used for excitation is shorter than the time scale of the electron-nuclear coherence transfer. This allows for the detection of the primary coherence transfer processes that drive the photo-CIDNP and visualization of the polarization buildup before it spreads into the system by nuclear spin diffusion and relaxes to thermal equilibrium (Daviso *et al.* 2008b). The transfer of nuclear polarization established by

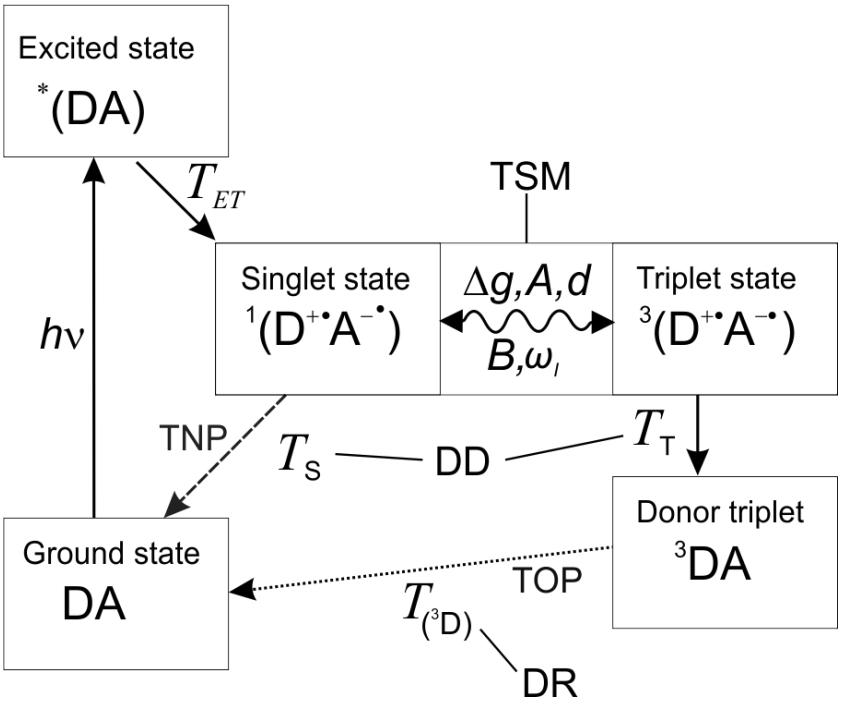

Figure 5.1: The electron-nuclear coherent mixing and chemical decay kinetics for the generation of photo-CIDNP in natural RCs at moderately high field, corresponding with 200-400 MHz ^{1}H NMR frequency. Three mechanisms are thought to be responsible for the buildup of net nuclear polarization in the solid-state, TSM, DD and DR. The evolution from the singlet state $^1(D^{+\bullet}A^{-\bullet})$ to the triplet state $^3(D^{+\bullet}A^{-\bullet})$ and back is accompanied by a transfer of fictitious electron polarization to the nuclei (Jeschke, 1997). In TSM net nuclear polarization is generated in the spin correlated radical pair due to the presence of both the pseudosecular part of the hyperfine interaction (*B*) and the coupling between the two electron spins (*d*), where the antisymmetry is broken in the presence of the nuclear Zeeman interaction (ω_I) in a fully coherent process. The TSM contribution is strongest at the matching condition $|A| \approx 2|d| \approx 2|\omega_I|$. In the DD mechanism, the formation of net nuclear polarization is based on different lifetimes for the singlet and the triplet radical pair states, T_S and T_T, respectively. In the DR, net nuclear polarization is thought to arise from opposite polarization in singlet and triplet radical pairs that do not cancel when part of the triplet-derived polarization relaxes during the triplet lifetime, $T_{(^3D)}$ (McDermott *et al.* 1998). This requires that the longitudinal relaxation time of the nuclei in the RC triplet is shortened to such an extent that it is comparable to $T_{(^3D)}$ (Jeschke and Matysik 2003; Daviso *et al.* 2007). The dashed arrow indicates the path of the transient nuclear polarization (TNP) generated in the singlet radical state and detected in the ground state. The dotted arrow indicates the path of the transiently obscured polarization (TOP) induced by the paramagnetic triplets. Nuclear polarization becomes observable when the excited triplet states decay to the ground state.

the photo-CIDNP effect by spin diffusion on the ms time scale was demonstrated in studies of ^{13}C ALA labeled RCs, with ^{13}C nuclei incorporated pairwise into the BChl cofactors. In addition, time-resolved photo-CIDNP experiments allow for the selective observation of nuclear polarization visualized through decay to the groundstate via the $^1(D^{+\bullet}A^{-\bullet})$ chemical species at $T_{(^3D)} > \Delta t > T_S$. As described earlier by Polenova and McDermott, the initial radical pair singlet is unpolarized and fully occupied at time, $t = T_{ET,}$ after which the molecular triplet species, ^{3}DA, and both singlet, $^1(D^{+\bullet}A^{-\bullet})$, and triplet, $^3(D^{+\bullet}A^{-\bullet})$, radical pair states get populated and polarized (Polenova and McDermott 1999). At $T_{(^3D)} > t > T_S$, the ground state is populated with a preference for a nuclear beta state due to the relative fast decay to the

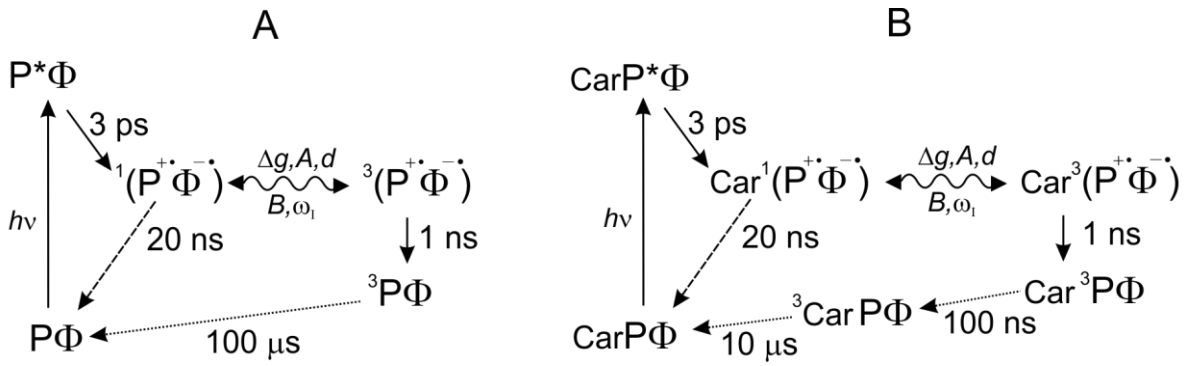

Figure 5.2: Kinetics and spin dynamics of electron transport for quinone-depleted RCs of the carotenoid-less strain R26 of *Rb. sphaeroides* (A) and for the corresponding wild type (B). After the absorption of a photon to produce the photochemically excited state of the primary donor P*, an electron is transferred to the primary acceptor Φ, a bacteriopheophytin cofactor. This leads to the initial singlet radical pair $^{1}(P^{+\bullet}\Phi^{-\bullet})$ in a non-stationary state, which can be represented as a polarized fictitious electron spin state (Jeschke 2008). Electron back transfer leads to the initial electronic ground state with a T_S of 20 ns. Due to hyperfine interaction with nuclei, the singlet radical pair coherently evolves into a triplet radical pair $^{3}(P^{+\bullet}\Phi^{-\bullet})$. Net nuclear polarization is produced by unbalancing the decay branches of the singlet and the triplet radical pair. (B) In *Rb. Spaeroides* WT the triplet donor ^{3}P is quenched by a nearby carotenoid, leading to a triplet excited state (^{3}Car) with a lifetime of ~10 μs. The dashed arrows indicate the path and timing of the transient nuclear polarization associated with the singlet radical state and detected in the ground state (Daviso 2008). The dotted arrows indicate path and timings of the transiently obscured polarization induced by paramagnetic triplets.

groundstate via the $^{1}(D^{+\bullet}A^{-\bullet})$ chemical species. From $t > T_{(^{3}D)}$ onward, all molecules are in the ground state and polarized (Polenova and McDermott 1999).

5.1.2 Photo-CIDNP buildup in bacterial RC

Time-resolved ns flash photo-CIDNP MAS NMR has been applied to bacterial RCs of *Rb. sphaeroides* WT and its carotenoid deficient mutant R26 to resolve the electronic structure of the primary electron donor and establish the mechanism of photo-CIDNP buildup (Daviso 2008; Daviso *et al*. 2009 and 2010b). Figure 5.2 summarizes the essentials of the decay kinetics and coherent spin dynamics. In WT RCs the Car is within van der Waals distance of the special pair. This leads to rapid quenching of the triplet donor via the formation of an excited ^{3}Car triplet state with a lifetime of ~10 μs. For the WT initially weak positive donor signals are observed due to the excess of nuclear polarization generated through decay to the groundstate via the singlet radical state before (see Figure 5.2 and Daviso *et al.* 2009). The initial rapid phase is followed by a gradual buildup of an entirely emissive spectrum reaching maximum signal intensity at Δt = 100 μs to match the $T(^{3}P)$, with a resonance profile that is similar to the entirely negative spectrum obtained with continuous illumination. In the R26 carotenoid-less mutant, maximum intensity was observed at Δt = 0 μs, no sign inversion occurred and the pattern of the light induced signals

in the aromatic region was similar to the spectral response observed with continuous illumination. In both WT and R26 maximum signal intensities for the aliphatic carbons are observed with NMR detection immediately following the laser pulse, *i.e.* with Δt = 0 µs (Daviso *et al.* 2010). These signals quickly diminish below the noise level upon increasing the Δt, which was attributed to polarization with opposite sign generated via recombination of the radical pair through the triplet branch versus recombination through the singlet branch (Poleneova and MCDermott, 1999). Based on experimental data and computational analysis, it was put forward that a predominant TSM contribution leads to the observation of emissive photo-CIDNP signals while a predominant DD contribution results in the observation of absorptive signals (Jeschke and Matysik, 2003; Daviso, 2008). In systems with a long living donor triplet, *e.g.* R26 mutants and PSII, an active DR mechanism will cause sign inversion of signals originating from the donor (Prakash *et al.*, 2006). On the other hand significant back transfer from a long living ^{3}P state into the radical pair will result in an inversion of both the donor and the acceptor signals (Chidsey *et al.*, 1985; de Winter and Boxer, 2003; Daviso, 2008 page 19).

Time-resolved photo-CIDNP experiments have not yet been reported for PSI and PSII. In this chapter we present time-resolved photo-CIDNP data obtained from uniformly ^{15}N and selectively 4-ALA ^{13}C labeled PSI and from PSII with ^{13}C at natural abundance, in order to study the mechanism of photo-CIDNP buildup prior to spin diffusion and the electronic structure of the active cofactors in PSI and PSII.

5.2 MATERIALS AND METHODS

5.2.1 Preparation of uniformly ^{15}N- and selectively ^{13}C labeled PSI and natural abundance PSII particles.

Uniformly ^{15}N labeled duckweed plants were grown under aseptic conditions on half-strength Hunter's medium (Posner 1967) with continuous illumination (20 µEm^{-2}s^{-1}) at 25 °C, as described in chapter 3 of this thesis (section 3.2.1). To provide a source of isotope labeled nitrogen, the KNO_3 in the medium was substituted by 5.5 mM of $^{15}NH_4{}^{15}NO_3$, and in addition $Ca(NO_3)\bullet 4H_2O$ was replaced by 4 mM $CaCl_2$. After 7 days plants were harvested, frozen in liquid nitrogen and stored at -80 °C until use. For selective ^{13}C labeling fully grown plants were exposed to 4-ALA δ-aminolevulinic acid (Cambridge Isotope Laboratories), isotopically ^{13}C labeled at carbon position 4. The labeled precursor was added in steps to a

final concentration of 1.4 mM in half-strength Hunter's medium at pH 4.8. After 7 days plants were harvested, frozen in liquid nitrogen and stored at -80 °C until further use. The PSI complex containing ~110 Chl/P700 (PSI-110 particles) was prepared according to the method described by Alia *et al.* 2004. Isolated D1D2 particles from duckweed plants with ^{13}C and ^{15}N at natural abundance were prepared as described earlier in Matysik *et al.* (Matysik 2000).

5.2.2 Time-resolved ns-flash photo-CIDNP MAS NMR experiments

The ns-flash photo-CIDNP MAS NMR experiments were performed with a DMX-200 or a DMX-400 NMR spectrometer (Bruker Biospin GmbH, Karlsruhe, Germany). The NMR probehead was coupled to a Nd:YAG laser (SpectraPhysics Quanta-Ray INDO 40-10, Irvine CA, USA) producing 532-nm laser flashes with an energy between 20 and 270 mJ at 1-4 Hz. For the current study laser flashes with an energy of 200 mJ have been applied. The electronic and optical coupling of the NMR probe with the laser, and the pulse sequence employed in time-resolved photo-CIDNP MAS NMR, are described in detail elsewhere (Daviso 2008). Laser flashes with a duration of ~8 ns were applied, and were separated by a variable evolution period Δt from the NMR $\pi/2$ detection pulse. After each repetitive cycle the residual polarization was erased with an NMR presaturation pulse sequence (Daviso *et al.* 2008b). All data reported in this chapter were obtained at a sample temperature of 235 K and with a spinning frequency of 8 kHz.

5.3 RESULTS AND DISCUSSION

5.3.1 Time-resolved photo-CIDNP experiments on uniformly ^{15}N labeled PSI

Figure 5.3 (see page 93), shows spectra obtained from uniformly ^{15}N labeled PSI-110 particles of duckweed collected with ns laser flashes and with Δt = 0, 10, 100 and 1000 µs (Figure 5.3A, black, green, orange and pink trace respectively). In addition, a spectrum recorded with continuous illumination is shown (Figure 5.3B). A principle difference between the time-resolved spectra in Figure 5.3A and the data obtained with continuous illumination in Figure 5.3B, is a sign inversion for the N-IV signals observed at 247.8, 250.1 and 253.0 ppm, and the N-III signal at 193.3 ppm. The N-II signal occurring at 206.3 ppm in trace B is not visible in trace A.

Table 5.1: ^{15}N chemical shifts for resonances observed by time-resolved photo-CIDNP MAS NMR. Data were obtained from uniformly ^{15}N labeled PSI from duckweed at 4.7 T with Δt = 0 µs, and are compared with literature values from steady state photo-CIDNP experiments and chemical shift predictions by quantum chemical calculations.

Chemical shifts						
Chl *a*	assignment atom	P_B	P_A	A_{0B}	A_0	A_{0A}
σ_{LS}[a]		σ_{SS}	σ_{SS}	σ_{SS}	σ_{SS}	σ_{SS}
186.0	N-I	**186.3 a**	**184.0 a**		**188.6 a**	
		195.6	*193.3*	*196.3*		*192.7*
206.5	N-II	**211.4 e**	**-**		**210.0 a**	
		210.0	*212.1*	*208.3*		*207.3*
189.4	N-III	**191.0 e**	**193.3 e**		**195.7 e**	
		196.9	*198.9*	*193.2*		*194.0*
247.0	N-IV	**254.3 e**	**250.1 a**		**247.8 a**	
		263.2	*255.5*	*252.1*	**253.0 a**	*248.3*
	His-N_τ	**225.4 a**	**-**			
		231.3	*239.5*			

[a] Boxer *et al.* (1974), data obtained in the liquid state from Chl *a* dissolved in $CDCL_3$. Abbreviations: σ, chemical shift, a, absorptive signal, e, emissive signal, LS liquid state, SS solid state. Bold printed chemical shifts represent experimental data, while italic printed chemical shifts are from quantum chemistry calculations (see Apendix B).

Quantum chemical calculations using a triple-zeta basis set and the SAOP model potential were performed to calculate the chemical shifts and ρ_i for the active cofactors in PSI (performed by Bela Bode, see Appendix B). Table 5.1 shows a tentative assignment of the ^{15}N photo-CIDNP signals obtained by time-resolved photo-CIDNP experiments on PSI in a magnetic field of 4.7 T and with Δt = 0 µs (Figure 5.3A, black trace). The assignment is based on the chemical shifts predicted by the calculations, printed in italic in Table 5.1. According to the calculations the cation is mainly localized on the P_B, which is in line with earlier QM/MM calculations and EPR and ENDOR experiments (Käss *et al.* 2001, Saito and Ishikita 2011).

The Mg^{2+} ions of the P_A and P_B cofactors are coordinated to respectively the His residues 680 and 660 of the protein backbone. The quantum chemical modeling predicts that part of the ρ_i is on the imidazole side chain of the histidine residue His680 that is in close proximity to the P_B donor. The chemical shift for the His-N_τ in the calculations is 231.3 ppm (see Table 5.1 and Appendix B). The signal appearing at 225.4 ppm in the datasets obtained from duckweed PSI with Δt = 0 (Figure 5.3A, black trace), is tentatively assigned to the His-N_τ that is coordinated to the Mg of P_B. The 225.4 ppm signal is not visible in the spectra obtained by continuous illumination of the PSI complex from duckweed (Figure 5.3B), while it has been observed earlier in photo-CIDNP MAS NMR data obtained by continuous

illumination of spinach PSI complex, when a short cycle delay of 0.4 s was applied (Diller *et al.* 2007).

The calculations predict mostly emissive signals for the ^{15}N nuclei of P_B and P_A after a single photocycle, except if a negative exchange coupling or unusually long triplet lifetimes were assumed. In line with the relatively short triplet lifetime of T_{3D} ~ 3 µs determined experimentally (Polm and Brettel 1998), mostly emissive photo-CIDNP signals are observed (Figure 5.3A). In addition to the emissive signals, absorptive signals of relatively weak intensity occur at 250.1, ~247, 225.4, 210.0, 188.6 and 186.3 ppm. According to the calculations, TSM leads to a pure emissive spectrum the DD mechanism would give rise to both emissive and absorptive signals. Since both absorptive and emissive signals are observed in the data presented in Figure 5.3A (black trace) the polarization buildup is in line with a dominant DD mechanism. The absorptive signals at 250.1, ~247, 225,4 and 186.3 ppm, have a maximum intensity at Δt = 0 µs (Figure 5.3, black trace) and disappear gradually upon increasing the Δt to 10 µs (Figure 5.3A, green trace) or 100 µs (signal at 188.6 ppm, Figure 5.3A, orange trace). The only exception is the absorptive signal observed at 210.0 ppm, which is present in both the time-resolved and the continuous illumination spectra and increases in intensity upon prolonging the delay time from 0 µs (Figure 5.3A, black trace) to 1 ms (Figure 5.3A, pink trace). The enhanced absorptive signals observed at Δt = 0 can be attributed to a fast decay of the radical pair via the singlet branch, which occurs at the ns timescale. The signal disappears due to the buildup of nuclear polarization with an opposite sign via the triplet branch upon increasing the Δt (see Figure 5.1). In contrast with the pure absorptive spectrum at Δt = 0 µs that was observed for the WT bacterial RC, the spectrum obtained from duckweed PSI shows strong emissive signals for Δt = 0 µs. In addition both absorptive and negative signals decrease in intensity upon increasing the delay time. This can be explained by the the triplet lifetime of $^3[P700^{+\bullet}A_0^{-\bullet}]$, which has been determined to be T_T ~3 µs (Polm and Brettel 1998). This is much shorter than the decay via the carotenoid triplet for the WT bacterial RC, which takes T_{3D} ~10 µs (see Figure 5.2B). Due to the short donor triplet lifetime in combination with the limited time resolution due to the finite NMR $\pi/2$ pulse length of 5 µs, both the polarization associated with the initial non-stationary $^1(D^{+\bullet}A^{-\bullet})$ singlet radical pair state and and the response due to the population of the $^3(D^{+\bullet}A^{-\bullet})$ triplet radical pair generated by the coherent evolution can be observed in the spectra obtained with Δt = 0 and only a residual excess of polarization associated with decay via the $^1(D^{+\bullet}A^{-\bullet})$ singlet radical pair state can be expected.

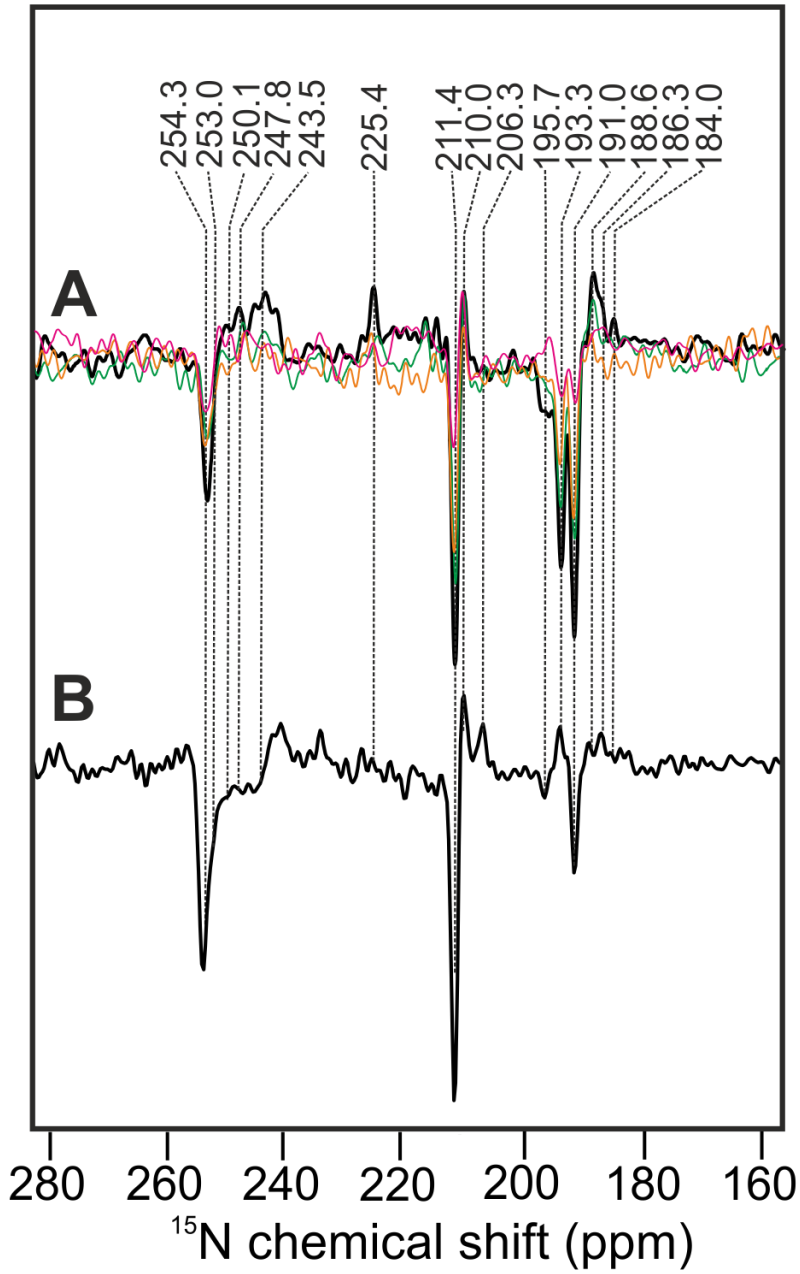

Figure 5.3: ^{15}N-photo-CIDNP MAS NMR spectra obtained from ^{15}N labelled duckweed PSI by ns-flash photo-CIDNP NMR with Δt = 0 µs (A, black trace), Δt = 10 µs (A, green trace), Δt = 100 µs (A, orange trace), Δt = 1 ms (A, pink trace) and by continuous illumination (B) of uniformly ^{15}N labeled PSI-110 particles of duckweed in a magnetic field of 4.7 T and at a temperature of 235K. For the continuous illumination experiments a recycle delay of 4 s was applied.

Upon prolonging the delay time to Δt = 1 ms, no further sign inversion was observed and the changes in relative intensity are small. For 100 µs < Δt < 1 ms (Figure 5.3, orange and pink trace, respectively), the response is different from the steady-state illumination spectrum. This contrasts with the time-resolved photo-CIDNP responses observed for the bacterial RC and for PSII. For these two systems there is apparently a good match between the time-resolved data at longer Δt and the response obtained by continuous illumination

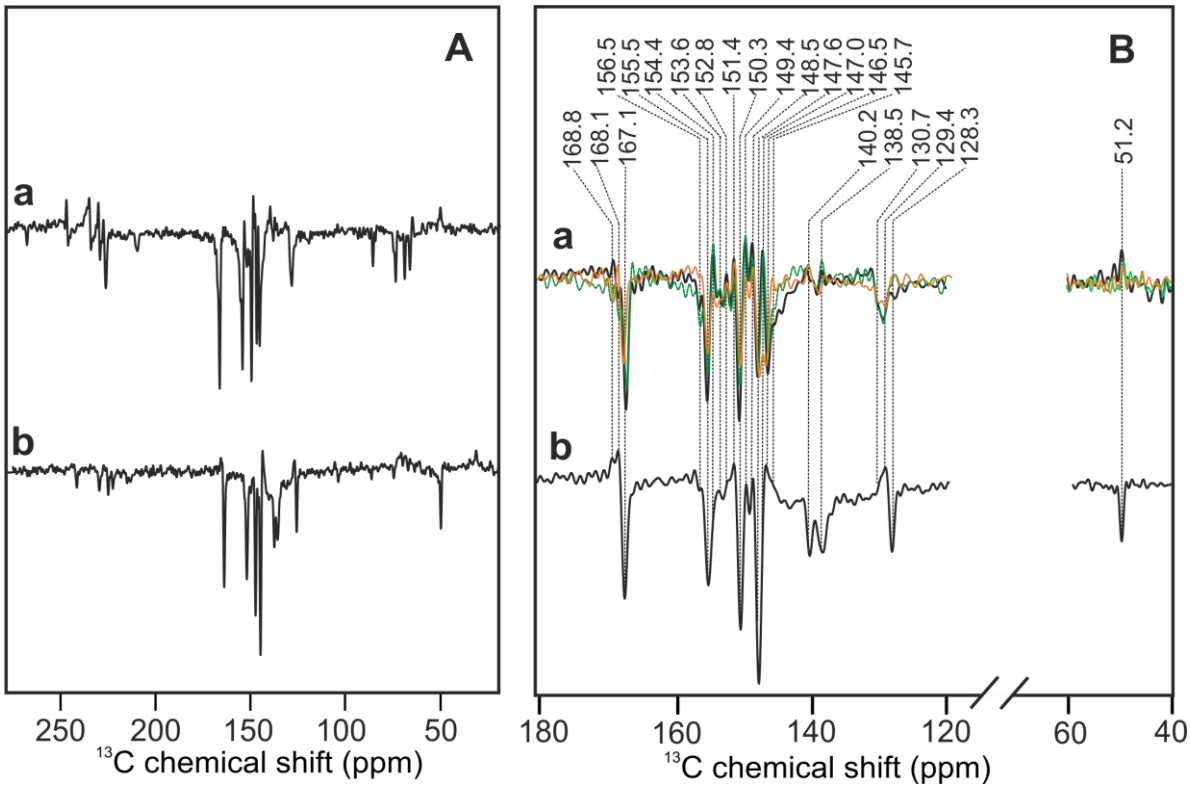

Figure 5.4: (A) ^{13}C photo-CIDNP MAS NMR spectra obtained by laser flash illumination with Δt = 0 µs (a, black trace) and by continuous illumination (b) of 4-ALA labeled PSI particles of duckweed. The signals occurring above 200 ppm and between 55 and 80 ppm are spinning sidebands. Figure B shows the aromatic and aliphatic regions of spectra a and b in A, with the dashed lines indicating the centerbands of the light induced signals. In addition the spectra collected with Δt = 10 µs (green trace) and Δt = 100 µs (orange trace) are depicted. The datasets were collected at a magnetic field strength of 9.4 T, with a recycle delay of 4 s, and using a spinning frequency of 8 kHz.

(Daviso *et al.* 2010 and Figure 5.6). A possible explanation could be that the high energy laser pulses induce trapping of the PSI system in a different state than for continuous illumination. The photo-CIDNP spectrum obtained by continuous illumination shows absorptive signals, while sign inversion is observed for signals associated with both the donor and acceptor upon comparison of the data obtained by continuous illumination. Hence the time-resolved data obatained with Δt = 0 could imply a long lived ^{3}D state. This provides additional support for the high functional flexibility of PSI discussed in chapters 3 and 6.

5.3.2 Time-resolved photo-CIDNP experiments on 4-ALA ^{13}C labeled PSI

Figure 5.4 shows spectra obtained from 4-ALA ^{13}C labeled PSI-110 particles of duckweed collected with ns-laser flashes with Δt = 0 µs (Figure 5.4a), and with continuous illumination (Figure 5.4b). The absorptive signals at 154.4, 152.8, 149.4, 148.5, 147.6, 140.2, 138.5, 128.5 and 51.2 ppm are more pronounced in the dataset obtained with time-resolved

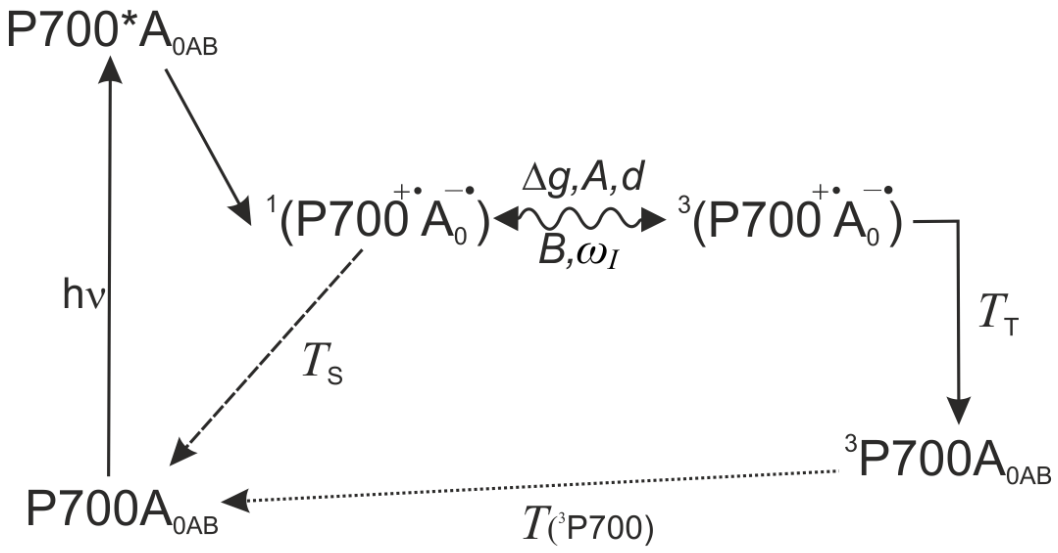

Figure 5.5: Reaction cycle in PSI with reduced F_X and bidirectional electron transfer over both the A and B cofactor branch. After absorption of a photon, ET occurs from the P700 donor to the primary acceptor A_0. Upon reduction of F_X the singlet radical pair lifetime (T_S) increases and the initial pure singlet states are converted into triplet radical pairs and back by coherent evolution. This leads to hyperpolarization of the nuclear states in a complex process, which occurs due to the difference of the *g* values between the two electrons, Δg, the secular part of the hyperfine interaction, *A*, the coupling between the two electrons, *d*, the pseudo-secular hyperfine coupling, *B*, and the nuclear Zeeman frequency, ω_I. The direction of the excitation and decay after light induced electron transfer from the P700 donor to the A_{0A} and A_{0B} Chl *a* acceptors of respectively the A and B cofactor branch, are shown in solid arrows. The radical pair generated upon illumination in PSI decays via the singlet or triplet branch back to the groundstate ($P700A_{0AB}$) with a triplet lifetime, $T_{(^3P700)}$ ~3 µs (Polm and Brettel 1998).

photo-CIDNP at Δt = 0 µs, compared to the same signals in the data that were collected with continuous illumination. In addition, the signals observed with 168.1, 146.5, 145.7, 130.7 and 129.4 ppm chemical shift are emissive in the time-resolved response (Figure 5.4Ba), and absorptive in the spectrum obtained by continuous illumination (Figure 5.4b). When the delay time between the laser pulse and NMR detection is increased to Δt = 10 µs and Δt = 100 µs, the emissive signals at 167.1, 150.3 and 155.5 ppm decrease in intensity. A similar trend is observed for the absorptive signal occurring at 148.5 ppm. It can be observed in the datasets with Δt = 0 µs and Δt = 10 µs, while for the dataset collected with the longer Δt = 100 µs there is no evidence for this response (Figure 5.4A, black, green and orange trace respectively). The aliphatic signal at 51.2 ppm decreases below the noise level for the datasets collected with Δt = 10 and 100 µs.

Based on the quantum chemical shift calculations using a triple-zeta basis set and the SAOP model potential in Appendix B, the response between 167.1 and 168.8 ppm is attributed to the C-19 of the Chl *a*. According to the calculations, the cation is mainly localized on the P_B, which is in line with previous QM/MM calculations and EPR and

ENDOR experiments (Davis *et al.* 1993; Käss *et al.* 2001, Saito and Ishikita 2011). Based on our calculations the response that appears most upfield at 168.8 ppm and has the strongest signal intensity in comparison to the other signals appearing in the C-19 region, is assigned to the P_B cofactor (Figure 5.4B and Appendix B).

The signal arising at 147.0 ppm appears as an absorptive signal of moderate intensity at Δt = 0 and Δt = 10 µs, while it appears as a strong emissive peak at Δt = 100 µs (Figure 5.4Ba) or when continuous illumination is applied (Figure 5.4b). Based on the quantum chemical calculations this signal is tentatively assigned to the C-8 of the P_A or P_B cofactor (see Appendix B). Yet due to the large signal overlap, especially in the region between 140 and 160 ppm and the high functional flexibility of PSI, it is difficult to arrive at a definite assignment of the NMR response at this point. Also the differences between the chemical shifts predicted for the three Chl *a* cofactors (P_B, A_{0A} and A_{0B}) and the one Chl *a*' cofactor (P_A) by calculations are very small (see Appendix B). 2-D and 3-D NMR experiments are proposed in chapter 6 to arrive at a conclusive signal assignment and determine the relative activity in electron transfer for the two cofactor branches in PSI.

Figure 5.5 shows a schematic representation of the spin dynamics of the electron transport in PSI. Both the primary ($P700^{+\bullet}A_0^{-\bullet}$) and subsequently the secondary ($P700^{+\bullet}A_1^{-\bullet}$) radical pair contribute to $^3P700$ buildup (Polm and Brettel 1998). In addition it has been demonstrated that in PSI both cofactor branches are active in ET (Fairclough *et al.* 2003; Ramesh *et al.* 2004; Poluektov *et al.* 2005; Santabarbara *et al.* 2005; Santabarbara *et al.* 2010). This increases the number of radical pairs that can contribute to P700 triplet buildup to four: $P700^{+\bullet}A_{0A}^{-\bullet}$, $P700^{+\bullet}A_{1A}^{-\bullet}$ $P700^{+\bullet}A_{0B}^{-\bullet}$, and $P700^{+\bullet}A_{1B}^{-\bullet}$. However due to the relative large distance between the P700 and the secondary acceptors A_{1A} and $A_{1B,}$ only the primary radical pairs, $P700^{+\bullet}A_{0A}^{-\bullet}$ and $P700^{+\bullet}A_{0B}^{-\bullet}$, are expected to occur at the magnetic field strengths of 4.7 and 9.4 T employed in the current study (Jeschke *et al.* 2011; Figure 5.5).

Upon illumination the PSI forms radical pairs with the electron donor P700 as the radical cation and either the Chl *a* cofactor A_{0A} on the A branch or A_{0B} on the B branch as the radical anion. The relative activity of the A and B branch is known to depend on the organism, cyanobacteria or green algae and plants, and the reduction state of the quinone A_{1A} (Ali *et al.* 2006). In cyanobacteria the relative activity of the B-branch is only 30% while in algae and green plants the activity of the A and B branches are about equal. However upon photo-accumulation of A_{1A}^- after the complete reduction of the F_X cluster, the relative

contribution of the B branch increases and becomes dominant (Santabarbara *et al.* 2006). This will be discussed further in chapter 6.

Reduction of the tightly bound phylloquinones in PSI is much less straightforward than the reduction of the quinones in PSII, which are promptly reduced upon the addition of the chemical reductant dithionite in the dark (Brettel and Golbeck 1995; Rigby *et al.* 1996; Kandrashkin and van der Est 2004; Karyagina *et al.* 2007). Upon dithionite incubation of PSI in the dark only the F_A and F_B clusters are partly reduced, 5 min of subsequent illumination at 205 K reduces the major part of the F_X clusters. When the temperature is increased, a longer photo-accumulation time is required to obtain a similarly large fraction of reduced F_X, *e.g.* a 200% increase of illumination time is required at 220 K (Santabarbara *et al.* 2006). Reduction of F_X causes the formation of the $P700^{+\bullet}A_1^{-\bullet}$ radical pair. Upon prolonged illumination at a high pH of 8 to 10.5, eventually all F_X will reduce. When F_X is reduced, forward ET past A_1 is blocked, which leads to the photo-accumulation of A_1^- and eventually A_0^-. It is suggested that the conditions during our photo-CIDNP experiments result in a relative slow reduction of the F_X cluster due to the relatively high temperature (235 K) and a pH of 9.5. Thus in the initial phase of the photo-CIDNP experiment the F_X will gradually become reduced, resulting in an increasing fraction of the $P700^{+\bullet}A_0^{-\bullet}$ radical pair, which evolves by coherent evolution of the electron-electron zero quantum coherence to the triplet radical and recombines to the $^3P700$ A_0 triplet (see Figure 5.5) allowing photo-CIDNP buildup. The change in the relative contribution of the A and B branch in ET and the changing fraction of reduced F_X, cause additional kinetic effects in the observed photo-CIDNP buildup in PSI, which complicates the interpretation. Due to the high similarity in the environment of the A_{0A} and A_{0B} cofactors and the minimal chemical shift dispersion of the ^{13}C signals, 2D NMR experiments will be required to visualize the relative participation of the two branches in ET (see chapter 6, section 5).

5.3.3 Time-resolved ^{13}C photo-CIDNP MAS NMR experiments on PSII

Spectrum B in figure 5.6 was measured with continuous illumination of PSII D1D2 particles from spinach. Figure 5.6A shows the polarization for the same sample at Δt = 0 µs, obtained by ns laser flash photo-CIDNP. Both spectra are very similar and for longer evolution time Δt = 10 µs and Δt = 1 ms (Figure 5.6A, black, green and pink trace respectively), no sign inversion was observed and changes in the signal pattern in the aromatic region remain

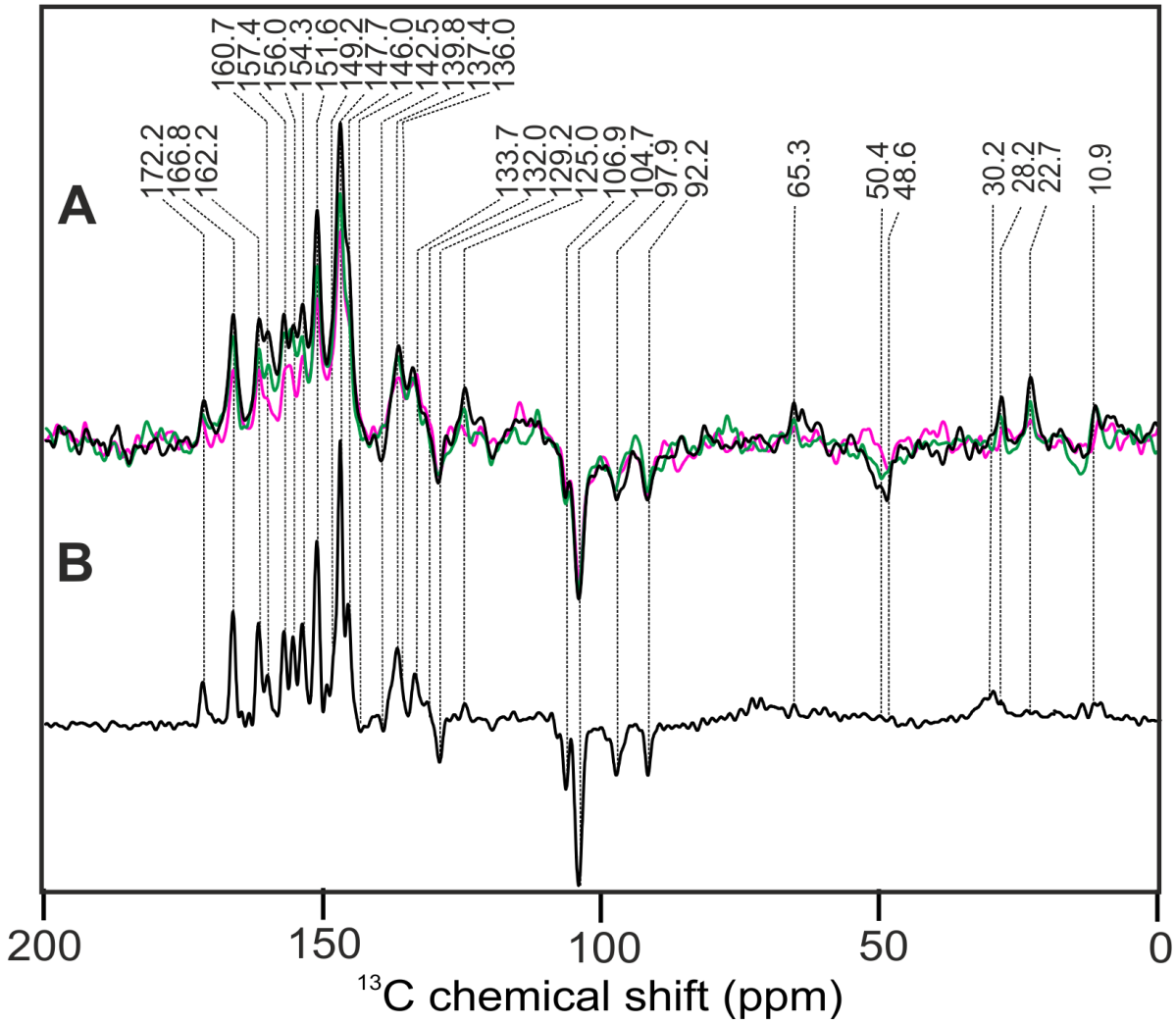

Figure 5.6: ^{13}C photo-CIDNP MAS NMR spectra collected from natural abundance D1D2 PSII particles of spinach with ns-flash photo-CIDNP NMR and (A) a Δt = 0 µs, black trace; Δt = 10 µs, green trace, and Δt = 1 ms, pink trace. The spectrum obtained by continuous illumination is shown in trace B. The data were collected in a magnetic field of 4.7 T and at a temperature of 235 K. Assigned MAS centerband signals are indicated with dashed vertical lines.

within the noise level. Maximum signal intensity was obtained at Δt = 0 µs, with the intensity of all signals decreasing upon prolonged evolution. The aliphatic carbons appear in the continuous illumination spectrum as broad signals of low intensity at 10 and 30 ppm (5.6B). Yet at Δt = 0 µs they are highly resolved and at maximum intensity (Figure 5.6B black trace) after which they disappear upon increasing the delay to 1 ms (Figure 5.6A).

The kinetic scheme of photo-CIDNP buildup in PSII systems was resolved in chapter 4 and is summarized in Figure 5.7. In PSII the negative polarization associated with the ($^3P_{D1}Phe_{D1}$) triplet is fully erased by the DR mechanism for the aromatic carbons at the (P_{D1}) donor side due to paramagnetic longitudinal relaxation occurring during the long lifetime of the ($^3P_{D1}Phe_{D1}$) triplet. Since the anisotropy for the aliphatic carbons is negligible,

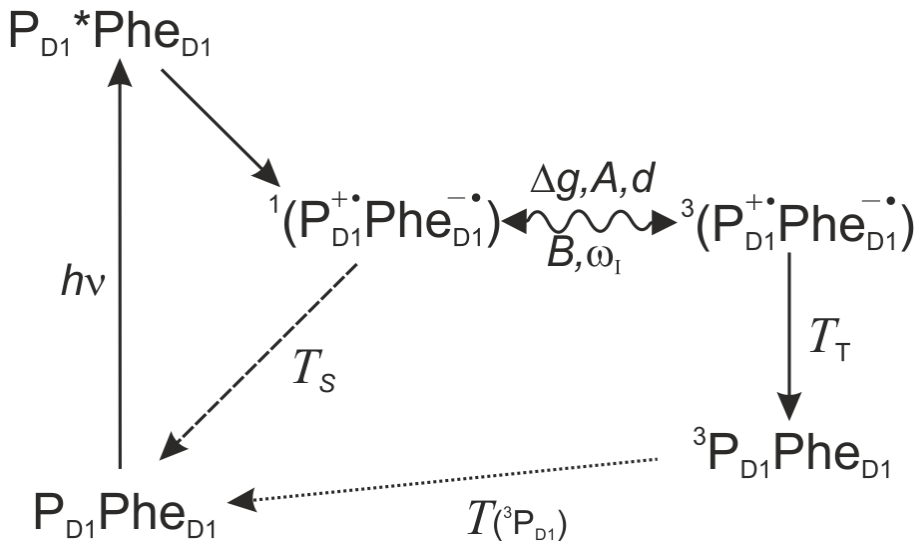

Figure. 5.7: Kinetics and spin dynamics of electron transport for quinone blocked PSII systems and for D1D2 preparations lacking both quinones. Upon removal or double reduction of Q_A the lifetime of the singlet radical pair $P_{D1}^{+\bullet}$ $Phe_{D1}^{-\bullet}$ increases from 20 ns to 250 ns allowing for coherent evolution to the triplet state and photo-CIDNP build-up by the TSM, DD and DR mechanisms.

the contributions from the TSM and DD mechanisms to net polarization buildup and the paramagnetic relaxation (DR) are very weak. The transient observation of the aliphatic signals that are visible at Δt = 0 µs is due to the fast (T_S ~ 250 ns) recombination of the singlet radical pair to the ground state during the NMR detection pulse. The lifetime of the triplet excited state in PSII is 1-3 ms (Hillmann *et al.* 1995; van Mieghem *et al.* 1995), which is considerably longer than the 100 µs found in R26 RCs (Daviso et al. 2009). Therefore the signals in the aliphatic region are gradually quenched by decay via the triplet branch upon increasing the Δt to 1 ms (Figure 5.6A, pink trace).

5.3.4 Conclusions and outlook

In this chapter the first time-resolved photo-CIDNP data from PSI has been presented, by applying ns- laser flash photo-CIDNP MAS NMR to uniformly ^{15}N and 4-ALA ^{13}C labeled PSI. The results suggest that the DD mechanism is the dominant mechanism of photo-CIDNP buildup in PSI. Furthermore the results are in agreement with bidirectional electron transfer and suggest that functional heterogeneity of PSI is an inherent property of PSI. This will be further discussed in chapter 6. To fully elucidate the photo-CIDNP buildup in PSI, where the four cofactors involved in primary ET resonate at similar chemical shift values, 2D and 3D experimentation are proposed in chapter 6. The kinetic effect caused by an increasing fraction of reduced F_X during the photo-CIDNP experiments and the

subsequent change in the relative activity of the A and B branch in ET have to be quantified. To eludiate this, extensive and systematic experimentation on freshly reduced PSI complex preparations by time-resolved photo-CIDNP will be required. The results obtained from D1D2 particles from spinach with ^{13}C at natural abundance reveal a photo-CIDNP buildup in PSII that resembles the buildup observed for *Rb. sphaeroides* R26 RCs. This is attributed to the relatively long triplet lifetime of 1 ms in PSII and 100 μs in R26, which contrasts with the short $T_{(^3D)}$ of 3 μs and 100 ns for the PSI and for *Rb. sphaeroides* WT RCs, respectively. In the next chapter possibilities for the application of ns laser flash photo CIDNP MAS NMR to labeled PSII will be discussed.

Chapter 6

Outlook

In this thesis new insights into the photochemical machinery of cyanobacterial and plant reaction centers have been presented. Through selective isotope labelling of cyanobacteria and plants, the primary ET events in PSI and PSII could be studied at the atomic level directly in whole cells or entire plants (see chapter 2 and 4). In this chapter we will provide perspectives on future studies with sparsely ^{13}C and ^{15}N labeled PSI and PSII protein complexes. In chapter 3 the functional flexibility and field dependence of PSI has been discussed based on data obtained from uniformly ^{15}N labeled PSI complex from different plant systems. The kinetics of the photo-CIDNP buildup presented in chapter 5 indicated that functional flexibility is an inherent property of PSI. In this chapter this discussion will be continued based on preliminary results obtained from 4-ALA ^{13}C labeled PSI complexes that were measured at different magnetic field strengths. In chapter 4 new evidence for the involvement of the protein matrix in ET in PSII RCs has been presented. In this chapter preliminary results obtained from ^{15}N-ALA labeled PSII will be presented that can further support the evidence for a histidine residue with some electron spin density ρ_i.

6.1 FIELD DEPENDANCE OF PHOTO-CIDNP BUILDUP

The magnetic field dependence of photo-CIDNP signals is a sensitive tool to study photo-CIDNP buildup mechanisms and investigate how the nuclear polarization depends on the magnetic parameters and on the lifetimes of the intermediate radical species (Jeschke 1997; Prakash *et al.* 2005). The field dependence of PSII and PSI has previously been studied by ^{13}C photo-CIDNP MAS NMR on unlabeled PSI and PSII preparations from spinach (Roy *et al.* 2007). PSII shows a field dependence similar to RCs of purple bacteria (Prakash *et al*. 2005), with maximum polarization at the lowest tested field of 4.7 T. In the meantime this trend has shown to extend to even lower fields of 2.35 T in PSII (data not shown), but due to the decrease in signal resolution the optimal field strength for PSII investigations remains 4.7 T. PSI of spinach on the other hand shows an optimal signal to noise ratio at 9.4 T (Roy *et al.* 2007). As discussed in chapter 3 of this thesis the same trend was found for PSI particles of duckweed based on a photo-CIDNP study of uniformly ^{15}N

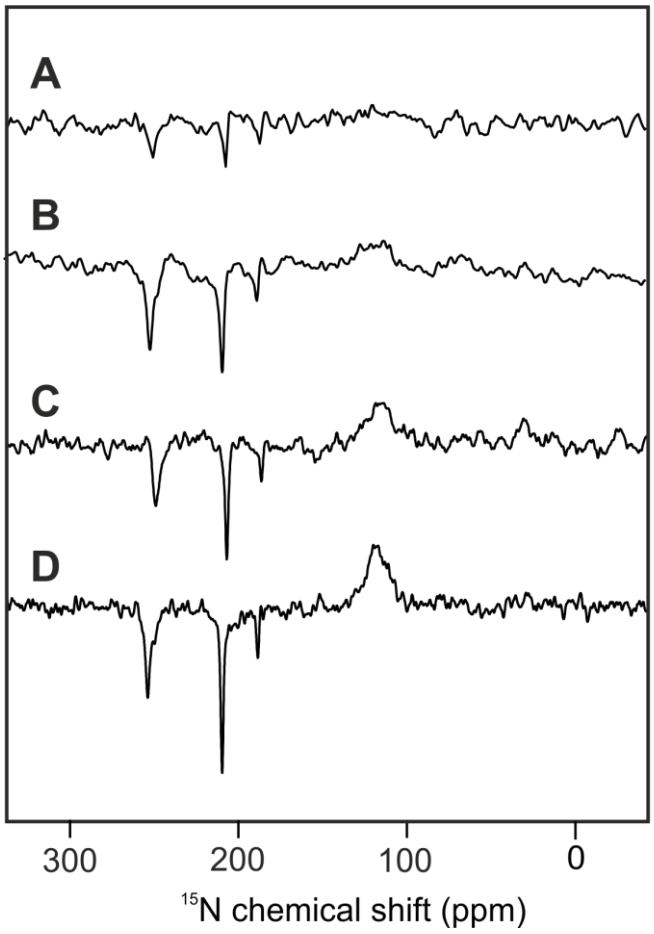

Figure 6.1 ^{15}N photo-CIDNP MAS NMR spectra obtained from the same pre-reduced sample of uniformly ^{15}N labeled PSI-110 particles of duckweed measured at magnetic field strengths of 2.35 T (A), 4.7 T (B), 7.1 T (C) and 9.4 T (D). All spectra have been obtained with a spinning frequency of 8 kHz, at a temperature of 235 K and with a recycle delay of 4 s. The light intensity was kept constant at 320 klux in all experiments. The number of scans was the same for the experiments that were performed at 235 K.

labeled PSI-110 particles. Figure 6.1 shows spectra obtained from uniformly ^{15}N labeled PSI-110 particles of duckweed and illustrates the increase in signal intensity observed upon increasing the magnetic field strength from 2.35 T to 9.4 T. As has been discussed in chapter 3, the field dependence observed for PSI confirms a different electronic structure for the radical pair compared to PSII and the bacterial RC. In addition, the data discussed in chapter 3 imply a functional flexibility of PSI in different plant species.

6.2 FUNCTIONAL FLEXIBILITY OF PSI

Figure 6.2 shows ^{13}C photo-CIDNP MAS NMR spectra obtained from selectively ^{13}C 4-ALA labeled PSI-110 particles from duckweed. Trace a shown in panel A of Figure 6.2 was collected by continuous illumination of a 4-ALA ^{13}C labeled PSI-110 complex

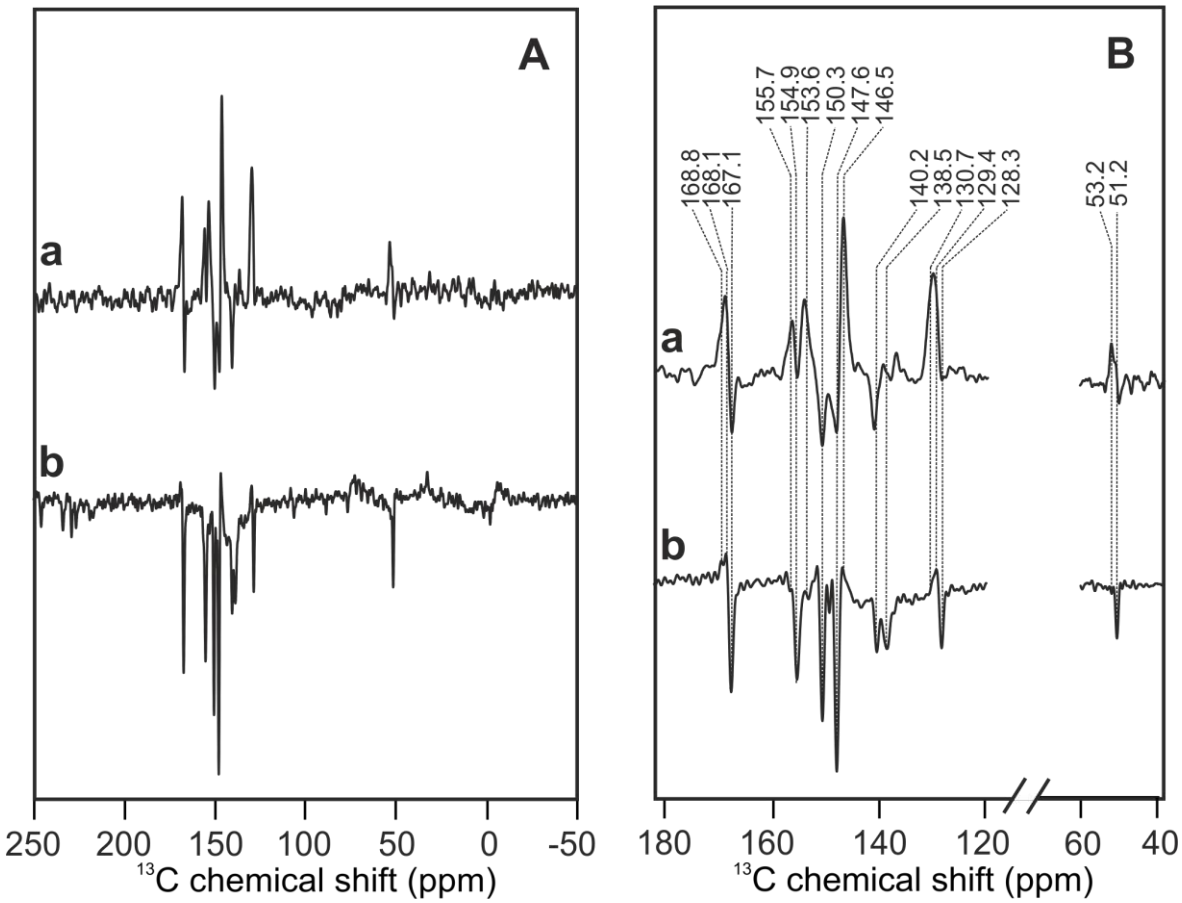

Figure 6.2: ^{13}C photo-CIDNP MAS NMR spectra obtained by continuous illumination of selectively ^{13}C 4-ALA labeled PSI-110 particles of duckweed at 4.7 T (a) and 9.4 T (b) at 235K and with a recycle delay of 4 s. Figure B shows the aromatic and aliphatic regions of spectra a and b in A in more detail, with the dashed lines indicating the centerbands of the observed light induced signals.

preparation, frozen directly inside the NMR probe in the dark while spinning slowly prior to NMR detection in a magnetic field of 4.7 T. Spectrum b in the left panel of Figure 6.2 was collected from a 4-ALA ^{13}C labeled PSI-110 in a magnetic field of 9.4 T. Figure 5.2B shows the aromatic and aliphatic regions with the light induced centerbands indicated by the dashed lines. The signal buildup for the isolated 4-ALA ^{13}C labeled PSI from duckweed was ~10 fold faster than the signal buildup in whole cells of cyanobacteria, and the signal to noise ratio was significantly improved (see chapter 2, Figure 2.3 and Figure 6.2). This is in agreement with the higher level of label incorporation in duckweed with P_{tot} = 75 ± 5 % as opposed to ~30 ± 5 % in cyanobacteria (See Appendix A and Figure 2.2, respectively) and the higher concentration of PSI RCs in preparations containing isolated PS-110 complexes as opposed to whole cells.

In Table 6.1, an overview is presented of the ^{13}C photo-CIDNP signals observed in the current work, and these results are compared with data from previous studies that were

Table 6.1: ^{13}C chemical shifts for photo-CIDNP signals obtained at 4.7 and 9.4 T, in comparison with literature data

Chemical shifts					
		n.a. Plant PSI	4-ALA Cyanobac PSI	4-ALA Plant PSI	
Chl *a*	assignment carbon atom	9.4 T	4.7 T	4.7 T	9.4 T
σ_{ss} [a]		σ [b]	σ [c]	σ [d]	σ [d]
170.0	**19**	167.1 e	166.9 e	168.3 a	168.8 a
				167.1 e	167.1 e
162.0	14	160.4 e			
155.9	**1**	154.8 e	154.8 e	153.6 a	154.9 e
154.4	**6**			155.7 a	
			149.8 e	150.3 e	150.3 e
154.0	16	152.6 e			
150.7	4	149.9 e			
147.2	**11**	147.2 e	147.6 e	146.5 a	146.5 a
147.2	9			147.6 e	147.6 e
146.2	**8**	144.2 e	144.2 e	140.7 e	140.2 e
138.0	**3**	138.6 e	138.6 e		138.5 e
136.1	2	~ 136 e			
134.0	12				
133.4	7	~ 132 e		129.8 a	130.7 a
					129.4 a
126.2	**13**		128.3 e		128.3 e
108.2	10	105.4 e	~ 104.5 e		
102.8	15				
98.1	5				
93.3	20				
51.4	**17**				51.2 e
				53.2 a	

[a] Boender *et al.* (1995), data obtained from solid aggregates of Chl *a*. [b]Alia *et al.* (2004), data obtained from isolated PSI particles from spinach. [c] data obtained from *Synechocytis* whole cells containing both PSI and PSII but showing pure PSI. [d] obtained from 4-ALA labeled isolated PSI from duckweed. Abbreviations: σ = chemical shift, a = absorptive signal, e = emissive signal

performed on a variety of PSI preparations from different organisms, at magnetic field strengths of 4.7 and 9.4 T. The chemical shifts of the positive features obtained from 4-ALA ^{13}C labeled PSI at 9.4 T match with the positive signals observed at 4.7 T (see Table 6.1). In earlier ^{13}C -photo-CIDNP studies on isolated PSI-110 particles from spinach, PSI has always shown a purely emissive spectrum (Alia *et al.* 2004; Diller *et al.* 2005). Likewise, as has been discussed in chapter 2, all signals assigned to PSI in the ^{13}C photo-CIDNP MAS NMR spectra obtained from whole cells of *Synechocystis* sp. PCC 6803 cyanobacteria were emissive. The similarity of the chemical shift patterns observed for the PSI of different organisms and at different experimental conditions, suggests that the electronic ground states

at the molecular level is largely species and preparation independent. The apparent changes in the signal intensity pattern confirm a large functional flexibility at the higher level of the protein complex, which depends both on the species and on the experimental conditions. PSII on the other hand shows little variation in both chemical shift and relative signal intensity pattern among different plant species, isolation states and experimental conditions (chapter 4 and Figure 5.6).

Upon prolonged illumination, *i.e.* an experimental time of more than ~20 h with continuous illumination at 235K, the positive features observed at 9.4 T (spectrum 6.2b) decrease in intensity (data not shown). On the other hand prolonged illumination at 4.7 T causes the negative signals shown in Figure 6.2a to diminish (data not shown). The same effect is observed in the data obtained from uniformly ^{15}N labeled PSI complex. Here the absorptive peaks observed in PSI samples from duckweed disappear upon prolonged illumination (see Figure 3.3A of freshly reduced PSI and Figure 6.1B of pre-reduced PSI for comparison). In addition, similar to the observations in cyanobacteria at 4.7 T (see Figure 2.5 page 48), the signal buildup rate for the emissive photo-CIDNP signals at 9.4 T increases upon prolonged illumination of isolated PSI complex from duckweed (data not shown). Further systematic experimentation has to be performed to quantify and understand the observed changes in the photo-CIDNP spectra of PSI upon prolonged illumination. Possible explanations for the light induced changes and the strong field dependence include (i) a change in the relative contribution of the TSM and DD mechanisms in the photo-CIDNP buildup or (ii) a change in the relative activity of the two cofactor branches in PSI ET at different conditions.

In PSI both cofactor branches are active in ET (Fairclough *et al.* 2003; Ramesh *et al.* 2004; Poluektov *et al.* 2005; Santabarbara *et al.* 2005; Santabarbara *et al.* 2010). Upon illumination the PSI forms radical pairs with the electron donor P700 as the radical cation and either the A_{0A} or A_{0B} Chl *a* cofactor as radical anion. The two radical pairs ($P700^{+\bullet}A_{0A}^{-\bullet}$ and $P700^{+\bullet}A_{0B}^{-\bullet}$) are generated in a pure singlet state and the initial electronic zero-quantum coherence is converted by the TSM and DD mechanisms into net nuclear polarization. The TSM mechanism breaks the symmetry of the coherent spin evolution in the correlated radical pair by state mixing due to anisotropic electron-electron dipolar coupling and pseudosecular hyperfine coupling. Coherence transfer is maximal when the difference of the electron Zeeman frequencies $\Delta\Omega$, the nuclear Zeeman frequency ω_I, and the secular part of the hyperfine interaction (A) fulfill the double matching condition $2|\Delta\Omega| = 2|\omega_I| = |A|$

(Jeschke, 1997, 1998; Jeschke and Matysik, 2003). In the DD mechanism the symmetry is broken due to the different lifetimes of the singlet and triplet radical pair state and the pseudosecular hyperfine coupling (Polenova and McDermott, 1999). For the DD mechanism only a single matching of conditions is required: $2|\omega_I| = |A|$ and the difference of the singlet and triplet radical pair lifetimes should be in the order of the inverse hyperfine coupling (Jeschke and Matysik, 2003). Since both $\Delta\Omega$ and $\underline{\omega_I}$ depend on the magnetic field, both the TSM and DD mechanisms produce the highest absolute nuclear polarization at a matching field but can generate polarization with opposite signs (Roy *et al.* 2007). Based on quantum chemistry calculations and the time-resolved data obtained from uniformly labeled PSI-110 particles discussed in chapter 5, section 3, it can be concluded that in PSI the DD mechanism is dominant. Previous simulations indicated an increase of the exchange coupling *J* between the $P700^{+\bullet}$ and $A_0^{-\bullet}$ radical anions by a factor of approximately 3 opposed to the bacterial RC, which can explain the field effect observed in PSI (Jeschke and Matysik 2003; Roy *et al.* 2007, Stoll and Schweiger 2006). It was suggested that the change in *J*-coupling arises from minor rearrangements of the cofactors, leading to a larger overlap between the molecular orbitals of the P700 donor and the accessory Chl *a* or between the molecular orbitals of the accessory Chl *a* and the primary acceptor A_0. A change in the *J*-coupling has a strong effect on the field dependence via the matching condition for Photo-CIDNP (Jeschke and Matysik 2003). While the local protein environment of the A_{0A} and A_{0B} Chl *a* cofactors and their relative orientation to the P700 donor are very similar (Jordan *et al.* 2001), the cation is mainly localized on P_B (Davis *et al.* 1993; Käss *et al.* 2001, Saito and Ishikita 2011). This could affect the relative strength of the exchange coupling between A_{0A} and A_{0B} to P_B and the optimal field for the observation of either the A_{0A} or A_{0B} electron acceptor.

The relative activity of the A and B branch depend on the organism and the reduction state of the quinone A_{1A} (Ali *et al.* 2006). In plants and green algae the A:B branch activity is about 50:50 but upon photo-accumulation of A_{1A}^- due to the complete reduction of the F_X cluster, the relative contribution of the B branch increases and becomes dominant (Santabarbara *et al.* 2006). In cyanobacteria a similar trend is visible, yet buildup of the contribution of the B branch takes longer and the resulting signal is weak with a maximum relative activity of 55 to 60% (Santabarbara *et al.* 2005 and 2006, Poluektov *et al.* 2005). As discussed in chapter 5 the conditions during our photo-CIDNP experiments result in a relatively slow F_X reduction with a gradual increase in the fraction of the $P700^{+\bullet}A_0^{-\bullet}$ radical pair during the experiment. This explains why upon continuous illumination of PSI during

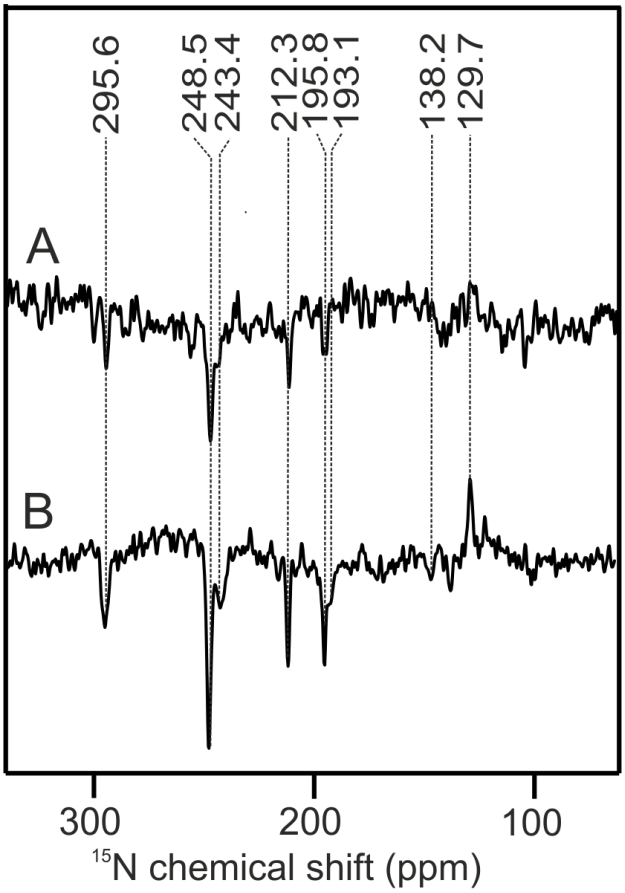

Figure 6.3 ^{15}N photo-CIDNP MAS NMR spectra obtained from ^{15}N-ALA labeled thylakoid (A), and uniformly ^{15}N labeled isolated PSII D1D2 complex from duckweed (B). Both spectra were measured at a magnetic field strength of 4.7 T and have been obtained with a spinning frequency of 8 kHz, a temperature of 235 K and a recycle delay of 4 s.

the NMR measurement the rate of signal buildup increases. In addition it provides a possible explanation for the observed light induced changes observed in cyanobacteria and duckweed. Full reduction of F_X causes the relative activity of the B branch to increase strongly while the participation of the A branch in ET decreases (Santabarbara *et al.* 2006). As noted before this alteration in the relative branch activity upon prolonged illumination is expected to be stronger in plants than in cyanobacteria (Poluektov *et al.* 2005; Santabarbara *et al.* 2006). This is in line with the pronounced light induced changes observed in the photo-CIDNP spectra obtained from duckweed plants (Figure 6.2) and the minor changes observed for *Synechocyctis* cyanobacteria (Figure 2.5, page 48).

6.3 ^{15}N PHOTO-CIDNP MAS NMR ON ^{15}N LABELED PSII

The signals at 136.0 and 132.0 ppm in the ^{13}C photo-CIDNP MAS NMR spectra obtained from PSII complexes with ^{13}C at natural abundance (see Figure 4.4B) provides

Table 6.2: ^{15}N chemical shifts of the photo-CIDNP signals obtained from ^{15}N-ALA labeled PSII in comparison to signals obtained from uniformly ^{15}N-labeled PSII and literature data

Assignment		Solution data	u-^{15}N PSII spinach	u-^{15}N PSII duckweed	^{15}N-ALA duckweed
cofactor	atom	σ^{a}_{LS}	$\sigma_{SS}{}^{b}$	$\sigma_{SS}{}^{c}$	$\sigma_{SS}{}^{c}$
Chl *a*	N-I	186.0		193.1 e	
	N-II	206.5	211.5 e	212.3 e	212.3 e
	N-III	189.4	195.3 e	195.8 e	195.8 e
	N-IV	247.0	247.6 e	248.5 e	248.5 e
Phe *a*	N-I	125.5		129.7 a	
	N-II	241.5		243.4 e	243.4 e
	N-III	133.9	138.3 e	138.2 e	
	N-IV	295.8	295.0 e	295.6 e	295.6 e

[a] Chl *a* and Phe *a* in $CDCl_2$, chemical shifts in ppm. Boxer *et al.* 1974.

[b] Uniformly ^{15}N labeled PSII D1D2 complex from spinach, chemical shifts in ppm. Diller *et al.* 2007.

[c] Uniformly ^{15}N labeled PSII D1D2 complex and ^{15}N-ALA labeled thylakoid from duckweed, chemical shifts in ppm. Abbreviations: σ = chemical shift, a = absorptive signal, e = emissive signal, u-^{15}N = uniformly ^{15}N labeled.

further support for a histidine residue with some spin density ρ_i in close proximity to the Chl *a* donor P_{D1} of PSII (Matysik *et al.* 2001; Diller *et al.* 2005). In this natural abundance spectrum not only ρ_i carrying carbons from the Chl *a* and Phe *a* cofactors appear. as is the case in selectively 3-, 4-, and 5-ALA ^{13}C labeled preparations but also ρ_i carrying carbons from the surrounding protein matrix will appear. Recently it has been suggested that a (B)Chl$^{\delta-}$-His$^{\delta+}$ partial charge transfer motif is a common denominator across photosynthetic RC complexes in plants and bacteria and that this interaction can help to establish a dynamic polaron mechanism for barrier-less electron transfer in photosynthetic complexes (Alia *et al.* 2013, Eisenmayer *et al.* 2012). Experiments with selectively ^{15}N-ALA label patterns would be of great interest to facilitate a final conclusion regarding the involvement of protein side chains as electron spin carriers in PSII. Figure 6.3A shows the preliminary results of ^{15}N photo-CIDNP MAS NMR applied to ^{15}N-ALA labeled thylakoid from duckweed. The quality of the data has to be further improved for final conclusions but a first comparison with data obtained from uniformly labeled ^{15}N PSII is still possible (Figure 6.3B). If ρ_i is located on a nitrogen atom of the protein matrix surrounding the RC cofactors, the corresponding photo-CIDNP signal will appear in the data collected from uniformly labeled PSII, and not in the data obtained from ^{15}N-ALA labeled PSII. The signals at 138.2 and

193.1 ppm in Figure 6.3 are weak and are difficult to resolve from the noise background in the data collected from ^{15}N-ALA labeled PSII. However, the sharp absorptive peak appearing at 129.7 ppm in the spectrum obtained from uniformly ^{15}N labeled PSII is interesting (Figure 6.3A). This is the only absorptive signal in Figure 6.3A and is very weak or absent in the spectrum obtained from ^{15}N-ALA labeled PSII (Figure 6.3B, Table 6.2). Based on the chemical shift the signal at 129.7 ppm can in principle be assigned to the N-I nitrogen of the Phe *a* acceptor (cf. Table 6.2). However, considering the relative strength of the 129.7 ppm signal in Figure 6.3B, it would be expected to be visible in Figure 6.3A as well, if it indeed originates from a nitrogen atom of the Phe *a* cofactor. Calculations using the TZP basis and the SAOP model have delivered reliable predictions for chemical shift and signal intensity patterns in PSI photo-CIDNP NMR spectra (see chapter 5 and Appendix B). Preliminary calculations using a similar approach for PSII provide no indication for sign reversal of the signal originating from the N-I of the Phe *a* donor in line with a different origin of the absorptive signal at 129.7 ppm. Further improvement of the spectral data from ^{15}N-ALA labeled PSII is required to arrive at a final conclusion on this point.

6.4 TIME-RESOLVED PHOTO-CIDNP EXPERIMENTS ON LABELED PSII

While continuous illumination spectra of 3, 4 and 5-ALA ^{13}C labeled duckweed PSII spectra are readily available (chapter 4), attempts to obtain reliable time-resolved ns-flash photo-CIDNP data of selectively ^{13}C labeled PSII in thylakoid, BBY and whole plants samples have consistently failed because of the high sensitivity of PSII to intense laser flashes. Due to the high cost of the ^{13}C-ALA precursor required for the preparation of labeled PSII, it was not possible to prepare a sufficient amount of selectively ^{13}C labeled D1D2 to compensate for the rapid degradation of the PSII activity for thylakoid, BBY and plant samples, which occurred even when the laser power was reduced to 80 mJ, compared with ~200 mJ in experiments on bacterial RC and PSI. The necessity to reduce the quinones in thylakoid, BBY and whole plant samples, causes additional sensitization of the already fragile PSII complex. Natural repair mechanisms which have shown to partly regenerate PSII activity in core preparations upon dark incubation after illumination at 4 °C or at room temperature, fail to function in the presence of sodium dithionite reductant (Braun *et al.* 1990). Hence further research to stabilize PSII during laser experiments is necessary. PSII from the cyanobacterial species *Thermococcus* (*T.*) *vulcanus* (Kamiya and Shen 2003), which is extremely stable (Hughes *et al.* 2010) might be a suitable candidate for additional

laser studies. As discussed in chapter 2 of this thesis, selective ^{13}C isotope labeling was successfull for *Synechocystis* sp. PCC 6803 cyanobacteria, and the closely related *T. vulcanus* may be a promising candidate for selective isotope labeling.

6.5 THE APPLICATION OF 2D AND 3D NMR EXPERIMENTS TO LABELED PSI AND PSII

As discussed in paragraph 5.3, quantum chemical calculations are very useful in assigning the photo-CIDNP MAS NMR response from PSI (using the TZP basis and SAOP model potential for best results, Bode *et al.* manuscript in preparation, appendix B) and the same procedure can be applied to PSII. In addition it is possible to apply 3D transferred-echo double resonance (TEDOR) (Jaroniec *et al.* 2002, Hing *et al.* 1992, Helmus *et al.* 2011) and frequency selective rotational-echo double-resonance (REDOR) (Jaroniec *et al.* 2001) MAS NMR to PSI an PSII samples which are both uniformly ^{15}N and selectively ^{13}C labeled. 3D TEDOR allows for the simultaneous measurement of multiple carbon-nitrogen distances in ^{13}C,^{15}N-labeled solids by ^{13}C-^{15}N coherence transfer and ^{15}N and ^{13}C frequency labeling for site-specific resolution while the detrimental effects of homonuclear ^{13}C-^{13}C *J*-couplings on the measurement of weak ^{13}C-^{15}N dipolar couplings are circumvented (Jaroniec *et al.* 2002). Through these experiments the signal assignment would be simplified due to the information that is encoded in the carbon-nitrogen couplings. This is relevant because the ^{15}N signals arising in PSII from the Chl *a* donor and Phe acceptor are well resolved, while the carbon spectra show considerable signal overlap also for the spectra obtained from selectively ^{13}C labeled samples. Frequency selective REDOR allows for the recoupling of a single ^{13}C-^{15}N dipolar interaction in a multiple spin system, while all remaining ^{13}C-^{15}N dipolar couplings and ^{13}C-^{13}C scalar couplings to the selected ^{13}C are suppressed. In this way local structural distortions of the cofactors can be probed like *e.g.* the involvement of the axial histidine, His-198, in the stabilization of the HOMO on P_{D1} in PSII (Diller 2008, Diller *et al.* 2007).

APPENDIX A

Determination of the level of isotope labeling in Synechocystis sp. PCC 6803 and duckweed by LC-MS.

Table A-1. LCMS peak intensities and calculated $^{L}I_t$ **and** P_n values for unlabeled and labeled Chl *a* isolated from *Synechocystis* sp. PCC 6803

m/z	^{U}I	$^{U}I_{\%}$	^{L}I	$^{L}I_t$	P_n
893.5	429304.0	1	190318.8	190318.8	0.545
894.5	288949.2	0.67	245637.4	117540.6	0.336
895.5	73242.9	0.17	147672.0	36089.6	0.103
896.5	26567.0	0.06	56997.8	876.1	0.003
897.5	7339.1	0.02	16776.9	2756.2	0.008
898.5	1579.5	0.00	5400.6	1162.7	0.003
899.5	0.0	0.00	4324.3	782.6	0.002
900.5	0.0	0.00	0.0	0.0	0.000
901.5	0.0	0.00	0.0	0.0	0.000

Table A-2. LCMS peak intensities and calculated $^{L}I_t$ **and** P_n values for unlabeled and labeled Chl *a* isolated from duckweed

m/z	^{U}I	$^{U}I_{\%}$	^{L}I	$^{L}I_t$	P_n
893.5	161481.0	1	118245.9	118245.9	0.289
894.5	120301.9	0.74	193086.8	104994.7	0.257
895.5	68342.5	0.42	173475.7	45211.2	0.111
896.5	9208.8	0.17	121856.1	36994.8	0.090
897.5	3323.8	0.02	75276.7	22594.0	0.055
898.5	1277.0	0.00	41455.4	6387.8	0.016
899.5	633.7	0.00	26502.6	10071.8	0.025
900.5	0.0	0.00	28208.2	16712.9	0.041
901.5	0.0	0.00	64674.5	47596.7	0.116

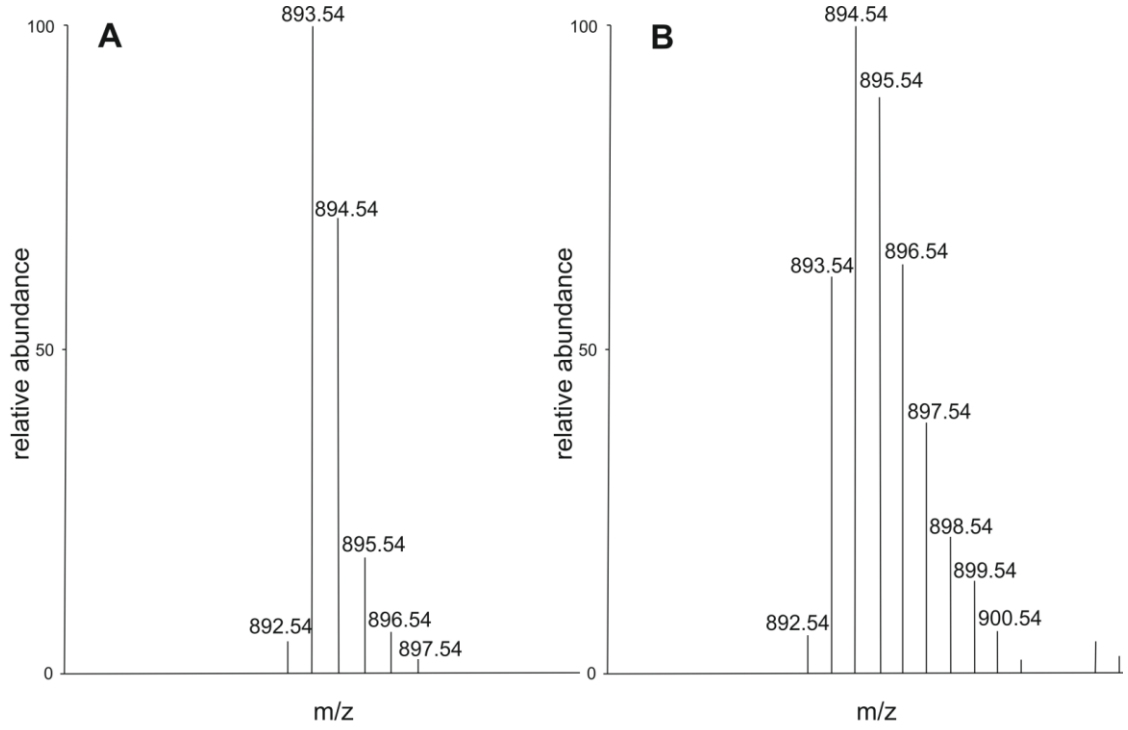

Figure-A 1: ^{13}C isotope incorporation determined by LCMS for Chl *a* isolated from duckweed leaves grown on unlabeled substrate (A) and with the ^{13}C 4-ALA precursor in the medium (B).

APPENDIX B

Quantum Chemistry Calculations on PSI

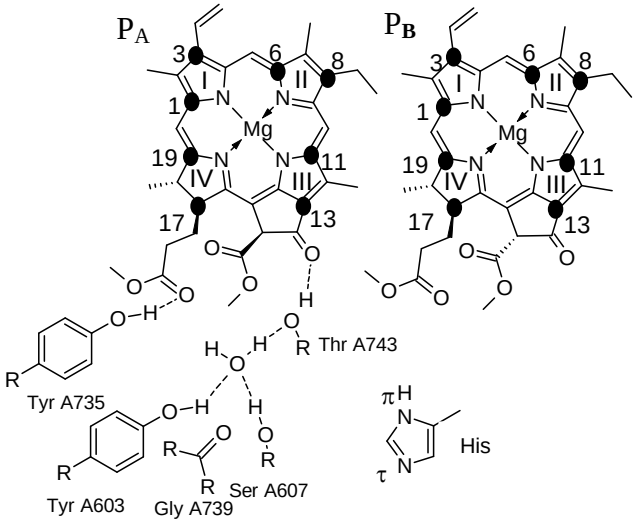

Appendix-B 1: The theoretical model used for the calculations on the PSI RC. Depicted are the two central Chls, P_A and P_B of the Chl *a*/Chl *a*' dimer P700, and the hydrogen bonds of P_A to the aminogroups of the surrounding protein matrix. The Mg atoms of the P_A and P_B cofactors are coordinated to respectively the His residues 680 and 660 of the protein backbone. A His residue is depicted and the π and τ nitrogen are indicated. The carbon atoms which are labeled in the ^{13}C 4-ALA treated plants are indicated by the black dots and numbered according to the IUPAC nomenclature.

Table Appendix-B 1: **Theoretically calculated ^{13}C and ^{15}N chemical shifts for photo-CIDNP signals expected from selected atoms within the PSI RC**

Carbon	**P_B**	**P_A**	**A_{0B}**	**A_{0A}**
C-1	153.7	155.0	154.3	154.7
C-3	143.7	142.1	143.3	143.1
C-6	154.3	154.1	153.9	153.8
C-8	147.3	147.0	149.4	149.4
C-11	152.9	152.5	153.1	152.8
C-13	134.6	135.0	135.8	134.8
C-17	59.0	58.9	60.3	60.5
C-19	166.6	167.4	168.7	168.4
Nitrogen	**P_B**	**P_A**	**A_{0B}**	**A_{0A}**
N-I	195.6	193.3	196.3	192.7
N-II	210.0	212.1	208.3	207.3
N-III	196.9	198.9	193.2	194.0
N-IV	263.2	255.5	252.1	248.3
His_Nπ	164.2	160.3		
His_Nτ	231.3	239.5		

Calculated chemical shifts in ppm for the 15N and 13C isotope labeled atoms in PSI. The system was truncated and all H-bonded amino-acid side chains were simplified to phenol, methanol or formaldehyde. The coordinates of heavy atoms were kept fixed. Histidines were truncated to methyl-imidazole and the methyl carbons were kept at fixed positions. The phytyl chain was truncated to methyl which was also fixed in the calculations. Optimization was done in Turbomole with the BP86 functional and the TZVP basis using the resolution of identity approximation. The structure published by Jordan et. al. 2011, PDB 2WSC was used as a starting point. The minimized structure was used for single point calculations in ADF. NMR shift calculations were performed using a triple-zeta basis and the SAOP model potential. The P_B Chl *a* and P_A Chl *a*' of P700 were treated as a dimer and the hydrogen bonds were taken into account.

REFERENCES

Acharya, K., V. Zazubovich, M. Reppert and R. Jankowiak **(2012)**. "Primary Electron Donor(s) in Isolated Reaction Center of Photosystem II from *Chlamydomonas reinhardtii*." *Journal of Physical Chemistry B 116* (16): 4860-4870.

Ali, K., S. Santabarbara, P. Heathcote, M. C. W. Evans and S. Purton **(2006).** "Bidirectional electron transfer in photosystem I" *Biochimica Et Biophysica Acta-Bioenergetics* 1757 (12): 1623-1633.

Alia, A., F. Buda, H. J. M. de Groot and J. Matysik **(2013)**. "Solid-state NMR of nanomachines involved in photosynthetic energy conversion." *Annual review Biophys (in press).*

Alia, E. Roy, P. Gast, H. J. van Gorkom, H. J. M. de Groot, G. Jeschke and J. Matysik **(2004)**. "Photochemically induced dynamic nuclear polarization in photosystem I of plants observed by ^{13}C magic-angle spinning NMR." *Journal of the American Chemical Society* 126 (40): 12819-12826.

Alia, A., P. K. Wawrzyniak, G. J. Janssen, F. Buda, J. Matysik and H. J. M. de Groot **(2009)**. "Differential Charge Polarization of Axial Histidines in Bacterial Reaction Centers Balances the Asymmetry of the Special Pair." *Journal of the American Chemical Society* 131 (28): 9626-9627.

Alia, A., B. Hulsebosch, H. J. van Gorkom, J. Raap, J. Lugtenburg, J. Matysik, H. J.M. de Groot, P. Gast **(2003)**. "Probing the electronic structure of Tyrosine radical $Y_D^{\bullet}$ in photosystem II by EPR spectroscopy using site specific isotope labelling in *Spirodela oligorrhiza*." *Chemical Physics* 294 (3): 459-469.

Alizadeh, S., P. J. Nixon, A. Telfer and J. Barber **(1995)**. "Isolation and characterization of the photosystem II reaction-center complex from a double mutant of *Chlamydomonas-reinhardtii*." *Photosynthesis Research* 43 (2): 165-171.

Allen, J. F., W. B. M. de Paula, S. Puthiyaveetil and J. Nield **(2011)**. "A structural phylogenetic map for chloroplast photosynthesis." *Trends in Plant Science 16* (12): 645-655.

Allen, M. M. **(1968)**. "Simple conditions for growth of unicellular blue-green algae on plates." *Journal of Phycology* 4 (1): 1-4.

Amunts, A., O. Drory and N. Nelson **(2007)**. "The structure of a plant photosystem I supercomplex at 3.4 Å resolution." *Nature* 447 (7140): 58-63.

Amunts, A., H. Toporik, A. Borovikova and N. Nelson **(2010)**. "Structure Determination and Improved Model of Plant Photosystem I." *Journal of Biological Chemistry* 285 (5): 3478-3486.

Anderson, J. M., W. S. Chow and J. Las Rivas **(2008)**. "Dynamic flexibility in the structure and function of photosystem II in higher plant thylakoid membranes: the grana enigma." *Photosynthesis Research* 98 (1-3): 575-587.

Barber, J. **(2003)**. "Photosystem II: the engine of life." *Quarterly Reviews Of Biophysics* 36 (1): 71-89.

Bargon, J. and H. Fischer **(1967)**. "Kernresonanz-Emissionslinien Wahrend Rascher Radikalreaktionen .2. Chemisch Induzierte Dynamische Kernpolarisation." *Zeitschrift Fur Naturforschung Part a-Astrophysik Physik Und Physikalische Chemie A* 22 (10): 1556-&.

Barter, L. M. C. and D. R. Klug **(2005)**. "A unified picture of energy and electron transfer in primary photosynthesis." *Chemical Physics* 319: 308-315.

Beale, S. I. and J. D. Weinstein **(1991)**. "Biochemistry and regulation of photosynthetic pigments in formation in plants and algae Biosynthesis of Tetrapyrroles." P. M. Jordan. Amsterdam, *Elsevier*. 19: 155-235.

Bennett, AE, C.M. Rienstra, M. Auger, K.V. Lakshmi, R.G. Griffin **(1995) "**Heteronuclear decoupling in rotating solids." *J. Chem. Phys.* 103: 6951–6958

Ben-Shem, A., F. Frolow and N. Nelson **(2003)**. "Crystal structure of plant photosystem I." *Nature* 426 (6967): 630-635.

Bernat, G., F. Morvaridi, Y. Feyziyev and S. Styring **(2002)**. "pH Dependence of the Four Individual Transitions in the Catalytic S-Cycle during Photosynthetic Oxygen Evolution." *Biochemistry* (41): 5830-5843.

Berthold, D. A., G. T. Babcock and C. F. Yocum **(1981)**. "A highly resolved, oxygen-evolving Photosystem-II preparation from spinach thylakoid membranes." *FEBS Letters* 134 (2): 231-234.

Berthold, T., E. D. von Gromoff, S. Santabarbara, P. Stehle, G. Link, O. G. Poluektov, P. Heathcote, C. F. Beck, M. C. Thurnauer and G. Kothe **(2012)**. "Exploring the Electron Transfer Pathways in Photosystem I by High-Time-Resolution Electron Paramagnetic Resonance: Observation of the B-Side Radical Pair $P700^{+}A_{1B}^{-}$ in Whole Cells of the Deuterated Green Alga *Chlamydomonas reinhardtii* at Cryogenic Temperatures." *Journal of the American Chemical Society* 134 (12): 5563-5576.

Biesiadka, J., B. Loll, J. Kern, K. D. Irrgang and A. Zouni **(2004)**. "Crystal structure of cyanobacterial photosystem II at 3.2 Å resolution: a closer look at the Mn-cluster." *Physical Chemistry Chemical Physics* 6 (20): 4733-4736.

Biggins, J. and P. Mathis **(1988)**. "Functional-role of vitamin-K1 in photosystem-I of the cyanobacterium *Synechocystis*-6803." *Biochemistry* 27 (5): 1494-1500.

Blankenship, R. E. **(2002)**. Molecular Mechanics of Photosynthesis. Oxford, Blackwell Science.

Blankenship, R. E., G. T. Babcock, J. T. Warden and K. Sauer **(1975)**. "Observation of a new EPR transient in chloroplasts that may reflect electron-donor to photosystem II at room-temperature." *Febs Letters* 51 (1): 287-293.

Boekema, E. J., P. E. Jensen, E. Schlodder, J. F. L. van Breemen, H. van Roon, H. V. Scheller and J. P. Dekker **(2001)**. "Green plant photosystem I binds light-harvesting complex I on one side of the complex." *Biochemistry* 40 (4): 1029-1036.

Boender, G. J., J. Raap, S. Prytulla, H. Oschkinat and H. J. M. Degroot **(1995)**. "MAS NMR structure refinement of uniformly ^{13}C enriched chlorophyll-a water aggregates with 2D dipolar correlation spectroscopy." *Chemical Physics Letters* 237 (5-6): 502-508.

Boghossian, A. A., M. H. Ham, J. H. Choi and M. S. Strano **(2011)**. "Biomimetic strategies for solar energy conversion: a technical perspective." *Energy & Environmental Science* 4 (10): 3834-3843.

Boxer, S. G., G. L. Closs and J. J. Katz **(1974)**. "Effect of magnesium coordination on ^{13}C and ^{15}N magnetic-resonance spectra of chlorophyll-a - relative energies of nitrogen n-pi-star states as deduced from a complete assignment of chemical-shifts." *Journal of the American Chemical Society* 96 (22): 7058-7066.

Braun, P. B., B. M. Greenberg and A. Scherz **(1990)**. "D 1 -D2-Cytochrome b559 Complex from the Aquatic Plant Spirodela oligorrhiza: Correlation between Complex Integrity, Spectroscopic Properties, Photochemical Activity, and Pigment Composition." *Biochemistry*: 10376-10387.

Breitmai, E. and W. Voelter **(1990)**. ^{13}C NMR "*Spectroscopy*" V. New York.

Breton, J., E. Nabedryk and W. Leibl **(1999)**. "FTIR study of the primary electron donor of photosystem I P700 revealing delocalization of the charge in $P700^{+}$ and localization of the triplet character in $^{3}P700$." *Biochemistry* 38 (36): 11585-11592.

Brettel, K. **(1997)**. "Electron transfer and arrangement of the redox cofactors in photosystem I." *Biochimica Et Biophysica Acta-Bioenergetics* 1318 (3): 322-373.

Brettel, K. and J. H. Golbeck **(1995)**. "Spectral and kinetic characterization of electron acceptor A_1 in a Photosystem I core devoid of iron-sulfur centers F_X, F_B and F_A." *Photosynthesis Research* 45 (3): 183-193.

Bricker, T. M., J. L. Roose, R. D. Fagerlund, L. K. Frankel and J. J. Eaton-Rye **(2012)**. "The extrinsic proteins of Photosystem II." *Biochimica Et Biophysica Acta-Bioenergetics* 1817 (1): 121-142.

Caffarri, S., K. Broess, R. Croce and H. van Amerongen **(2011)**. "Excitation Energy Transfer and Trapping in Higher Plant Photosystem II Complexes with Different Antenna Sizes" *Biophysical Journal 1*00 (17): 2094-2103

Camara-Artigas, A., D. Brune and J. P. Allen **(2002)**. "Interactions between lipids and bacterial reaction centers determined by protein crystallography." *Proceedings of the National Academy of Sciences of the United States of America* 99 (17): 11055-11060.

Camara-Artigas, A., C. Magee, A. Goetsch and J. P. Allen **(2002)**. "The structure of the heterodimer reaction center from Rhodobacter sphaeroides at 2.55 Å resolution." *Photosynthesis Research* 74 (1): 87-93.

Cardona, T., A. Sedoud, N. Cox and A. W. Rutherford **(2012)**. "Charge separation in Photosystem II: A comparative and evolutionary overview." *Biochimica Et Biophysica Acta-Bioenergetics* 1817 (1): 26-43.

Chidsey, E.D., L. Takiff, R.A. Goldstein and S.G. Boxer (1985). "Effect of magnetic fields on the triplet state lifetime in photosynthetic reaction centers: Evidence for thermal repopulation of the initial radical pair." *Proceedings of the National Academy of Sciences of the United States of America* 82 (20): 6850-6854.

Closs, G. L. and L. E. Closs **(1969)**. "Induced dynamic nuclear spin polarization in reactions of photochemically and thermally generated triplet diphenylmethylene." *Journal of the American Chemical Society* 91 (16): 4549-4550.

Cocivera, M. **(1968)**. "Optically induced overhauser effect in solution. Nuclear magnetic resonance emission." *Journal of the American Chemical Society* 90 (12): 3261-&.

Cogdell, R. J., T. D. Howard, R. Bittl, E. Schlodder, I. Geisenheimer and W. Lubitz **(2000)**. "How carotenoids protect bacterial photosynthesis." *Philosophical Transactions of the Royal Society of London Series B-Biological Sciences* 355 (1402): 1345-1349.

Cohen, R. O., G. Z. Shen, J. H. Golbeck, W. Xu, P. R. Chitnis, A. I. Valieva, A. van der Est, Y. Pushkar and D. Stehlik **(2004)**. "Evidence for asymmetric electron transfer in cyanobacterial photosystem I: Analysis of a methionine-to-leucine mutation of the ligand to the primary electron acceptor A_0." *Biochemistry* 43 (16): 4741-4754.

Cox, N., J. L. Hughes, A. W. Rutherford and E. Krausz, Eds. **(2010)**. "On the assignment of PSHB in D1/D2/cytb(559) reaction centers." *Proceedings of the tenth international meeting on hole burning, single molecule and related spectroscopies: science and applications-hbsm.*

Cox, N., J. L. Hughes, R. Steffen, P. J. Smith, A. W. Rutherford, R. J. Pace and E. Krausz **(2009)**. "Identification of the Q_Y excitation of the primary electron acceptor of photosystem II: CD determination of its coupling environment." *The journal of physical chemistry*. B 113: 12364-12374.

Croce, R., M. Mozzo, T. Morosinotto, A. Romeo, R. Hienerwadel and R. Bassi **(2007)**. "Singlet and triplet state transitions of carotenoids in the antenna complexes of higher-plant Photosystem I." *Biochemistry* 46 (12): 3846-3855.

Dashdorj, N., W. Xu, R. O. Cohen, J. H. Golbeck and S. Savikhin **(2005)**. "Asymmetric electron transfer in cyanobacterial photosystem I: Charge separation and secondary

electron transfer dynamics of mutations near the primary electron acceptor A_0." *Biophysical Journal* 88 (2): 1238-1249.

Dau, H. and I. Zaharieva **(2009**). "Principles, efficiency, and blueprint character of solar-energy conversion in photosynthetic water oxidation." Accounts of chemical research, 42 (12): 1861-1870

Davis, I. H., P. Heathcote, D. J. Maclachlan and M. C. W. Evans **(1993)**. "Modulation Analysis of the Electron-Spin Echo Signals of in-Vivo Oxidized Primary Donor ^{14}N Chlorophyll Centers in Bacterial, P870 and P960, and Plant Photosystem-I, P700, Reaction Centers." *Biochimica Et Biophysica Acta* 1143 (2): 183-189.

Daviso, E. **(2008)**. "The solid State Photo-CIDNP effect", Leiden Universiteit.

Daviso, E., A. Diller, A. Alia, J. Matysik and G. Jeschke **(2008b)**. "Photo-CIDNP MAS NMR beyond the T-1 limit by fast cycles of polarization extinction and polarization generation." *Journal of Magnetic Resonance* 190 (1): 43-51.

Daviso, E, A. Diller, P. Gast, A. Alia, J. Lugtenburg, M.G. Müller and J. Matysik **(2010)**. "Action Spectroscopy on Dense Samples of Photosynthetic Reaction Centers of *Rhodobacter sphaeroides* WT Based on Nanosecond Laser-Flash ^{13}C Photo-CIDNP MAS NMR." *Applied Magnetic Resonance* 38 (1): 105-116.

Daviso, E., G. J. Janssen, A. Alia, G. Jeschke, J. Matysik and M. Tessari **(2011)**. "A 10 000-fold Nuclear Hyperpolarization of a Membrane Protein in the Liquid Phase via Solid-State Mechanism." *Journal of the American Chemical Society* 133 (42): 16754-16757.

Daviso, E., G. Jeschke and J. Matysik **(2007)**. "Photo CIDNP MAS NMR." *Biophysical Techniques in Photosynthesis II*. T. J. Aartsma and J. Matysik. Dordrecht, Springer. II: 385-399.

Daviso, E, S. Prakash, A. Alia, P. Gast, G. Jeschke and J. Matysik **(2010b)** "Nanosecond-Flash ^{15}N Photo-CIDNP MAS NMR on Reaction Centers of *Rhodobacter sphaeroides* R26." *Applied Magnetic Resonance* 37 (1-4): 49-63.

Daviso, E., S. Prakash, A. Alia, P. Gast, J. Neugebauer, G. Jeschke and J. Matysik **(2009)**. "The electronic structure of the primary electron donor of reaction centers of purple bacteria at atomic resolution as observed by photo-CIDNP ^{13}C NMR." *Proceedings of the National Academy of Sciences of the United States of America* 106: 22281-22286.

Deisenhofer, J., O. Epp, K. Miki, R. Huber and H. Michel **(1984)**."X-ray structure-analysis of a membrane-protein complex-electron-density map at 3 Å resolution and a model of the chromophores of the photosynthetic reaction centert from *Rhodopseudomonas viridis*." *Journal of Molecular Biology* 180 (2): 385-398.

Deisenhofer, J., O. Epp, K. Miki, R. Huber and H. Michel **(1985)**."Structure of the protein subunits in the photosynthetic reaction center of *Rhodopseudomonas viridis* at 3 Å resolution." *Nature* 318 (6047): 618-624.

Dekker, J. P. and R. van Grondelle **(2000)**. "Primary charge separation in Photosystem II." *Photosynthesis Research* 63 (3): 195-208.

Dexter, D. L. **(1953)**. "A theory of sensitized luminescence in solids." *Journal of Chemical Physics* 21 (5): 836-850.

Diller, A., Alia, E. Roy, P. Gast, H. J. van Gorkom, J. Zaanen, H. J. M. de Groot, C. Glaubitz and J. Matysik **(2005)**. "Photo-CIDNP solid-state NMR on photosystems I and II: What makes P680 special?" *Photosynthesis Research* 84 (1-3): 303-308.

Diller, A., P. Gast, G. Jeschke, A. Alia and J. Matysik **(2008).** "^{13}C Photo-CIDNP MAS NMR on the LH1-RC Complex of *Rhodopseudomonas Acidophila.*" *Energy from the Sun*. J. Allen, E. Gantt, J. Golbeck and B. Osmond. Dordrecht: 10606-10614.

Diller, A., S. Prakash, A. Alia, P. Gast, J. Matysik and G. Jeschke **(2007)**. "Signals in solid-state photochemically induced dynamic nuclear polarization recover faster than signals obtained with the longitudinal relaxation time." *Journal of Physical Chemistry* B 111 (35): 10606-10614.

Diller, A., E. Roy, P. Gast, H. J. van Gorkom, H. J. M. de Groot, C. Glaubitz, G. Jeschke, J. Matysik and A. Alia **(2007)**. "^{15}N photochemically induced dynamic nuclear polarization magic-angle spinning NMR analysis of the electron donor of photosystem II." *Proceedings of the National Academy of Sciences* 104 (31): 12767-12771.

Diner, B. A. and F. Rappaport **(2002)**. "Structure, dynamics, and energetics of the primary photochemistry of photosystem II of oxygenic photosynthesis." *Annual Review of Plant Biology* 53: 551-580.

Diner, B. A., E. Schlodder, P. J. Nixon, W. J. Coleman, F. Rappaport, J. Lavergne, W. F. J. Vermaas and D. A. Chisholm **(2001)**. "Site-directed mutations at D1-His198 and D2-His197 of photosystem II in *Synechocystis* PCC 6803: Sites of primary charge separation and cation and triplet stabilization." *Biochemistry* 40 (31): 9265-9281.

Durrant, J. R., L. B. Giorgi, J. Barber, D. R. Klug and G. Porter **(1990)**. "Characterization of triplet-states in isolated photosystem-II reaction centers - oxygen quenching as a mechanism for photodamage." *Biochimica et Biophysica Acta* 1017 (2): 167-175.

Durrant, J. R., D. R. Klug, S. L. S. Kwat, R. V. A. N. Grondellet, G. Porter and J. A. N. P. Dekkert **(1995)**. "A multimer model for P680, the primary electron donor of photosystem II." *Nature* 92: 4798-4802.

Egorova-Zachernyuk, T., B. van Rossum, C. Erkelens and H.J.M. de Groot **(2008)**. "Characterisation of uniformly ^{13}C, ^{15}N-labeled bacteriochlorophyll a and bacteriopheophytin a in solution and in solid state: complete assignment of the ^{13}C, ^{1}H and ^{15}N chemical shifts." *Magnetic Resonance in Chemistry* 46 (11): 1074-1083.

Egorova Zachernyuk, T. A., B. van Rossum, G. J. Boender, E. Franken, J. Ashurst, J. Raap, P. Gast, A. J. Hoff, H. Oschkinat and H. J. M. De Groot **(1997)**. "Characterization of pheophytin ground states in *Rhodobacter sphaeroides* R26 photosynthetic reaction centers from multispin pheophytin enrichment and 2-D ^{13}CMAS NMR dipolar correlation spectroscopy." *Biochemistry* 36 (24): 7513-7519.

Eisenmayer, T. J., H. J. M. de Groot, E.van de Wetering, J. Neugebauer, F. Buda **(2012)**. "Mechanism and Reaction Coordinate of Directional Charge Separation in Bacterial Reaction Centers" *Physical Chemical Letters* 3: 694– 697

Emerson R and Chalmers R.V. **(1958)**. "Speculations concerning the function and phylogenetic significance of the accessory pigments in algae." *Phycological Society of American News Bulletin* 11: 51-56.

Ermler, U., G. Fritzsch, S. K. Buchanan and H. Michel **(1994)**. "Structure of the photosynthetic reaction center from *Rhodobacter sphaeroides* at 2.65 Å resolution cofactors and protein cofactor interactions." *Structure* 2 (10): 925-936.

Fairclough, W. V., A. Forsyth, M. C. W. Evans, S. E. J. Rigby, S. Purton and P. Heathcote **(2003)**. "Bidirectional electron transfer in photosystem I: electron transfer on the PsaA side is not essential for phototrophic growth in Chlamydomonas." *Biochimica Et Biophysica Acta-Bioenergetics* 1606 (1-3): 43-55.

Fajer, J., D. C. Brune, M. S. Davis, A. Forman and L. D. Spaulding **(1975)**. "Primary charge separation in bacterial photosynthesis - oxidized chlorophylls and reduced pheophytin." *Proceedings of the National Academy of Sciences of the United States of America* 72 (12): 4956-4960.

Feikema, W. O., P. Gast, I. B. Klenina and I. I. Proskuryakov **(2005)**. "EPR characterisation of the triplet state in photosystem II reaction centers with singly reduced primary acceptor Q A." *Biochimica et Biophysica Acta* 1709: 105-112.

Feldman, K. S., D. K. Hester and J. H. Golbeck **(2007)**. "A relationship between amide hydrogen bond strength and quinone reduction potential: Implications for photosystem I and bacterial reaction center quinone function." *Bioorganic & Medicinal Chemistry Letters* 17 (17): 4891-4894.

Frank, H. A. and R. J. Cogdell **(1996)**. "Carotenoids in photosynthesis." *Photochemistry and Photobiology* 63 (3): 257-264.

Frank, H. A., O. Hansson and P. Mathis **(1989)**. "EPR and optical changes of the photosystem II reaction center produced by low temperature illumination." *Photosynthesis Research* 20: 279-289.

Frese, R. N., M. Germano, F. L. de Weerd, I. H. M. van Stokkum, A. Y. Shkuropatov, V. A. Shuvalov, H. J. van Gorkom, R. van Grondelle and J. P. Dekker **(2003)**. "Electric field effects on the chlorophylls, pheophytins, and beta-carotenes in the reaction center of photosystem II." *Biochemistry* 42 (30): 9205-9213.

Fromme, P., P. Jordan and N. Krauss **(2001)**. "Structure of photosystem I." *Biochimica Et Biophysica Acta-Bioenergetics* 1507 (1-3): 5-31.

Ganapathy, S., G. T. Oostergetel, P. K. Wawrzyniak, M. Reus, A. G. M. Chew, F. Buda, E. J. Boekema, D. A. Bryant, A. R. Holzwarth and H. J. M. de Groot **(2009)**. "Alternating syn-anti bacteriochlorophylls form concentric helical nanotubes in chlorosomes." *Proceedings of the National Academy of Sciences of the United States of America* 106 (21): 8525-8530.

Ghanotakis, D. F., D. M. Demetriou and C. F. Yocum **(1987)**. "Isolation and characterization of an oxygen-evolving photosystem-II reaction center core preparation and a 28 kDa Chl-alpha-binding protein." *Biochimica et Biophysica Acta* 891 (1): 15-21.

Goez, M. **(1997)**. Photochemically Induced Dynamic Nuclear Polarization. *Advance in Photochemistry*. D. C. Neckers, D. H. Volman and G. von Bünau. New York, Wiley: 63-163.

Golbeck, J. **(2004)**. “hotosynthetic Reaction Centers: So little time, so much to do.

Goldstein, R. A. and S. G. Boxer **(1987)**. "Effects Of Nuclear-Spin Polarization On Reaction Dynamics In Photosynthetic Bacterial Reaction Centers." *Biophysical Journal* 51 (6): 937-946.

Gorkom, H. J. and J. P. M. Schelvis **(1993)**. "Kok's oxygen clock: What makes it tick? The structure of P680 and consequences of its oxidizing power." *Photosynthesis Research* 38: 297-301.

Govindjee and E. Rabinowitch **(1960)**. "Two forms of chlorophyll a invivo with distinct photochemical functions." *Science* 132 (3423): 355-356.

Graber, P. and H. T. Witt **(1976)**. "Relations between electrical potential, pH gradient, proton flux and phosphorylation in photosynthetic membrane." *Biochimica et Biophysica Acta* 423 (2): 141-163.

Groot, M. L., N. P. Pawlowicz, L. van Wilderen, J. Breton, I. H. M. van Stokkum and R. van Grondelle **(2005)**. "Initial electron donor and acceptor in isolated photosystem II reaction centers identified with femtosecond mid-IR spectroscopy." *Proceedings of the National Academy of Sciences of the United States of America* 102 (37): 13087-13092.

Groot, M. L., F. vanMourik, C. Eijckelhoff, I. H. M. Van Stokkum, J. P. Dekker and R. vanGrondelle **(1997)**. "Charge separation in the reaction center of photosystem II studied as a function of temperature." *Proceedings of the National Academy of Sciences of the United States of America* 94 (9): 4389-4394.

Guergova-Kuras, M., B. Boudreaux, A. Joliot, P. Joliot and K. Redding **(2001)**. "Evidence for two active branches for electron transfer in photosystem I." *Proceedings of the National Academy of Sciences of the United States of America* 98 (8): 4437-4442.

Gupta, K. B. S. S. **(2011)**. Spin-torch experiments on reaction centers of Rhodobacter sphaeroides, Leiden University.

Guskov, A., A. Gabdulkhakov and A. Zouni **(2010)**. :"Recent progress in the crystallographic studies of photosystem II" *European Journal of Chemical Physics and Physical Chemistry* 11:1160–1171.

Hanley, J., Y. Deligiannakis, A. Pascal, P. Faller, A.W. Rutherford **(1999)**. "Carotenoid oxidation in Photosystem II." *Biochemistry* 38: 8189–8195.

Helmus, J. J., K. Surewicz, M. I. Apostol, W. K. Surewicz and C. P. Jaroniec **(2011)**. "Intermolecular Alignment in Y145Stop Human Prion Protein Amyloid Fibrils Probed by Solid-State NMR Spectroscopy." *Journal of the American Chemical Society* 133 (35): 13934-13937.

Herrin, D. L., J. F. Battey, K. Greer and G. W. Schmidt **(1992)**. "Regulation of chlorophyll apoprotein expression and accumulation - requirements for carotenoids and chlorophyll." *Journal of Biological Chemistry* 267 (12): 8260-8269.

Hillmann, B., K. Brettel, F. van Mieghem, A. Kamlowski, A. W. Rutherford and E. Schlodder **(1995)**. "Charge Recombination Reactions in Photosystem II. 2. Transient Absorbance Difference Spectra and Their Temperature Dependence." *Biochemistry* 34 (14): 4814-4827.

Hillmann, B. and E. Schlodder **(1995)**. "Electron-transfer reactions in photosystem-II core complexes from *Synechococcus* at low-temperature - difference spectrum of $P680^{+}$ Q_A^{-}/P680 Q_A at 77 K." *Biochimica Et Biophysica Acta-Bioenergetics* 1231 (1): 76-88.

Hing, A. W., S. Vega and J. Schaefer **(1992)**. "Transferred-echo double-resonance NMR." *Journal of Magnetic Resonance* 96 (1): 205-209.

Hoff, A. J. and J. Amesz **(1991)**. Visible absorption spectroscopy of chlorophylls. Chlorophylls. H. Sheer. Boca Raton, CRC Press Inc.: 723-738.

Holt, N. E., G. R. Fleming and K. K. Niyogi **(2004)**. "Toward an understanding of the mechanism of nonphotochemical quenching in green plants." *Biochemistry* 43 (26): 8281-8289.

Holzwarth, A. R., M. G. Müller, J. Niklas and W. Lubitz **(2006)**. "Ultrafast transient absorption studies on photosystem I reaction centers from *Chlamydomonas reinhardtii*. 2: Mutations near the P700 reaction center chlorophylls provide new insight into the nature of the primary electron donor." *Biophysical Journal* 90 (2): 552-565.

Holzwarth, A. R., M. G. Müller, M. Reus, M. Nowaczyk, J. Sander and M. Rögner **(2006)**. "Kinetics and mechanism of electron transfer in intact photosystem II and in the isolated reaction center: Pheophytin is the primary electron acceptor." *Proceedings of the National Academy of Sciences of the United States of America* 103 (18): 6895-6900.

Hore, P. J. and R. W. Broadhurst **(1993)**. "Photo-CIDNP of Biopolymers." *Progress in Nuclear Magnetic Resonance Spectroscopy* 25: 345-402.

Hughes, J. L., N. Cox, A. W. Rutherford, E. Krausz, T.-L. Lai, A. Boussac and M. Sugiura **(2010)**. "D1 protein variants in photosystem II from *Thermosynechococcus elongatus* studied by low temperature optical spectroscopy." *Biochimica et biophysica acta* 1797: 11-19.

Hunter, C. N., F. Daldal, M. C. Thurnauer and J. T. Beatty **(2008)**. "The Purple Photosynthetic Bacteria." Dordrecht, Springer.

Ishikita, H., B. Loll, J. Biesiadka, W. Saenger and E.-W. Knapp **(2005)**. "Redox potentials of chlorophylls in the photosystem II reaction center." *Biochemistry* 44 (10): 4118-4124.

Ishikita, H., W. Saenger, J. Biesiadka, B. Loll and E.-W. Knapp **(2006)**. "How photosynthetic reaction centers control oxidation power in chlorophyll pairs P680, P700, and P870." *Proceedings of the National Academy of Sciences of the United States of America* 103 (26): 9855-9860.

Jankowiak, R., M. Ratsep, J. Hayes, V. Zazubovich, R. Picorel, M. Seibert and G. J. Small **(2003)**. "Primary charge-separation rate at 5 K in isolated photosystem II reaction centers containing five and six chlorophyll a molecules." *Journal of Physical Chemistry* B 107 (9): 2068-2074.

Janssen, G. J., E. Daviso, M. Son, H. J. M. Groot, A. Alia and J. Matysik **(2010)**. "Observation of the solid-state photo-CIDNP effect in entire cells of cyanobacteria *Synechocystis*." *Photosynthesis Research* 104 (2-3): 275-282.

Jaroniec, C. P., C. Filip and R. G. Griffin **(2002)**. "3D TEDOR NMR experiments for the simultaneous measurement of multiple carbon-nitrogen distances in uniformly ^{13}C, ^{15}N-labeled solids." *Journal of the American Chemical Society* 124 (36): 10728-10742.

Jaroniec, C. P., B. A. Tounge, J. Herzfeld and R. G. Griffin **(2001)**. "Frequency selective heteronuclear dipolar recoupling in rotating solids: Accurate ^{13}C-^{15}Ndistance measurements in uniformly ^{13}C, ^{15}N-labeled peptides." *Journal of the American Chemical Society* 123 (15): 3507-3519.

Jensen, P. E., A. Haldrup, L. Rosgaard and H. V. Scheller **(2003)**. "Molecular dissection of photosystem I in higher plants: topology, structure and function." *Physiologia Plantarum* 119 (3): 313-321.

Jeschke, G. **(1997)**. "Electron-electron-nuclear three-spin mixing in spin-correlated radical pairs." *Journal of Chemical Physics* 106 (24): 10072-10086.

Jeschke, G. **(1998)**. "A new mechanism for chemically induced dynamic nuclear polarization in the solid state." *Journal of the American Chemical Society* 120 (18): 4425-4429.

Jeschke, G., B. C. Anger, B. E. Bode and J. Matysik **(2011)**. "Theory of Solid-State Photo-CIDNP in the Earth's Magnetic Field." *Journal of Physical Chemistry A* 115 (35): 9919-9928.

Jeschke, G. and J. Matysik **(2003)**. "A reassessment of the origin of photochemically induced dynamic nuclear polarization effects in solids." *Chemical Physics* 294 (3): 239-255.

Joliot, P. and A. Joliot **(1999)**. "In vivo analysis of the electron transfer within photosystem I: Are the two phylloquinones involved?" *Biochemistry* 38 (34): 11130-11136.

Jordan, P., P. Fromme, H. T. Witt, O. Klukas, W. Saenger and N. Krauss **(2001)**. "Three-dimensional structure of cyanobacterial photosystem I at 2.5 Å resolution." *Nature* 411 (6840): 909-917.

Joya, K.S., N.K. Subbaiyan, F.D. Souza, and H.J.M. de Groot **(2012) "**Surface-Immobilized Single-Site Iridium Complexes for Electrocatalytic Water Splitting" *Angewandte Chemie Int. Ed.*, 51, 9601 –9605

Kamiya, N. and J. R. Shen **(2003)**. "Crystal structure of oxygen-evolving photosystem II from *Thermosynechococcus vulcanus* at 3.7 Å resolution." *Proceedings of the National Academy of Sciences of the United States of America* 100 (1): 98-103.

Kamlowski, A., L. Frankemoller, A. van der Est, D. Stehlik and A. R. Holzwarth **(1996)**. "Evidence for delocalization of the triplet state $^{3}P680$ in the D1-D2-cyt b559 complex of photosystem II." Berichte Der Bunsen-Gesellschaft-Physical *Chemistry Chemical Physics* 100 (12): 2045-2051.

Kammel, M., J. Kern, W. Lubitz and R. Bittl **(2003)**. "Photosystem II single crystals studied by transient EPR: the light-induced triplet state." *Biochimica Et Biophysica Acta-Bioenergetics* 1605 (1-3): 47-54.

Kandrashkin, Y. and A. van der Est **(2004)**. "Electron spin polarization of the excited quartet state of strongly coupled triplet-doublet spin systems." *Journal of Chemical Physics* 120 (10): 4790-4799.

Kaptein, R. and J. L. Oosterhoff **(1969)**. "Chemically induced dynamic nuclear polarization II : (Relation with anomalous ESR spectra)." *Chemical Physics Letters* 4 (4): 195.

Karyagina, I., Y. Pushkar, D. Stehlik, A. van der Est, H. Ishikita, E.-W. Knapp, B. Jagannathan, R. Agalarov and J. H. Golbeck **(2007)**. "Contributions of the protein environment to the midpoint Potentials of the A_1 phylloquinones and the F_X iron-sulfur cluster in photosystem I." *Biochemistry* 46 (38): 10804-10816.

Käss, H., E. Bittersmannweidlich, L. E. Andreasson, B. Bonigk and W. Lubitz **(1995)**. "ENDOR and ESEEM of the ^{15}N-labeled radical cations of chlorophyll *a* and the primary donor P-700 in photosystem-I." *Chemical Physics* 194 (2-3): 419-432.

Käss, H., P. Fromme and W. Lubitz **(1996)**. " Quadrupole parameters of nitrogen nuclei in the cation radical P-700(center dot+) determined by ESEEM of single crystals of photosystem I." *Chemical Physics Letters* 257 (1-2): 197-206.

Käss, H., P. Fromme, H. T. Witt and W. Lubitz **(2001)**. "Orientation and electronic structure of the primary donor radical cation P-700$^{+\bullet}$ in photosystem I: A single crystals EPR and ENDOR study." *Journal of Physical Chemistry* B 105 (6): 1225-1239.

Käss, H., W. Lubitz, G. Hartwig, H. Scheer, D. Noy and A. Scherz **(1998)**. "ENDOR studies of substituted chlorophyll cation radicals." *Spectrochimica Acta Part a-Molecular and Biomolecular Spectroscopy* 54 (9): 1141-1156.

Käss, H., J. Rautter, B. Bonigk, P. Hofer and W. Lubitz **(1995)**. "2D ESEEM of the ^{15}N Labeled Radical Cations of Bacteriochlorophyll a and of the Primary Donor in Reaction Centers of *Rhodobacter-Sphaeroides*." *Journal of Physical Chemistry* 99 (1): 436-448.

Kitagawa, Y., K. Matsuda and J. Hasegawa **(2011)**. "Theoretical study of the excited states of the photosynthetic reaction center in photosystem II: Electronic structure, interactions, and their origin." *Biophysical Chemistry* 159 (2-3): 227-236.

Knip, K. **(2011)**. Technici verliezen greep op Fukushima. NRC, NRC media: 2-3.

Koivuniemi, A., E. Swiezewska, E. M. Aro, S. Styring and B. Andersson **(1993)**. "Reduced content of the quinone acceptor Q_A in photosystem II complexes isolated from thylakoid membranes after prolonged photoinhibition under anaerobic conditions." *FEBS Letters* 327 (3): 343-346.

Kok, B., B. Forbush and M. McGloin **(1970)**. "Cooperation of charges in photosynthetic O_2 evolution, 1. A linear 4 step mechanism." *Photochemistry and Photobiology* 11 (6): 457-&.

Kouril, R., N. van Oosterwijk, A. E. Yakushevska and E. J. Boekema **(2005)**. "Photosystem I: a search for green plant trimers." *Photochemical & Photobiological Sciences* 4 (12): 1091-1094.

Kramer, D. M., C. A. Sacksteder and J. A. Cruz **(1999)**. "How acidic is the lumen?" *Photosynthesis Research* 60 (2-3): 151-163.

Kruip, J., D. Bald, E. Boekema and M. Rögner **(1994)**. "Evidence for the existence of trimeric and monomeric photosystem-I complexes in thylakoid membranes from cyanobacteria." *Photosynthesis Research* 40 (3): 279-286.

Leeuwen, P. J. V., M. C. Nieveen, E. J. V. D. Meent, J. P. Dekker and H. J. van Gorkom **(1991)**. "Rapid and simple isolation of pure photosystem II core and reaction center particles from spinach." *Photosynthesis Research* 100: 149-153.

Lendzian, F., R. Bittl, A. Telfer and W. Lubitz **(2003)**. "Hyperfine structure of the photoexcited triplet state ^{3}P680 in plant PSII reaction centres as detennined by pulse ENDOR spectroscopy." *Biochimica Et Biophysica Acta-Bioenergetics* 1605 (1-3): 35-46.

Li, X. H. and T. X. Fan **(2011)**. "Artificial Photosynthesis." *Progress in Chemistry* 23 (9): 1841-1853.

Li, Y. J., A. van der Est, M. G. Lucas, V. M. Ramesh, F. F. Gu, A. Petrenko, S. Lin, A. N. Webber, F. Rappaport and K. Redding **(2006)**. "Directing electron transfer within photosystem I by breaking H-bonds in the cofactor branches." *Proceedings of the National Academy of Sciences of the United States of America* 103 (7): 2144-2149.

Lin, X., H. a. Murchison, V. Nagarajan, W. W. Parson, J. P. Allen and J. C. Williams **(1994)**. "Specific alteration of the oxidation potential of the electron donor in reaction centers from *Rhodobacter sphaeroides*." *Proceedings of the National Academy of Sciences of the United States of America* 91: 10265-10269.

Loll, B., J. Kern, W. Saenger, A. Zouni and J. Biesiadka **(2005)**. "Towards complete cofactor arrangement in the 3.0 A resolution structure of photosystem II." *Nature* 438: 1040-1044.

Lubitz, W. **(2003)**. "Photochemical processes in photosynthesis studied by advanced electron paramagnetic resonance techniques." *Pure and Applied Chemistry* 75 (8): 1021-1030.

Lubitz, W., F. Lendzian and R. Bittl **(2002)**. "Radicals, radical pairs and triplet states in photosynthesis." *Accounts of Chemical Research* 35 (5): 313-320.

Madjet, M. E.-A., F. Mueh and T. Renger **(2009)**. "Deciphering the Influence of Short-Range Electronic Couplings on Optical Properties of Molecular Dimers: Application to "Special Pairs" in Photosynthesis." *Journal of Physical Chemistry* B 113 (37): 12603-12614.

Magnitskii, S. G. and A. N. Tikhonov **(1998)**. "Determination of intrathylakoid pH from the exchange broadening of the ESR spectrum of TEMPO amine spin label in chloroplasts." *Biofizika* 43 (1): 69-76.

Martinez-Junza, V., M. Szczepaniak, S. E. Braslavsky, J. Sander, M. Nowaczyk, M. Rögner and A. R. Holzwarth **(2008)**. "A photoprotection mechanism involving the D2 branch in photosystem II cores with closed reaction centers." *Photochemical & Photobiological Sciences* 7 (11): 1337-1343.

Mathies, G., M. C. van Hemert, P. Gast, K. B. S. S. Gupta, H. A. Frank, J. Lugtenburg and E. J. J. Groenen **(2011)**. "Configuration of Spheroidene in the Photosynthetic Reaction Center of *Rhodobacter sphaeroides*: A comparison of wild-type and reconstituted R26." *Journal of Physical Chemistry* A 115 (34): 9552-9556.

Mathur, S., P. Singh, P. Mehta and A. Jajoo **(2011)**. "Effects of high temperature and low pH on photosystem II photochemistry in spinach thylakoid membranes." *Biologia Plantarum* 55 (4): 747-751.

Mattoo, A. K., H. Hoffmanfalk, J. B. Marder and M. Edelman **(1984)**. "Regulation of Protein-Metabolism - Coupling of photosynthetic electron-transport to invivo degradation of the rapidly metabolized 32-kilodalton protein of the chloroplast membranes." *Proceedings of the National Academy of Sciences of the United States of America* 81 (5): 1380-1384.

Matysik, J. **(2000)**. "Photochemically induced nuclear spin polarization in reaction centers of photosystem II observed by ^{13}C-solid-state NMR reveals a strongly asymmetric electronic structure of the $P680^{+\bullet}$ primary donor chlorophyll." *Proceedings of the National Academy of Sciences* 97 (18): 9865-9870.

Matysik, J., Alia, J. G. Hollander, T. Egorova-Zachernyuk, P. Gast and H. J. M. de Groot **(2000)**. "A set-up to study photochemically induced dynamic nuclear polarization in

photosynthetic reaction centres by solid-state NMR." *Indian Journal of Biochemistry & Biophysics* 37 (6): 418-423.

Matysik, J., A. Diller, E. Roy and A. Alia **(2009)** "The solid-state photo-CIDNP effect." *Photosynthesis Research* DOI: 10.1007/s11120-009-9403-9.

Matysik, J., E. Schulten, Alia, P. Gast, J. Raap, J. Lugtenburg, A. J. Hoff and H. J. M. de Groot **(2001)**. "Photo-CIDNP ^{13}C-magic angle spinning NMR on bacterial reaction centres: Exploring the electronic structure of the special pair and its surroundings." *Biological Chemistry* 382 (8): 1271-1276.

McDermott, A., M. G. Zysmilich and T. Polenova **(1998)**. "Solid state NMR studies of photoinduced polarization in photosynthetic reaction centers: mechanism and simulations." *Solid State Nuclear Magnetic Resonance* 11 (1-2): 21-47.

Moran, R. and D. Porath **(1980)**. "Chlorophyll determination in intact tissues using N,N-dimethylformamide." *Plant Physiology* 65 (3): 478-479.

Muh, F., C. Glockner, J. Hellmich and A. Zouni **(2012)**. "Light-induced quinone reduction in photosystem II." *Biochimica Et Biophysica Acta-Bioenergetics* 1817 (1): 44-65.

Müller, M. G., C. Slavov, R. Luthra, K. E. Redding and A. R. Holzwarth **(2010)**. "Independent initiation of primary electron transfer in the two branches of the photosystem I reaction center." *Proceedings of the National Academy of Sciences* 107 (9): 4123-4128.

Mullet, J. E., J. J. Burke and C. J. Arntzen **(1980)**. "Chlorophyll proteins of Photosystem-I." *Plant Physiology* 65 (5): 814-822.

Myers, J. A., K. L. M. Lewis, F. D. Fuller, P. F. Tekavec, C. F. Yocum and J. P. Ogilvie **(2010)**. "Two-Dimensional Electronic Spectroscopy of the D1-D2-cyt b559 Photosystem II Reaction Center Complex." *Journal of Physical Chemistry Letters 1* (19): 2774-2780.

Nakamura, A., T. Suzawa, Y. Kato and T. Watanabe **(2011)**. "Species dependence of the redox potential of the primary electron donor P700 in photosystem i of oxygenic photosynthetic organisms revealed by spectroelectrochemistry." *Plant and Cell Physiology* 52 (5): 815-823.

Nanba, O. and K. Satoh **(1987)**. "Isolation of a photosystem-II reaction center consisting of D1 and D2 polypeptides and cytochrome-b-559." *Proceedings of the National Academy of Sciences of the United States of America* 84 (1): 109-112.

Nilsson Lill, S. O. **(2011)**. "On the dimerization of chlorophyll in photosystem II." *Physical Chemistry Chemical Physics*: 16022-16027.

Novoderezhkin, V. I., E. G. Andrizhiyevskaya, J. P. Dekker and R. van Grondelle **(2005)**. "Pathways and timescales of primary charge separation in the photosystem II reaction center as revealed by a simultaneous fit of time-resolved fluorescence and transient absorption." *Biophysical Journal* 89 (3): 1464-1481.

Novoderezhkin, V. I., J. P. Dekker and R. van Grondelle **(2007)**. "Mixing of exciton and charge-transfer states in Photosystem II reaction centers: Modeling of stark spectra with modified redfield theory." *Biophysical Journal* 93 (4): 1293-1311.

Novoderezhkin, V. I., E. Romero, J. P. Dekker and R. van Grondelle **(2011)**. "Multiple charge-separation pathways in photosystem II: Modeling of Transient Absorption Kinetics." *Physical Chemistry Chemical Physics* 12 (3): 681-688.

Nowaczyk, M. M., J. Sander, N. Grasse, K. U. Cormann, D. Rexroth, G. Bernat and M. Roegner **(2010)**. "Dynamics of the cyanobacterial photosynthetic network: Communication and modification of membrane protein complexes." *European Journal of Cell Biology* 89 (12): 974-982.

Ohad, I., D. J. Kyle and C. J. Arntzen **(1984)**. "Membrane-protein damage and repair - removal and replacement of inactivated 32-kilodalton polypeptides in chloroplast membranes." *Journal of Cell Biology* 99 (2): 481-485.

Plato, M., N. Krauss, P. Fromme and W. Lubitz **(2003)**. "Molecular orbital study of the primary electron donor P700 of photosystem I based on a recent X-ray single crystal structure analysis." *Chemical Physics* 294 (3): 483-499.

Polenova, T. and A. E. McDermott **(1999)**. "A coherent mixing mechanism explains the photoinduced nuclear polarization in photosynthetic reaction centers." *Journal Of Physical Chemistry B* 103 (3): 535-548.

Polm, M. and K. Brettel **(1998)**. "Secondary pair charge recombination in photosystem I under strongly reducing conditions: Temperature dependence and suggested mechanism." *Biophysical Journal* 74 (6): 3173-3181.

Poluektov, O. G., S. V. Paschenko, L. M. Utschig, K. V. Lakshmi and M. C. Thurnauer **(2005)**. "Bidirectional electron transfer in photosystem I: Direct evidence from high-frequency time-resolved EPR spectroscopy." *Journal of the American Chemical Society* 127 (34): 11910-11911.

Posner, H. B. **(1967)**. "Aquatic vascular plants." Methods in Developmental Biology. F. A. Wilt, Wessel, S.N.K. New York, Crowel: 131-317.

Powles, S. B. **(1984)**. "Photoinhibition of photosynthesis induced by visible-light." *Annual Review of Plant Physiology and Plant Molecular Biology* 35: 15-44.

Prakash, S. **(2006)**. "Photo-CIDNP studies on reaction centers of *Rhodobacter sphaeroides*." PhD Thesis, Universiteit Leiden.

Prakash, S., Alia, P. Gast, H. J. M. de Groot, G. Jeschke and J. Matysik **(2005)**. "Buil-up kinetics of light induced nuclear polarization observed in RCs of *Rhodobacter sphaeroides*." Photosynthesys: Fundamental Aspect to Global Perpectives. A. van der Est and A. Bruce. Montréal, Allen Press: 301-302.

Prakash, S., Alia, P. Gast, H. J. M. de Groot, G. Jeschke and J. Matysik **(2005)**. "Magnetic field dependence of photo-CIDNP MAS NMR on photosynthetic reaction centers of Rhodobacter sphaeroides WT." *Journal Of The American Chemical Society* 127 (41): 14290-14298.

Prakash, S., Alia, P. Gast, H. J. M. de Groot, J. Matysik and G. Jeschke **(2006)**. "Photo-CIDNP MAS NMR in intact cells of *Rhodobacter sphaeroides* R26: Molecular and atomic resolution at nanomolar concentration." *Journal of the American Chemical Society* 128 (39): 12794-12799.

Prakash, S., Alia, P. Gast, G. Jeschke, H. J. M. de Groot and J. Matysik **(2003)**. "Photochemically induced dynamic nuclear polarisation in entire bacterial photosynthetic units observed by ^{13}C magic-angle spinning NMR." *Journal of Molecular Structure* 661: 625-633.

Prakash, S., A. Alia, P. Gast, H. J. M. de Groot, G. Jeschke and J. Matysik **(2007)**. "^{13}C chemical shift map of the active cofactors in photosynthetic reaction centers of Rhodobacter sphaeroides revealed by photo-CIDNP MAS NMR." *Biochemistry* 46 (31): 8953-8960.

Prokhorenko, V. I. and A. R. Holzwarth **(2000)**. "Primary processes and structure of the photosystem II reaction center: A photon echo study." *Journal of Physical Chemistry* B 104 (48): 11563-11578.

Ptushenko, V., D.A. Cherepanov, L.I. Krishtalik, A.Y. Semenov **(2008)**. "Semi-continuum electrostatic calculations of redox potentials in photosystem I." *Photosynthesis Research* 97:55–74

Pulles, M. P. J., H. J. van Gorkom and G. A. M. Verschoor **(1976)**. "Primary reactions of photosystem II at low pH 2. light-induced changes of absorbance and electron spin resonance in spinach chloroplasts." *Biochimica et Biophysica Acta* 440: 98-106.

Ramesh, V. M., K. Gibasiewicz, S. Lin, S. E. Bingham and A. N. Webber **(2004)**. "Bidirectional electron transfer in photosystem I: Accumulation of A_0^- in A-side or B-side mutants of the axial ligand to chlorophyll A_0." *Biochemistry* 43 (5): 1369-1375.

Rappaport, F., M. Blanchard-desce and J. Lavergne **(1994)**. "Kinetics of electron transfer and electrochromic change during the redox transitions of the photosynthetic oxygen-evolving complex." *Biochimica et Biophysica Acta* 1184: 178-192.

Raszewski, G., W. Saenger and T. Renger **(2005)**. "Theory of optical spectra of photosystem II reaction centers: Location of the triplet state and the identity of the primary electron donor." *Biophysical Journal* 88 (2): 986-998.

Raszewski, G., B. A. Diner, E. Schlodder and T. Renger **(2008)**. "Spectroscopic properties of reaction center pigments in photosystem II core complexes: revision of the multimer model." *Biophysical Journal* 95 (1): 105-119.

Rautter, J., F. Lendzian, C. Schulz, A. Fetsch, M. Kuhn, X. Lin, J. C. Williams, J. P. Allen and W. Lubitz **(1995)**. "Endor studies of primary donor cation-radical in mutant reaction centers of Rhodobacter-sphaeroides with altered hydrogn-bond interactions." *Biochemistry* 34 (25): 8130-8143.

Redding, K., A. Jasaitis, R. Luthra, M. Byrdin, C. Slavov, M. Müller, B. Bullock, A. Holzwarth and F. Rappaport **(2007)**. "Directionality of electron transfer within photosystem I." *Photosynthesis Research* 91 (2-3): 139-139.

Rigby, S. E. J., M. C. W. Evans and P. Heathcote **(1996)**. "ENDOR and special triple resonance spectroscopy of A_1 of photosystem I." *Biochemistry* 35 (21): 6651-6656.

Rigby, S. E. J., J. H. A. Nugent and P. J. Omalley **(1994)**. "ENDOR and special triple-resonance studies of chlorophyll cation radicals in photosystem-II." *Biochemistry* 33 (33): 10043-10050.

Riley, K., R. Jankowiak, M. Ratsep, G. J. Small and V. Zazubovich **(2004)**. "Evidence for highly dispersive primary charge separation kinetics and gross heterogeneity in the isolated photosystem II reaction center of green plants." *Journal of Physical Chemistry* B 108 (29): 10346-10356.

Riley, K., V. Zazubovich, R. Jankowiak and G. J. Small **(2004)**. "Spectral hole burning studies of the isolated photosystem II reaction center of green plants." *Biophysical Journal* 86 (1): 12A-12A.

Rochaix, J.-D. **(2011)**. "Reprint of: Regulation of photosynthetic electron transport." *Biochimica et Biophysica Acta* 1807 (8): 878-886.

Rögner, M., P. J. Nixon and B. A. Diner **(1990)**. "Purification and characterization of photosystem-I and photosystem-II core complexes from wild-type and phycocyanin-deficient strains of the cyanobacterium *Synechocystis* PCC-6803." *Journal of Biological Chemistry* 265 (11): 6189-6196.

Romberger, S. P. and J. H. Golbeck **(2010)**. "The bound iron–sulfur clusters of Type-I homodimeric reaction centers." *Photosynthesis Research* 104 (2-3): 333-346.

Romero, E., I. H. M. van Stokkum, V. I. Novoderezhkin, J. P. Dekker and R. van Grondelle **(2010)**. "Two Different Charge Separation Pathways in Photosystem II." *Biochemistry* 49 (20): 4300-4307.

Romero, E, B.A. Diner, P.J. Nixon, W.J. Coleman, J. Wiliam, J.P. Dekker, and R. van Grondelle **(2012)**. "Mixed Exciton-Charge-Transfer States in Photosystem II: Stark Spectroscopy on Site-Directed Mutants." *Biophysical Journal* 103 (2):185-194.

Roth, H. D. **(1996)**. "Dependence of the yield of a radical-pair reaction in the solid-state on orientation" in a Magnetic-Field. Encyclopedia of Nuclear Magnetic Resonance. D. M. Grant and R. K. Harris. Chichester, Wiley. II: 1337-1350.

Roy, E., Alia, P. Gast, H. van Gorkom, H. J. M. de Groot, G. Jeschke and J. Matysik **(2007)**. "Photochemically induced dynamic nuclear polarization in the reaction center of the green sulphur bacterium Chlorobium tepidum observed by ^{13}C MAS NMR." *Biochimica Et Biophysica Acta-Bioenergetics* 1767 (6): 610-615.

Roy, E., A. Diller, Alia, P. Gast, H. J. van Gorkom, H. J. M. de Groot, G. Jeschke and J. Matysik **(2007)**. "Magnetic field dependence of ^{13}C photo-CIDNP MAS NMR in plant photosystems I and II." *Applied Magnetic Resonance* 31 (1-2): 193-204.

Roy, E., T. Rohmer, P. Gast, G. Jeschke, A. Alia and J. Matysik **(2008)**. "Characterization of the primary radical pair in reaction centers of Heliobacillus mobilis by ^{13}C photo-CIDNP MAS NMR." *Biochemistry* 47 (16): 4629-4635.

Rutherford, A.W., P. Faller, **(2003).** "Photosystem II: evolutionary perspectives" *Philosophical Transactions of the Royal Society* B 358: 245–253.

Rutherford, A.W., W. Nitschke, **(1996)** "Photosystem II and the quinone–iron-containing reaction centers: comparisons and evolutionary perspectives", Origin and evolution of biological energy conversion, H. Baltscheffsky, CVH, New York: 43–175.

Saito, K., T. Ishida, M. Sugiura, K. Kawakami, Y. Umena, N. Kamiya, J.-R. Shen and H. Ishikita **(2011)**. "Distribution of the Cationic State over the Chlorophyll Pair of the photosystem II Reaction Center." *Journal of the American Chemical Society* 133 (36): 14379-14388.

Saito, K. and H. Ishikita **(2011)**. "Cationic state distribution over the p700 chlorophyll pair in photosystem I." *Biophysical Journal* 101 (8): 2018-2025.

Saito, K., J. R. Shen and H. Ishikita **(2012)**. "Influence of the Axial Ligand on the Cationic Properties of the Chlorophyll Pair in Photosystem II from *Thermosynechococcus vulcanus*." *Biophysical Journal* 102 (11): 2634-2640.

Santabarbara, S., S. Kuprov, I. Fairclough and A. P. Casazza **(2010)**. "Bidirectional Electron Transfer in the Reaction Centre of Photosystem I." *Journal of Integrative Plant Biology* 52 (8): 735-749.

Santabarbara, S., I. Kuprov, W. V. Fairclough, S. Purton, P. J. Hore, P. Heathcote and M. C. W. Evans **(2005)**. "Bidirectional electron transfer in photosystem I: Determination of two distances between $P700^+$ and A_1^- in spin-correlated radical pairs." *Biochemistry* 44 (6): 2119-2128.

Santabarbara, S., I. Kuprov, P. J. Hore, A. Casal, P. Heathcote and M. C. W. Evans **(2006)**. "Analysis of the spin-polarized electron spin echo of the [$P700+A_1^-$] radical pair of photosystem I indicates that both reaction center Subunits are competent in electron transfer in cyanobacteria, green algae, and higher plants." *Biochemistry* 45 (23): 7389-7403.

Santabarbara, S., I. Kuprov, O. Poluektov, A. Casal, C. A. Russell, S. Purton and M. C. W. Evans **(2010)**. "Directionality of Electron-Transfer Reactions in Photosystem I of Prokaryotes: Universality of the Bidirectional Electron-Transfer Model." *Journal of Physical Chemistry B* 114 (46): 15158-15171.

Scheller, H. V., P. E. Jensen, A. Haldrup, C. Lunde and J. Knoetzel **(2001)**. "Role of subunits in eukaryotic Photosystem I." *Biochimica Et Biophysica Acta-Bioenergetics* 1507 (1-3): 41-60.

Schlodder, E., T. Renger, G. Raszewski, W. J. Coleman, P. J. Nixon, R. O. Cohen and B. A. Diner **(2008)**. "Site-directed mutations at D1-Thr179 of photosystem II in *Synechocystis* sp PCC 6803 modify the spectroscopic properties of the accessory

chlorophyll in the D1-branch of the reaction center." *Biochemistry* 47 (10): 3143-3154.

Schmid, V. H. R., K. V. Cammarata, B. U. Bruns and G. W. Schmidt **(1997)**. "In vitro reconstitution of the photosystem I light-harvesting complex LHCI-730: Heterodimerization is required for antenna pigment organization." *Proceedings of the National Academy of Sciences of the United States of America* 94 (14): 7667-7672.

Schulten, E. A. M., J. Matysik, Alia, S. Kiihne, J. Raap, J. Lugtenburg, P. Gast, A. J. Hoff and H. J. M. de Groot **(2002)**. "^{13}CMAS NMR and photo-CIDNP reveal a pronounced asymmetry in the electronic ground state of the special pair of Rhodobacter sphaeroides reaction centers." *Biochemistry* 41 (27): 8708-8717.

Schuster, G., R. Timberg and I. Ohad **(1988)**. "Turnover of thylakoid photosystem-II proteins during photoinhibition of *Chlamydomonas-reinhardtii*." *European Journal of Biochemistry* 177 (2): 403-410.

Seibert, M., Ed. **(1993)**. The photosynthetic reaction center. New York, Academic Press.

Setif, P. and K. Brettel **(1993)**. "Forward electron-transfer from phylloquinone-A(1) to iron-sulfur centers in spinach photosystem-I." *Biochemistry* 32 (31): 7846-7854.

Shibata, Y, S. Nishi, K. Kawakami, J.R. Shen and T. Renger **(2013).** "Photosystem II Does Not Possess a Simple Excitation Energy Funnel: Time-Resolved Fluorescence Spectroscopy Meets Theory." Journal of the American Chemical Society 135 (18): 6903-6914.

Srinivasan, N., I. Karyagina, R. Bittl, A. van der Est and J. H. Golbeck **(2009)**. "Role of the hydrogen bond from Leu722 to the A_{1A} phylloquinone in photosystem I." *Biochemistry* 48 (15): 3315-3324.

Stoll, S. and A. Schweiger **(2006)**. "EasySpin, a comprehensive software package for spectral simulation and analysis in EPR." *Journal of Magnetic Resonance* 178 (1): 42-55.

Stroebel, D., Y. Choquet, J. L. Popot and D. Picot **(2003)**. "An atypical haem in the cytochrome b(6)f complex." *Nature* 426 (6965): 413-418.

Styring, S. and A. W. Rutherford **(1988)**. "Deactivation kinetics and temperature dependence of the S-state transitions in the oxygen-evolving system of photosystem II measured by EPR spectroscopy." *Science* 933: 378-387.

Styring, S., J. Sjöholm and F. Mamedov **(2012)**. "Two tyrosines that changed the world: Interfacing the oxidizing power of photochemistry to water splitting in photosystem II." *Biochimica et Biophysica Acta* 1817 (1): 76-87.

Suzuki, H., M. Sugiura and T. Noguchi **(2005)**. "pH dependence of the flash-induced S-state transitions in the oxygen-evolving center of photosystem II from *Thermosynechoccocus elongatus* as revealed by Fourier transform infrared spectroscopy." *Biochemistry* 44 (5): 1708-1718.

Takahashi, R., K. Hasegawa and T. Noguchi **(2008)**. "Effect of charge distribution over a chlorophyll dimer on the redox potential of P680 in photosystein II as studied by density functional theory calculations." *Biochemistry* 47 (24): 6289-6291.

Tang, D., R. Jankowiak, M. Seibert, C. F. Yocum and G. J. Small **(1990)**. "Excited-state structure and energy-transfer dynamics of 2 different preparations of the reaction center of photosystem-II - a hole-burning study." *Journal of Physical Chemistry* 94 (17): 6519-6522.

Tang, D. M., R. Jankowiak, M. Seibert and G. J. Small **(1991)**. "Effects of detergent on the excited-state structure and relaxation dynamics of the photosystem-II reaction center - a high-resolution hole burning study " *Photosynthesis Research* 27 (1): 19-29.

Telfer, A. **(2005)**. "Too much light? How beta-carotene protects the photosystem II reaction centre." *Photochemical & Photobiological Sciences* 4 (12): 950-956.

Tetenkin, V. L., B. A. Gulyaev, M. Seibert and A. B. Rubin **(1989)**. "Spectral properties of stabilized D1/D2/cytochrome-b-559 in the photosystem-II reaction center complex - effects of triton X-100 on the redox state of pheophytin, and beta-carotene." *FEBS Letters* 250 (2): 459-463.

Thamarath, S. S., A. Alia, E. Daviso, D. Mance, J. H. Golbeck and J. Matysik **(2012)**. "Whole Cell Nuclear Magnetic Resonance Characterization of Two Photochemically Active States of the Photosynthetic Reaction Center in Heliobacteria." *Biochemistry* 51 (29): 5763-5773.

Thamarath, S.S., J. Heberle, P. J. Hore, T. Kottke and J. Matysik **(2010)**. "Solid-State Photo-CIDNP Effect Observed in Phototropin LOV1-$C_{57}S$ by ^{13}C Magic-Angle Spinning NMR Spectroscopy." *Journal of the American Chemical Society* 132 (44): 15542-15543.

Thurnauer, M.C. and J.R. Norris **(1980)**. "An electron-spin echo phase-shift observed in photosynthetic algae - possible evidence for dynamic radical pair interactions." *Chemical Physics Letters* 76 (3): 557-561.

Tracewell, C.A., J.S. Vrettos, J.A. Bautista, H.A. Frank, G.W. Brudvig **(2001)**. "Carotenoid photooxidation in Photosystem II" *Archives of Biochemistry and Biophysics* 385: 61–69.

Trebst, A. **(1986)**. "The topology of the plastoquinone and herbicide binding peptides of photosystem-II in the thylakoid membrane." *Zeitschrift Fur Naturforschung C-a Journal of Biosciences* 41 (1-2): 240-245.

Trubitsin, B. V. and A. N. Tikhonov **(2003)**. "Determination of a transmembrane pH difference in chloroplasts with a spin label tempamine." *Journal of Magnetic Resonance* 163 (2): 257-269.

Umena, Y., K. Kawakami, J. R. Shen and N. Kamiya **(2011)**. "Crystal structure of oxygen-evolving photosystem II at a resolution of 1.9 Å." *Nature* 473 (7345): 55-U65.

van der Vos, R., P. J. van Leeuwen, P. Braun and A. J. Hoff **(1992)**. "Analysis of the optical absorbency spectra of D1-D2-cytochrome b-559 complexes by absorbency-detected magnetic-resonance - structural-properties of P680." *Biochimica et Biophysica Acta* 1140 (2): 184-198.

van Kan, P. J. M., S. C. M. Otte, F. A. M. Kleinherenbrink, M. C. Nieveen, T. J. Aartsma and H. J. Vangorkom **(1990)**. "Time-resolved spectroscopy at 10k of the photosystem-II reaction center - deconvolution of the red absorption-band." *Biochimica et Biophysica Acta* 1020 (2): 146-152.

van Leeuwen, P. J., M. C. Nieveen, E. J. Vandemeent, J. P. Dekker and H. J. Vangorkom **(1991)**. "Rapid and simple isolation of pure photosystem II core and reaction center particles from spinach." *Photosynthesis Research* 28 (3): 149-153.

van Mieghem, F., K. Brettel, B. Hillman, A. Kamlowski, A. W. Rutherford and E. Schlodder **(1995)**. "Charge Recombination Reactions in Photosystem II. 1. Yields, Recombination Pathways, and Kinetics of the Primary Pair." *Biochemistry* 34 (14): 4798-4813.

van Mieghem, F. J. E., K. Satoh and A. W. Rutherford **(1991)**. "A chlorophyll tilted 30-degrees relative to the membrane in the photosystem-II reaction center. ." *Biochimica et Biophysica Acta* 1058 (3): 379-385.

van Mieghem, F. J. E., G. F. W. Searle, A. W. R and T. J. Schaafsma **(1992)**. "The influence of the double rcduction of Q_A on the fluorescence decay kinetics of photosystem II." *Biochimica et Biophysica Acta* 1100: 198-206.

Vass, I., S. Styring, T. Hundal, a. Koivuniemi, E. Aro and B. Andersson **(1992)**. "Reversible and irreversible intermediates during photoinhibition of photosystem II: stable

reduced Q_A species promote chlorophyll triplet formation." *Proceedings of the National Academy of Sciences of the United States of America* 89 (4): 1408-1412.

Wang, J., D. Gosztola, S. V. Ruffle, C. Hemann, M. Seibert, M. R. Wasielewski, R. Hille, T. L. Gustafson and R. T. Sayre **(2002)**. "Functional asymmetry of photosystem II D1 and D2 peripheral chlorophyll mutants of *Chlamydomonas reinhardtii*." *Proceedings of the National Academy of Sciences of the United States of America* 99 (6): 4091-4096.

Ward, H. R. and R. G. Lawler **(1967)**. "Nuclear Magnetic Resonance Emission And Enhanced Absorption In Rapid Organometallic Reactions." *Journal Of The American Chemical Society* 89 (21): 5518-&.

Watanabe, T., M. Kobayashi, A. Hongu, M. Nakazato, T. Hiyama and N. Murata **(1985)**. "Evidence that a chlorophyll-a' dimer constitutes the photochemical-reaction center-1 (P700) in photosynthetic apparatus." *FEBS Letters* 191 (2): 252-256.

Webber, A. N. and W. Lubitz **(2001)**. "P700: the primary electron donor of photosystem I." *Biochimica Et Biophysica Acta-Bioenergetics* 1507 (1-3): 61-79.

Wientjes, E., G. T. Oostergetel, S. Jansson, E. J. Boekema and R. Croce **(2009)**. "The Role of Lhca Complexes in the Supramolecular Organization of Higher Plant Photosystem I." *Journal of Biological Chemistry* 284 (12): 7803-7810.

Wirtz, A. C., M. C. van Hemert, J. Lugtenburg, H. A. Frank and E. J. J. Groenen **(2007)**. "Two stereoisomers of spheroidene in the Rhodobacter sphaeroides R26 reaction center: A DFT analysis of resonance raman spectra." *Biophysical Journal* 93 (3): 981-991.

Witt, H. T. **(1996)**. "Structure Analysis of Single Crystals of Photosystem I by X-Ray, EPR and ENDOR." Oxygenic Photosynthesis: The Light Reactions. D. R. Ort and C. F. Yocum. Dordrecht, Kluwer Academic Publoshers. 4: 363-375.

Woodbury, N. W. and J. P. Allen **(1995)**. "The pathway, kinetics and thermodynamics of electron transfer in wild type and mutant reaction centers of purple nonsulfur bacteria." Anoxygenic photosynthetic bacteria: advances in photosynthesis. R. E. Blankenship, M. T. Madigan and C. E. Bauer. Dordrecht, Kluwer Academic Publishers: 527-557.

Xiong, J., S. Subramaniam and Govindjee **(1998)**. "A knowledge-based three dimensional model of the Photosystem II reaction center of *Chlamydomonas reinhardtii*." *Photosynthesis Research* 56 (3): 229-254.

Xue, Y. F., M. Okvist, O. Hansson and S. Young **(1998)**. "Crystal structure of spinach plastocyanin at 1.7 Å resolution." Protein Science 7 (10): 2099-2105.

Yang, X., Y. H. Zhang, Z. L. Yang, L. J. Chen, J. L. He and R. F. Wang **(2009)**. "pH Dependence of Photosynthetic Behavior of Plant Photosystem I Particles." *Russian Journal of Plant Physiology* 56 (5): 599-606.

Yao, D. C. I., D. C. Brune, D. Vavilin and W. F. J. Vermaas **(2012)**. "Photosystem II component lifetimes in the cyanobacterium *Synechocystis sp* strain PCC 6803 small cab-like proteins stabilize biosynthesis intermediates and affect early steps in chlorophyll synthesis." *Journal of Biological Chemistry* 287 (1): 682-692.

Yeates, T. O., H. Komiya, D. C. Rees, J. P. Allen and G. Feher **(1987)**. "Structure of the reaction center from *Rhodobacter-sphaeroides* R-26 - membrane-protein interactions." *Proceedings of the National Academy of Sciences of the United States of America* 84 (18): 6438-6442.

Zazubovich, V., R. Jankowiak, K. Riley, R. Picorel, M. Seibert and G. J. Small **(2003)**. "How fast is excitation energy transfer in the photosystem II reaction center in the low temperature limit? Hole burning vs photon echo." *Journal of Physical Chemistry B* 107 (12): 2862-2866.

Zouni, A., H. T. Witt, J. Kern, P. Fromme, N. Krauss, W. Saenger and P. Orth **(2001)**. "Crystal structure of photosystem II from Synechococcus elongatus at 3.8 Å resolution." *Nature* 409 (6821): 739-743.

Zysmilich, M. G. and A. McDermott **(1994)**. "Photochemically Induced Dynamic Nuclear-Polarization In The Solid-State ^{15}N Spectra Of Reaction Centers From Photosynthetic Bacteria *Rhodobacter-Sphaeroides* R-26." *Journal of the American Chemical Society* 116 (18): 8362-8363.

Zysmilich, M. G. and A. McDermott **(1996)**. "Photochemically Induced Nuclear Spin Polarization in Bacterial Photosynthetic Reaction Centers : Assignments of the ^{15}N SSNMR Spectra." *Journal of the American Chemical Society* 7863 (5): 5867-5873.

SUMMARY

Photosynthesis is the process by which photosynthetic organisms convert solar energy into chemical energy. Photosynthesis in plants, algae and cyanobacteria releases oxygen and is referred to as oxygenic photosynthesis. The primary photosynthetic processes of energy conversion occur inside the reaction center (RC), a pigment-protein complex located at the heart of the photosynthetic complexes. Among all the photosynthetic RCs only PSII provides a redox reaction that is sufficiently strong to oxidize water. PSII consists of a protein matrix with highly tuned cofactors facilitating electron transfer (ET) with quantum efficiency close to 100%. The cofactor arrangement in the PSII RC shows a strong similarity to that found in bacterial RCs of purple bacteria, yet the oxidation potentials differ greatly. Despite extensive research, the exact nature of the exceptionally high redox potential of PSII and the role of the protein matrix in establishing this redox potential are still unknown. The electrons flow from PSII to PSI, a complex optimized to provide a strong reductant which is used for the formation of NADPH. While the electron flow in PSII is strictly asymmetric, in PSI different levels of bidirectionality indicate functional flexibility of this complex. This raises the question whether the electronic architecture of PSI varies across different plant sources and influences the electronic ground state of P700.

Photo-CIDNP (chemically induced nuclear polarization) is non-Boltzmann nuclear magnetization caused by photochemical reactions and can be observed by NMR spectroscopy as strongly enhanced absorptive or emissive signals. For RC studies photo-CIDNP has proven to be a powerful tool. It provides selective excitation of cofactors, electron density profiles in the ground state from the chemical shifts, excited state profiles from the signal intensities and gives insight into the kinetic stabilization of photosynthetic intermediates and other transient species. When used in a time-resolved manner, photo-CIDNP provides access to molecular dynamics from correlation signals in two-dimensional dipolar spectroscopy.

Photo-CIDNP studies on PSI and PSII have been limited to the isolated complexes due to difficulties with incorporating selective isotope labels into plant RCs. In this thesis photo-CIDNP solid state NMR with selective isotope labeling has been applied to get direct access to the heart of large PSII and PSI photosynthetic complexes in intact and isolated systems of *Spirodela oligorrhiza* and *Synechocystis* sp. PCC 6803. For the first time the direct observation of selective atoms within the heart of the PSII and PSI complexes by

experiments on entire plants and whole cells is reported. In this way the conservation of the electronic structure of the PSII electron donor at various levels of biological preparations have been addressed and the electron spin density (ρ_i) in the active cofactors of PSI has been constructed. In addition the functional heterogeneity of the PSI electron donor among different plant species was probed.

In **chapter 2** experiments have been performed on selective ^{13}C- isotope labeled whole cells of *Synechocystis* sp. PCC 6803 cyanobacteria. The results demonstrate for the first time the occurrence of the solid-state photo-CIDNP effect in cyanobacteria. In addition, the observed photo-CIDNP features suggested a remarkable conservation of the electronic properties of the photochemical machineries from plants and cyanobacteria. The observation of the photo-CIDNP effect directly in whole cells implies that photo-CIDNP MAS NMR studies on oxygenic photosystems are not limited to isolated plant photosystems.

Chapter 3 reports experiments that have been performed on ^{15}N- isotope labeled PSI-110 particles from spinach and duckweed. The results demonstrate a strict conservation of the electronic ground state of the PSI electron donor among different plant systems, while simultaneously a large flexibility of the PSI was observed in terms of its electronic architecture. Despite the highly optimized redox properties of P700, PSI shows functional heterogeneity in terms of the relative participation of the two branches in ET. The results discussed in this chapter reveal that these variations do not affect P700 but remain in the periphery.

In **chapter 4** experiments have been performed on D1D2 and PSII core complexes from spinach and duckweed and on selectively ^{13}C- labeled duckweed. The solid-state photo-CIDNP effect in conjunction with selective isotope incorporation allows for the observation of NMR signals from the primary radical pair of PSII, directly from thylakoid membranes, as well as from entire plants. The data presented here demonstrate that the photochemical machinery is remarkably robust and remains essentially unaffected by the various preparation procedures, this is important for the validation of results obtained from the extensively studied D1D2 complex. In addition the results presented in this chapter show that the electronic structures of the PSII electron donor in spinach and duckweed are identical. Analysis of the spectra obtained from selectively ^{13}C- labeled thylakoid membranes showed clearly that the radical pair in PSII is formed by a single Chl *a* and a single Phe *a*. In addition the involvement of the protein matrix and the mechanism of photo-CIDNP buildup in larger PSII systems have been discussed in this chapter.

In **chapter 5** time-resolved ns-flash photo-CIDNP MAS NMR experiments on PSI and PSII have been discussed. The results are in agreement with bidirectional electron transfer in PSI and the photo-CIDNP buildup is PSI is discussed. As expected, a significant contribution of the DR mechanism in the photo-CIDNP buildup is observed in PSII, which is not detected for PSI. The results show that the photo-CIDNP buildup in PSII resembles the buildup observed for *Rb. sphaeroides* R26, due to the long triplet lifetime.

Finally, **chapter 6** contains an outlook for applications of photo-CIDNP to selectively labeled PSII and PSI and 2- and 3-dimensional MAS NMR experiments are proposed. The observed field effect and light induced changes in various experiments on PSI particles are discussed and the first data obtained from selectively ^{15}N-ALA labeled PSII is presented. Based on the preliminary data presented in Chapter 6, the relative participation of the two cofactor branches in ET in PSI and the involvement of a histidine with spin density ρ_i in ET in PSII is discussed.

SAMENVATTING

Fotosynthese is het proces waarmee fotosynthetische organismen zonne-energie omzetten in chemische energie. Tijdens de fotosynthetische reacties in planten, algen en cyanobacteriën komt zuurstof vrij, dit wordt oxygene fotosynthese genoemd. De primaire fotosynthetische processen van energieomzetting vinden plaats in het reactiecentrum (RC), een pigment-eiwitcomplex gelokaliseerd in het hart van het fotosynthetische complex. Van alle RC bezit uitsluitend fotosysteem II (PSII) een reductieve kracht die sterk genoeg is om water te oxideren. PSII bestaat uit een eiwitmatrix met zeer nauwkeurig afgestelde cofactoren die de elektron overdracht faciliteren met een kwantumefficiëntie van bijna 100%. De ordening van de cofactoren in het PSII RC vertoont sterke overeenkomsten met die in bacteriële RC van purperbacteriën terwijl de oxidatieve potentialen sterk verschillen. Ondanks uitgebreid onderzoek is het geheim achter deze buitengewone hoge redox potentiaal en de rol van de omringende eiwitmatrix nog niet ontrafeld. De elektronen stromen van PSII naar PSI, een complex met een sterk reductieve kracht, die wordt gebruikt voor het aanmaken van NADPH. Hoewel de elektronenstroom in PSII strikt asymmetrisch is, vertoont PSI een veel grotere flexibiliteit en kan elektron overdracht via beide cofactor takken plaatsvinden. De vraag die hieruit voortvloeit, is of the elektronische architectuur van het PSI complex varieert tussen verschillende plantsoorten en ook de elektronische grondtoestand van P700 beïnvloedt.

Photo-CIDNP (photo-chemically induced nuclear polarization) is non-Boltzmann kernmagnetisatie die wordt veroorzaakt door fotochemische reacties en kan met behulp van NMR spectroscopie worden geobserveerd als zeer versterkte negatieve en positieve NMR signalen. Photo-CIDNP is een uitstekend geschikt gereedschap voor het bestuderen van fotosynthetische RC. Het biedt de mogelijkheid tot selectieve excitatie van cofactoren, het construeren van elektrondichtheidprofielen via de intensiteit van de signalen en het verschaft ook inzicht in de kinetische stabilisatie van fotosynthetische intermediairen en andere transiente soorten. Toegepast in de tijdopgeloste modus, geeft photo-CIDNP via gecorreleerde signalen in 2-dimensionale dipolaire spectroscopie toegang tot de moleculaire dynamiek.

Photo-CIDNP studies van PSI en PSII waren vooralsnog beperkt tot het meten van geïsoleerde complexen vanwege de moeilijkheid om planten RC-selectief te labelen met ^{13}C- en ^{15}N-isotopen. In dit proefschrift is photo-CIDNP vaste stof NMR in combinatie met

selectieve isotoopverrijking toegepast om directe toegang tot het hart van de grote PSII en PSI complexen binnenin zowel intacte en geïsoleerde systemen van kroos en *Synechocystis* sp. PCC 6803 te krijgen en selectieve atomen in het RC te bestuderen. Hiermee kon het behoud van de elektronische structuur van de PSII elektron donor in verschillende biologische preparaties worden onderzocht en de elektronspindichtheid (ρ_i) in de actieve cofactoren van PSI worden geconstrueerd. Daarnaast is de functionele heterogeniteit van de PSI elektron donor in verschillende planten soorten onderzocht.

Hoofdstuk 2 rapporteert over de resultaten die zijn verkregen middels het uitvoeren van experimenten op selectief ^{13}C- isotoop gelabelde hele cellen van de cyanobacterie *Synechocystis* sp. PCC 6803. De in dit hoofdstuk besproken resultaten tonen voor het eerst het vaste-stof photo-CIDNP effect in cyanobacteriën aan. Daarnaast suggereren de geobserveerde photo-CIDNP signalen een buitengewoon complete overeenkomst van de elektronische eigenschappen van de fotosynthetische machinerie tussen planten en cyanobacteriën. Het feit dat het photo-CIDNP effect direct kan worden geobserveerd middels experimenten met hele cellen, betekent dat photo-CIDNP MAS NMR studies van oxygene fotosystemen niet zijn beperkt tot geïsoleerde plantfotosystemen.

In **Hoofdstuk 3** worden de resultaten van experimenten met uniform ^{15}N- isotoop gelabelde PSI-110 deeltjes van spinazie en kroos besproken. De resultaten demonstreren een stikte conservatie van de elektronische grondtoestand van de PSI elektrondonor tussen verschillende plantsystemen terwijl tegelijkertijd een zeer grote flexibiliteit wordt geconstateerd wat betreft de elektronische architectuur. Ondanks de zeer geoptimaliseerde redox eigenschappen van P700, vertoont PSI functionele heterogeniteit wat betreft de relatieve participatie van de twee cofactor takken in elektron overdracht. De besproken resultaten in dit hoofdstuk laten zien dat deze variaties de P700 niet beïnvloeden maar zich beperken tot de periferie.

Hoofdstuk 4 beschrijft de experimenten die zijn gedaan met D1D2 en PSII core-complexen van spinazie en kroos en met selectief ^{13}C- isotoop gelabeld kroos. Het vaste stof photo-CIDNP effect in conjunctie met selectieve ^{13}C isotoop verrijking maakt het mogelijk om NMR signalen van het primaire radicaalkoppel van PSII te observeren direct in preparaties van thylakoide membranen en ook hele kroosplanten. De besproken data demonstreren dat de fotosynthetische machinerie opmerkelijk robuust is en in essentie niet wordt beïnvloed door verschillende sample bereidingsprocedures en isolatie. Dit is belangrijk bij het valideren van resultaten die zijn verkregen van het uitgebreid bestudeerde D1D2

complex. Verder tonen de in dit hoofdstuk besproken resultaten aan dat de elektronische structuren van de PSII elektron donor in spinazie en kroos identiek zijn. Analyse van de verkregen spectra van selectief ^{13}C- gelabeld thylakoide membraan toont duidelijk aan dat het radicaalkoppel in PSII wordt gevormd door een enkele Chl *a* en één Phe *a* molecuul. Daarnaast is in dit hoofdstuk de invloed van de eiwitmatrix en het mechanisme achter de photo-CIDNP opbouw in grotere PSII systemen besproken.

In **hoofdstuk 5** zijn tijd opgeloste ns-flash photo-CIDNP MAS NMR experimenten aan PSI en PSII besproken. De resultaten zijn in overeenstemming met een elektronoverdracht via beide cofactortakken en de opbouw van photo-CIDNP in PSI is in dit hoofdstuk uiteengezet. Een significante bijdrage van het DR mechanisme in de opbouw van photo-CIDNP is geobserveerd in PSII maar niet gedetecteerd bij photo-CIDNP opbouw in PSI. De resultaten tonen aan dat de opbouw van photo-CIDNP in PSII overeenkomt met de opbouw in *Rb. sphaeroides* R26 vanwege de lange levensduur in beide systemen.

Tenslotte bevat **hoofdstuk 6** een vooruitblik naar de toepassing van photo-CIDNP op selectief gelabeld PSII en PSI en worden mogelijke 2- en 3-dimenionale MAS NMR experimenten voorgesteld. Het waargenomen veldeffect en de licht geïnduceerde veranderingen in de verschillende experimenten op PSI deeltjes worden besproken en de eerste data die zijn verkregen van selectief ^{15}N-ALA gelabeld PSII worden gepresenteerd.

Gebaseerd op de preliminaire data in hoofdstuk 6 wordt de relatieve participatie van de twee cofactor takken in de elektron overdracht in PSI en de betrokkenheid van een histidine met partiële spindichtheid (ρ_i) besproken.

LIST OF PUBLICATIONS

A. Alia, P.K. Wawrzyniak, G.J. Janssen, F. Buda, J. Matysik. and H.J.M. de Groot. **(2009)** "Differential charge polarization of axial Histidines in Bacterial Reaction Centers Balances the Asymmetry of the Special Pair." *J. Am. Chem. Soc.*, 131(28): 9626-7 http://pubs.acs.org/doi/abs/10.1021/ja9028507

G. J. Janssen, E. Daviso, M. van Son, J. Matysik, and A. Alia **(2010)**. "Observation of the solid-state photo-CIDNP effect in entire cells of cyanobacteria *Synechocystis* sp. PCC-6803." *Photosynth. Res., 104*, 275-282. http://www.springerlink.com/content/b068n17um89p1m0k/

E. Daviso, G.J. Janssen, A. Alia, G. Jeschke, J. Matysik, and M. Tessari **(2011)**. "A 10 000-fold Nuclear Hyperpolarization of a Membrane Protein in the Liquid Phase via Solid-State Mechanism." *J. Am. Chem. Soc., 133*: 16754-16757. http://pubs.acs.org/doi/abs/10.1021/ja206689t?mi=sgirgo&af=R&pageSize=20&searchText=Proton+exchange+membrane

G. J. Janssen, E. Roy, J. Matysik, and A. Alia **(2012)**. "^{15}N Photo-CIDNP MAS NMR To Reveal Functional Heterogeneity in Electron Donor of Different Plant Organisms." *App. Mag. Res., 42*: 57-67. http://www.springerlink.com/content/k1kr74n933756h4v/

G.J. Janssen, J. Matysik, H.J.M. de Groot and A. Alia. "Photochemically induced dynamic nuclear polarization NMR on photosystem II obtained directly from plants reveals remarkable similarity and robustness of the radical pair across species" *Manuscript in preparation*

G.J. Janssen, K.B. Gupta, B. Bode, J. Matysik, H.J.M. de Groot and A. Alia. "Time-resolved photo-CIDNP MAS NMR on PSI and PSII from plants." *Manuscript in preparation*

CURRICULUM VITAE

On the 27th of April 1984 I was born in London, Great Britain after which my family soon moved to Amsterdam. I attended the anthroposophic Geert Grote primary School and the Sint Nicolaas Lyceum in Amsterdam. In 2002 after obtaining my gymnasium diploma I moved to Leiden to study Chemistry at Leiden University. In 2005 I took my bachelor's degree and started the master Physical and Theoretical Chemistry. In the same year Prof. J. van den Broek started the first year of the Science Communication track, which I followed and which greatly widened my horizon. During my bachelor I did a laboratory project in genetics, studying the REV1 domain of the BRCT protein. My Master thesis was based on a computational study using quantum chemical calculations to investigate the anti cancer drug Bleomycin. In addition I completed two external projects, the first in Teylers museum in Haarlem titled "Science communication in the 19th century" and the second at Williams College in the United States where I investigated the self-organizing power of sugar polymers in a research aimed to develop drug delivery vehicles. In my extracurricular space I completed Italian courses at the Leiden University Language School up to level 5. In the summer of 2007 Dr. J. Matysik gave me the exceptional opportunity to attend the Spin Chemistry meeting in Venice as a master student. In September 2007, I started my PhD under the supervision of Dr. A. Alia in the Solid State NMR group at Leiden University led by Prof. dr. H.J.M. de Groot. During my PhD time, I attended the Advanced NMR course (2007) held at Bruker in Kahrlsuhe, and the theoretical "Solid-State NMR School" (2007) in Denmark. I had the opportunity to present my PhD work through poster presentations at various international conferences. These include the 4th EUROMAR meeting in Saint Petersburg, Russia (2008), the 43rd Meeting of the Dutch NMR-DG in Eindhoven, the Netherlands (2008), the NWO Spectroscopy and Theory meeting in Lunteren, the Netherlands (2009), the 44th meeting of the Dutch NMR-DG in Leiden, the Netherlands (2009), the NWO Spectroscopy and Theory in Veldhoven, the Netherlands (2010), the Discussion Meeting and Joint Benelux/German MR Conference in Münster, Germany (2010), the 6th EUROMAR meeting in Florence, Italy (2010) and the Spin Chemistry Meeting 2011 in Noordwijk, the Netherlands. From April 2012 to January 2013, while completing this thesis, I have been working as consultant at People in Science; an agency specialized in recruitment of science professionals. In Feburary 2013 I have started as Director Business Development at Crystallics; a company specialized in solid state drug research services.